The role of the GID complex
at the primary cilium.

Dissertation

zur Erlangung des akademischen Grades des

Doktor rerum medicarum (Dr. rer. medic)

für das Fachgebiet Molekulare Medizin

vorgelegt

der Medizinischen Fakultät

der Martin-Luther-Universität Halle-Wittenberg

von Friederike Hantel (M.Sc. Biochemie)

geboren am 21.09.1990 in Kiel

Betreuer: Prof. Thorsten Pfirrmann

1. Gutachter: Prof. Julia Groß, Potsdam
2. Gutachter: PD Frank Bartel, Halle

Datum der Verteidigung: 16.02.2023

Abstract

The primary cilium is involved in many signalling pathways in mammalian cells. It acts as a signalling hub for many important pathways, including the Hedgehog signalling pathway (Hh). Sonic hedgehog (Shh) can be activated via the canonical signalling route, involving proteins of the GLI family, which localise to the primary cilium. A study by Boldt et al. located the mammalian homologue to the GID (glucose induced degradation deficient) complex in close proximity to the primary cilium. The GID complex was first discovered in *Saccharomyces cerevisiae*. However, little is known about the mammalian GID complex and the roles it plays, especially regarding primary cilia.

The investigations conducted in this work led to the hypothesis that the human GID complex plays an important role in the regulation of Shh signalling. Experiments using qPCR could show that in cells with a dysfunctional GID complex, relative mRNA levels of two key components of the Shh pathway, *Gli1* and *Ptch1*, were significantly reduced. Further investigations using immunofluorescence techniques led to the result that the localisation of all investigated components of the Shh signalling pathway did not differ between the WT and the KO cell lines. However, when relative amounts of these proteins were quantified using ImageJ software, differences in the relative amount of GLI1, GLI2 and PTCH1 were observed. In subsequent immunofluorescence experiments it was shown that four components of the GID complex, ARMc8, MKLN1, RMND5a, and TWA1, are located at the primary cilium. This further underlines the existence of an important relationship between these organelles and the GID complex. This work could also suggest putative novel interacting partners for GID4, the subunit of the GID complex responsible for substrate recognition. For this, GID4 was over expressed in HEK293 cells and immunoprecipitation was performed. Also, BioID experiments were performed to further identify novel GID4 interacting partners in cooperation with Dr Ori's lab in Jena. However, the putative GID4 interacting partners need further investigation and verification.

In summary, this thesis underscores the interplay between the primary cilia and the GID complex in mammalian cells. It could be demonstrated that cells deficient in the GID complex have a modified Shh signalling pathway. Additionally, four subunits of the GID complex were shown to localise to the primary cilia, further strengthening the hypothesis of an intricate relationship between these two players. Lastly, putative novel interacting partners for GID4 could be proposed.

Referat

Das primäre Cilium ist an vielen Signalwegen in Säugetierzellen beteiligt. Es fungiert als Signalknotenpunkt für viele wichtige Signalwege, einschließlich des Hedgehog-Signalwegs (Hh). Sonic Hedgehog (Shh) kann über den kanonischen Signalweg aktiviert werden, an dem Proteine der GLI-Familie beteiligt sind, die im primären Zilium lokalisiert sind. Eine Studie von Boldt et al. lokalisierte das Säuger-Homolog zum GID-Komplex (glucose induced degradation deficient) in unmittelbarer Nähe des primären Ziliums. Der GID-Komplex wurde zuerst in *Saccharomyces cerevisiae* entdeckt. Allerdings ist wenig über den Säugetier-GID-Komplex und die Rolle, die er spielt, insbesondere in Bezug auf primäre Zilien, bekannt.

Die in dieser Arbeit durchgeführten Untersuchungen führten zu der Hypothese, dass der humane GID-Komplex eine wichtige Rolle bei der Regulation des Shh-Signalwegs spielt. qPCR Experimente konnten zeigen, dass in Zellen mit einem dysfunktionalen GID-Komplex die relativen mRNA-Spiegel von zwei Schlüsselkomponenten des Shh-Signalwegs, *Gli1* und *Ptch1*, signifikant reduziert waren. Weitere Untersuchungen mit Immunfluoreszenztechniken führten zu dem Ergebnis, dass sich die Lokalisierung aller untersuchten Komponenten des Shh-Signalwegs zwischen den WT- und den KO-Zelllinien nicht unterschied. Als jedoch die relativen Mengen dieser Proteine mit der ImageJ-Software quantifiziert wurden, wurden Unterschiede in der relativen Menge von GLI1, GLI2 und PTCH1 beobachtet. In nachfolgenden Immunfluoreszenzexperimenten wurde gezeigt, dass vier Komponenten des GID-Komplexes, ARMc8, MKLN1, RMND5a und TWA1, am primären Zilium lokalisiert sind. Dies unterstreicht weiter die Existenz einer wichtigen Beziehung zwischen diesen Organellen und dem GID-Komplex. Diese Arbeit konnte auch mutmaßliche neue Interaktionspartner für GID4 vorschlagen, die Untereinheit des GID-Komplexes, die für die Substraterkennung verantwortlich ist. Dazu wurde GID4 in HEK293-Zellen überexprimiert und es wurde eine Immunpräzipitation durchgeführt. Als nächstes wurden BioID-Experimente durchgeführt, um in Zusammenarbeit mit dem Labor von Dr. Ori in Jena neue GID4-Interaktionspartner weiter zu identifizieren. Die mutmaßlichen GID4-Interaktionspartner müssen jedoch weiter untersucht und verifiziert werden.

Zusammenfassend unterstreicht diese Arbeit das Zusammenspiel zwischen den primären Zilien und dem GID-Komplex in Säugetierzellen. Es konnte gezeigt werden, dass GID-defiziente Zellen einen modifizierten Shh-Signalweg aufweisen. Darüber hinaus wurde gezeigt, dass sich vier Untereinheiten des GID-Komplexes an den primären Zilien lokalisieren, was die Hypothese einer komplizierten Beziehung zwischen diesen beiden Akteuren weiter stärkt. Schließlich konnten mutmaßliche neuartige Interaktionspartner für GID4 vorgeschlagen werden.

I Table of content

II List of Figures

III List of Tables

IV List of Abbreviations

A_{260}	Absorption at 260 nm
A_{280}	Absorption at 280 nm
aa	amino acid
alas	5-aminolevulinate synthase
AMPK	AMP-activated protein kinase
BCA	bicinchoninic acid
BSA	bovine serum albumin
bp	base pair
cDNA	complementary DNA
Ctrl	control
DAPI	4′,6-diamidino-2-phenylindole
DNA	deoxyribonucleic acid
DMSO	dimethylsulfoxide
DMEM	Dulbecco's Modified Eagle's Medium
dNTP	deoxynucleicotide triphosphate
E. coli	*Escherichia coli*
EDTA	Ethylenediaminetetraacetic acid
EGTA	ethylene glycol-bis(β-aminoethyl ether)-N,N,N′,N′-tetraacetic acid
ER	endoplasmic reticulum
EtBr	ethidium bromide
EtOH	ethanol
FBS	fetal bovine serum
GAPDH	glycerinhaldehyde-3-phosphate-dehydrogenase
h	hour
HEK	human embryonic kidney
Hh	Hedgehog
hprt	hypoxanthine-guanine phosphoribosyltransferase
IF	immunofluorescence
IFT	intraflagella transport
Kan	Kanamycin
Kb	kilo base
LB	lysogeny broth
kDa	kilodalton
KO	knock out
MeOH	Methanol
min	minute
mRNA	messenger RNA

Myc	V-myc avian myelocytomatosis viral oncogene homolog
NES	nuclear localisations signal
NLS	nuclear export signal
PBS	phosphate buffered saline
PAGE	polyacrylamide gel electrophoresis
PC	primary cilium
PCR	polymerase chain reaction
qPCR	quantitative PCR
PFA	paraformaldehyde
PKA	protein kinase A
PHAX	phosphorylated adaptor for RNA export
RNA	ribonucleic acid
rpm	revolutions per minute
rt	room temperature
SD	standard deviation
SDS	sodium dodecyl sulfate
Shh	Sonic Hedghog
TBE	tris/borate/EDTA
TBS	tris buffered saline
TBS-T	tris buffered saline-Tween 20
Tris	tris(hydroxymethyl)aminomethane
TZ	transition zone
UV	ultraviolet
VC	vector control
VDAC1	voltage-dependent anion channel 1 protein
WT	wild type

1 Introduction

1.1 The primary cilium – the cell's antenna

The primary cilium is a sensory non-motile organelle which protrudes like an antenna from the cell's surface [1]. It is involved in various signal transduction pathways and a disruption in the primary cilia's function can have severe consequences [2]. Diseases caused by malfunctions of cilia are called ciliopathies [3]. The severity of each ciliopathy depends on the extent to which ciliogenesis or cilium function is affected [4]. In contrast to many other cell organelles, the primary cilium is typically formed during quiescence or the G1 phase of the cell cycle [5]. In many ways, primary cilia resemble the motile cilia found on respiratory epithelia, however primary cilia are mostly present as a single organelle per cell [6]. Also, the functions of motile cilia are well understood while the primary cilia were regarded to have little importance. This opinion has changed and it is now well known that primary cilia play important roles in the development and function of most organs of the human body [6].
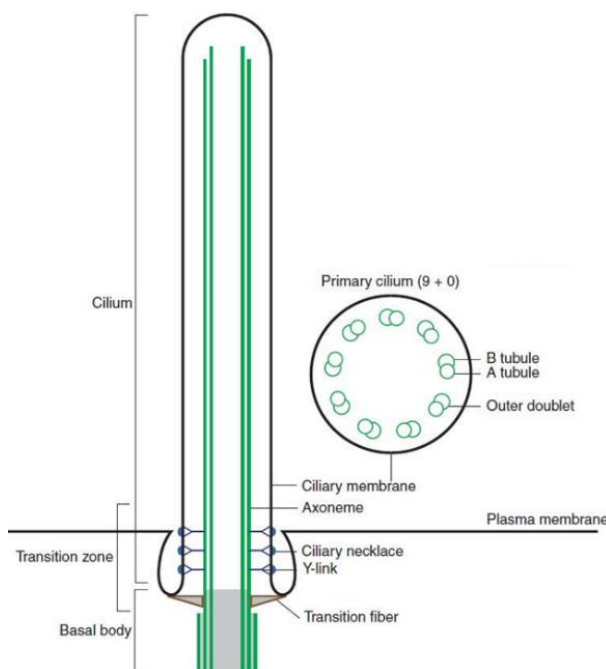
Figure 1 The primary cilium. Schematic structure of the primary cilium showing a longitudinal section on the left and a cross section on the right. Adapted from [7].

1.1.1 Structure of the primary cilium

Structurally, primary cilia are composed of the axoneme, a microtubule-based cytoskeleton [8]. It consists of nine pairs of radially arranged microtubules which are post-translationally acetylated to support the long ciliary structure. Motile cilia carry an additional central pair of microtubules [8]. A cilium is rooted to the basal body, a structure that is derived from centrioles [9]. A schematic structure of the primary cilium is shown in Figure 1.1. Prior to cell division,

disassembly of the primary cilium is required. This allows the centriole to detach from the plasma membrane in order to duplicate and segregate during cell division [10].

The ciliary membrane is a continuous yet specialized portion of the plasma membrane with a unique lipid and protein composition [11]. It is enriched in signalling receptors that are critical for vertebrate development and tissue homeostasis, such as components of the Hedgehog (Hh) pathway and Wnt signalling pathway [10].

1.1.2 Ciliogenesis

The process during which a cilium is formed is called ciliogenesis. This process begins when the cell exits the mitotic cycle in response to mitogen deprivation or differentiation cues [1]. Ciliogenesis is initiated when small vesicles are recruited to the distal appendages of the mother centriole, called distal appendage vesicles (DAVs) [2]. When the centriolar distal appendages are associated with the primary cilium they are called transition fibres [12]. After attachment, the DAVs fuse to form a larger vesicle, called primary ciliary vesicle, that caps the distal centriole[2]. It increases in size due to vesicular trafficking [1] which results in the growth of the ciliary membrane [13] and also starts to form the axoneme from its tip [12]. The nascent cilium is now enclosed by a double membrane [1]. The base however remains structurally distinct and forms the transition zone [12]. Finally, the cilium migrates to the plasma membrane where the ciliary sheath fuses with the plasma membrane to establish a continuity of these two compartments [1].

1.1.3 Transition zone and ciliary gate

As mentioned above, a part called transition zone is constructed during the formation of the axoneme [2]. This involves the recruitment of intraflagellar transport (IFT) particles [2], since all ciliary proteins need to be transported to the primary cilium from the cytoplasm [14]. This transition zone is located at the base of the cilium and is part of the ciliary gate [15], a structure that ensures that the cilium is separated from the rest of the cell [13]. It is important that the cilium maintains an environment which is distinct from the cytosol [13] which is why the ciliary gate controls selective protein entry to and exit from the primary cilium [15]. In loss of function studies performed with different components of the transition zone it was shown that it plays a crucial role in both ciliogenesis and the control of ciliary composition [13].

So-called transition fibres connect the distal part of the basal body to the base of the ciliary membrane [13]. They also play an important role in IFT during which they serve as a docking station for particles on their way to the cilia [13]. It has also been shown that transition zone proteins can localize to different structures (e.g., centrosome, centriolar satellites, cell junctions) and can interact with components from different machineries like the BBSome and the IFT [15]: They seem to work together for the efficient import and export of proteins and other ciliary processes [15]. The proximal axoneme and the ciliary membrane are connected

within the transition zone by electron-dense structures called Y-links [13]. These structures connect each microtubule doublet of the axoneme to the ciliary membrane [13]. Another structure characteristic for the transition zone is the ciliary necklace, a specialized part of the membrane which is typically built by rows of membrane particles encircling the base of the axoneme [15]. It has been suggested that this gated entry of proteins to the cilia utilizes some of the same molecules and mechanisms which function in the gated entry to the nuclear compartment [11]. Both organelles use a barrier that controls the entry of small molecules by diffusion and a gate that enables the selective transport of larger molecules [11]. In both cases, Importin and the small GTPase Ran are involved in the import of proteins [7].

1.1.4 Intraflagellar Transport

The transport process mediating ciliary assembly and the import and export of ciliary proteins is called intraflagellar transport (IFT) [2]. Figure 1.2 shows an overview of the IFT machinery. This bidirectional transport system utilizes the axoneme to transport ciliary components from the cell body to the distal end of the cilium [7]. This is called the anterograde IFT [16] and it is thought to be powered by a heterotrimeric kinesin-2 [16]. When anterograde IFT trains reach the tip of the cilia, they remodel into retrograde trains and return to the ciliary base [17]. It has been observed that more IFT trains are leaving the ciliary tip than entering it, leading to the conclusion that anterograde trains fragment at least partially at the tip [17]. The retrograde transport is mediated by dynein-2 [18]. Additionally, BBSomes move on IFT trains through cilia in most systems and can hence be regarded as an additional IFT subcomplex [18]. During ciliogenesis all components which are required for cilia assembly are transported to the growing tip in this fashion [16]. However, the IFT system is also necessary for ciliary maintenance and a variety of ciliary functions after the cilium has been fully assembled [7]. For example, IFT is responsible for the localization of signal-transduction proteins to cilia which include receptors for Hh and Wnt signalling [15]. Defects in IFT proteins in mammals were found to affect signalling pathways and cause ciliopathies [19].

Each train is a large protein complex, consisting of IFT-A and IFT-B [17]. These complexes interact with kinesin-II, dynein-2 and a variety of cargoes [17]. IFT-A and IFT-B are loosely associated [14] and are thought to perform different roles in retrograde and anterograde IFT respectively [19]. The IFT-A subcomplex is currently thought to consist of six proteins (IFT144, 140, 139, 122, 121, and 43) and IFT-B is thought to be comprised of 16 subunits (IFT172, 88, 81, 74, 70, 57, 56, 54,52, 46,38,27, 25, 22, and 20) [19].

Transition fibres are involved in regulating protein trafficking both during ciliogenesis and in the mature cilia [13]. IFT trains assemble and bind their cargoes [19] near the transition fibres, i.e., at the basal body of the cilium [17]. The train then moves through the transition zone [17] and proceeds along the B-tubule of the microtubule doublet [17] to the ciliary tip [19]. When this destination is reached, the ciliary cargoes are unloaded and the IFT train is remodelled [19].

The anterograde motor is inactivated and the retrograde motor is activated [19] to allow the train to return via the A-tubule [17] to the ciliary base [19].Here, the IFT particles are recycled for the next cycle of transportation [19]. While this outline of the IFT cycle is well accepted, most of the underlying molecular mechanisms are still poorly understood [19].
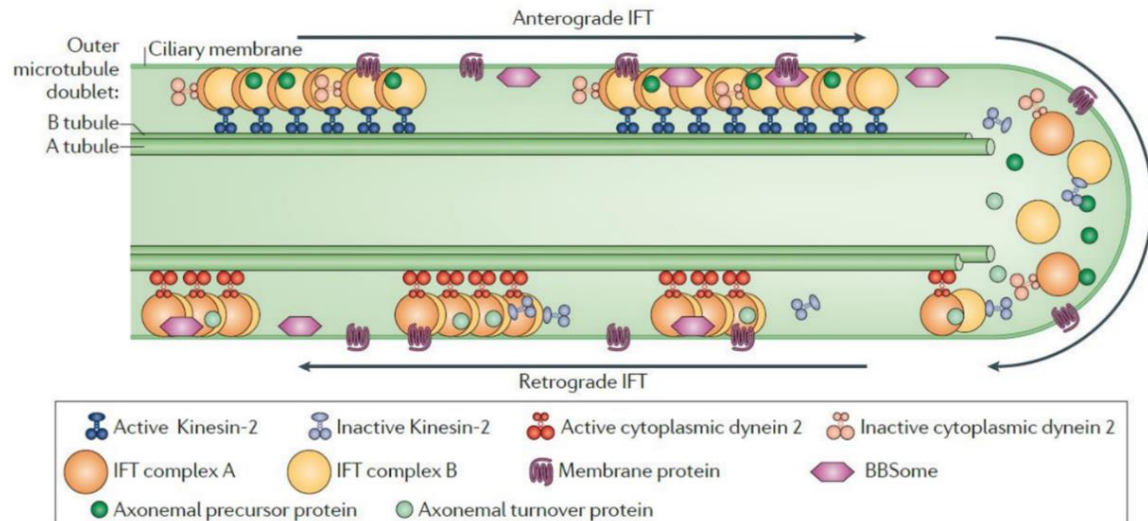
Figure 2 Overview of the IFT machinery. Cargo is transported to the ciliary tip by kinesin-2 in anterograde IFT. This includes inactive dynein-2, IFT complex A, IFT complex B and the BBSome. At the ciliary tip, the complex disassembles and axonemal proteins are released, before it is reassembled and moved back to the basal body by dynein-2 [14].

Membrane vesicle transport to the cilia is thought to be mediated by Rab small GTPases [7]. Rab8 interacts with the IFT machinery to facilitate vesicle trafficking to the cilia [7].

The IFT-B protein IFT20 is localized both to the basal body and is associated with the Golgi apparatus and thus required for the transport of proteins to the cilia [7]. Also involved in this process are Rab small GTPases [7]. Rab8 for example is thought to be involved in ciliogenesis by interacting with the IFT machinery and thereby mediating vesicle trafficking to cilia [7].

1.1.5 The BBSome

The BBSome is a multiprotein complex composed of eight BBS proteins (BBS1, BBS2, BBS4, BBS5, BBS7, BBS8, BBS9, and BBS18/BBIP10) and the small GTPase BBS3/Arl6 [18]. Defects in the BBSome cause the ciliopathy Bardet-Biedl syndrome (BBS) in humans [16]. The BBSome is thought to be an adapter for the transport of ciliary membrane proteins [18] and to move via IFT trains through the cilia [16]. One hypothesis suggests that BBSome-dependent retrograde transport plays a role in ciliary protein homeostasis [16]. Thus, it could scavenge non-ciliary proteins leaking into cilia and/or regulate the concentration of specific groups of ciliary signalling proteins in the cilia [18].

1.2 Shh signalling

In 1980 the Hedgehog (Hh) gene was first discovered in the fruit fly *Drosophila melanogaster* by Nüsslein-Volhard and Wieschaus [20]. In mammals, it is crucial for the organogenesis of almost all organs and also plays an important role in regeneration and homeostasis [21]. Three different mammalian Hh proteins have been described, Sonic-hedgehog (Shh), Indian-Hedgehog (Ihh), and Desert-Hedgehog (Dhh). While Dhh is restricted to the gonads, Shh and Ihh play important and sometimes overlapping roles in several tissues. Shh plays an important part in nervous system cell type specification, while Ihh is crucial for endochondral ossification during skeletal development [22]–[24]. In vertebrates, the primary cilium (described in detail above) plays an important role in Hh signalling, to wit, it carries the receptor for Shh and PTCH1 on the ciliary membrane [21]. This pathway is usually tightly regulated in healthy adult tissues and a hyperactivation may contribute to the development of solid tumours [25]. Figure 1.3 gives an overview of the Hh signalling in primary cilia.

The Shh pathway can be activated by either canonical signalling or non-canonical signalling [21]. The canonical signalling route is activated when Shh binds to and inactivates its receptor PTCH1 which is localized on the ciliary membrane [21]. While Shh is absent, the active PTCH1 inhibits the transmembrane protein Smo and thus prevents ciliary accumulation of it [25], [26]. In the absence of an active signalling pathway, Smo is ubiquitinated and removed from the cilia [27].

After binding of Shh to PTCH1, PTCH1 is transported out of the cilia and degraded. Now, active Smo accumulates in the cilia and initiates the Shh downstream signalling cascade [28]. The cellular mechanisms involved in these translocation steps are poorly understood [27]. However, this process seems to rely on IFT, since defects in IFT27 and components of the BBSome lead to an accumulation of Smo in cilia without subsequent activation of the pathway [27]. The pathway downstream of Smo leads to the translocation of Gli family proteins to the nucleus which trigger the transcription of target genes, including PTCH1 and GLI1 resulting in a negative and positive feedback loop, respectively [21].

The three GLI proteins, GLI1, GLI2 and GLI3, are transcription factors, carrying zinc finger motifs. GLI1 appears as a full-length transcriptional activator, whereas GLI2 and GLI3 can be processed to either act as an activator (GLI2A, GLI3A) or as a repressor (GLI2R, GLI3R) [29], [30].However, it seems like GLI2A and GLI3R are the more common forms of the two factors which means that GLI2 acts mainly as an activator while GLI3 mainly acts as a repressor of transcriptional activities [21]. While there is no activation of the Shh pathway, GLI3 remains in the GLI3R form. Upon activation, Smo converts GLI3R to the active GLI3A form [21]. Seemingly, GLI2 accumulates in the cilia upon Shh activation and is able to overcome the negative regulation of GLI3 [31]. GLI2 however, seems to shuttle between the cilium and the cytoplasm in the inactive state of the signalling pathway. It seems like dynein-2, the retrograde ciliary motor, actively shuttles both GLI2 and Smo out of the cilium to prevent their

accumulation [31]. After Shh activation, this transport process is altered and Smo and GLI2 accumulate in the cilia [31]. It has been reported that GLI2 is primarily located at the ciliary tip, although another study suggests GLI2 to be localized in the entire cilium [31]. Finally, GLI2 will be transported to the nucleus in its active GLI2A form [31].
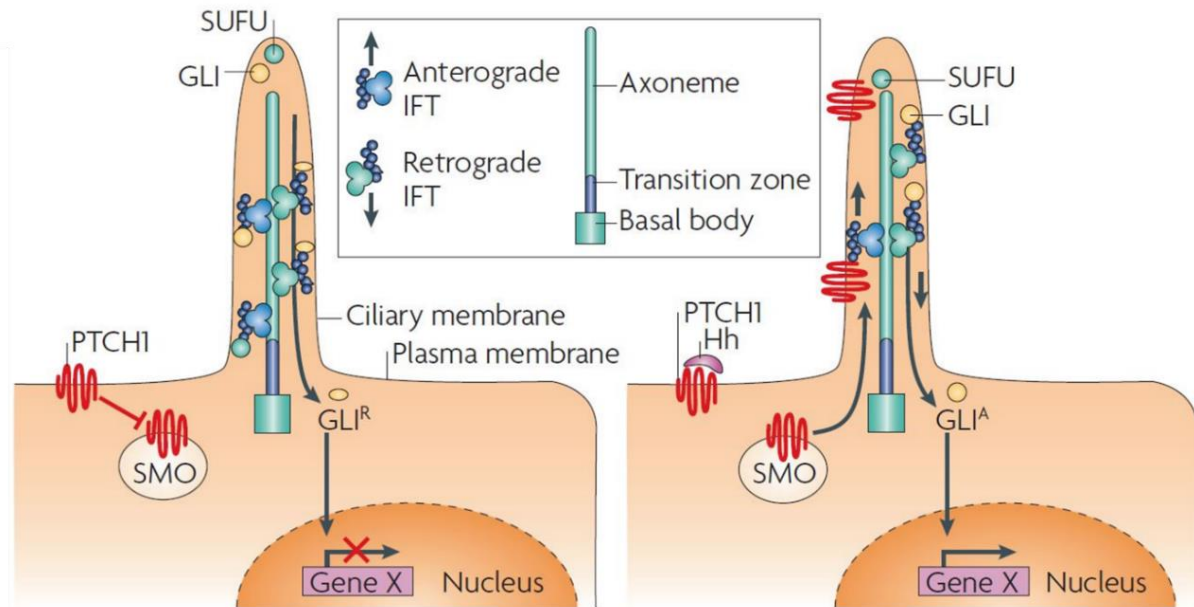
Figure 3 The Hedgehog (Hh) signalling pathway in primary cilia. In the absence of a Hh activator, the transcription factor GLI is processed at the ciliary tip to its repressor form (GLIR) and gene expression is turned off. Upon Hh activation, Smo is accumulates at the ciliary tip which leads to the translocation of active GLI (GLIA) to the nucleus and activation of target gene expression. Adapted from [3].

GLI1 and GLI3 are closely related proteins, however they differ greatly when it comes to proteasomal degradation [32]. In the absence of Hh stimulation, GLI3 is partially degraded, i.e., processed by the proteasome to create the repressor form GLI3R [32]. GLI1 on the other hand is degraded completely [32]. Another way to regulate GLI proteins can be acetylation. GLI1 and GLI2 can be acetylated by the enzyme histone deacetylase 1(HDAC1) at lysine 518 and 757, respectively [33]. This promotes the transcriptional activation of the signalling pathway and is turned off by degradation of HDAC1, mediated by an E3 ubiquitin ligase complex [33].

Another component of the Hh signalling pathways worth mentioning is Suppressor of Fused (SUFU) [34]. When the pathway is inactive, SUFU binds directly to the GLI proteins and inhibits their translocation to the nucleus and thus prevents the activation of the pathway [21], [34]. The exact mechanisms are not yet understood, although it could be shown that GLI proteins retained in the cytoplasm by SUFU are subsequently degraded or processed and are in this way involved in inhibiting Shh signalling [21].

1.3 Ubiquitination

1.3.1 Ubiquitin

Ubiquitin (Ub) is a small 76 amino acid long protein and one of the most common post translational modifiers. Ub can be linked to the lysine residues of substrate proteins and is thus involved in the regulation of countless different cellular processes [35]. Modification of substrates can occur either with a single Ub or with several Ub linked together in a polyubiquitin chain [36].To covalently attach Ub to a lysin moiety of a substrate protein, the C-terminus of the Ub and the ε-amino group of the lysin form an isopeptide bond. This is catalysed by three enzymes, called E1, E2 and E3 enzymes [37]. Also, Ub carries seven lysins and can be ubiquitinated at any of them to form different types of polyubiquitin chains [36]. The crystal structure of ubiquitin is shown in Figure 1.4.
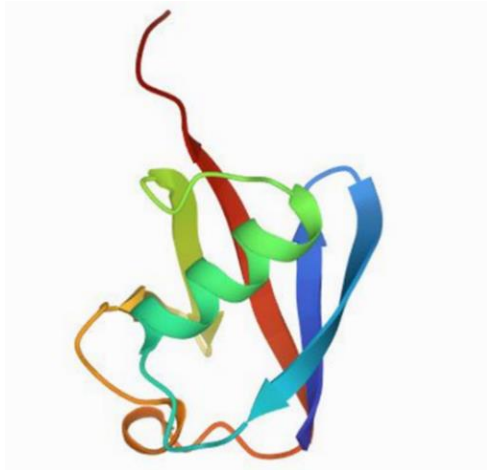
Figure 4 Crystal structure of ubiquitin, a small 76 amino acid and 8.58 kDa protein, one of the most common post translational modifiers [38]

If substrates are destined for degradation via the Ub-proteasome system (UPS), ubiquitination occurs mostly in form of a Lys-11- or Lys-48-linked polyUb chain which acts as a signal for proteasomal degradation [39]. The UPS plays a major role in cellular protein homeostasis (proteostasis) by degrading proteins that are either dysfunctional or no longer needed [35], [40].

1.3.2 Ub binding

The first step in ubiquitination is the activation of Ub by ubiquitin activating enzyme (E1) in an ATP-dependent fashion [41] resulting in a thioester bond between an E1 active site cysteine and the Ub C terminus [37] (see Figure 1.5 (1)). Next, Ub is transferred to the active site cysteine of one of ~40 different (in mammals) ubiquitin-conjugating enzymes (E2) [42] in a transthioesterification reaction to yield an E2~Ub thioester intermediate [37] [41] (see Figure 1.5. (2)). Then, a ubiquitin protein ligase (E3) binds both the E2~Ub thioester and the substrate and transfers the Ub from the active site cysteine of the E2 to a primary amine on a lysin side

chain or the N terminus of the substrate protein [37] [41] (Figure 1.5 (3)). This highlights the importance of E3 ligases as they are responsible for both substrate recognition [43] and increasing the rate of Ub transfer [37].
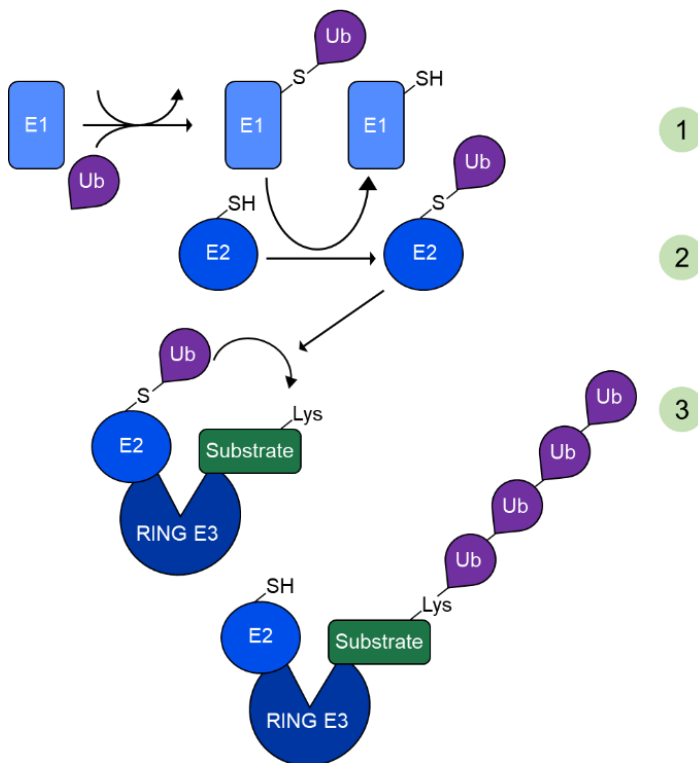
Figure 5 Mechanism of RING E3 ligases. Ubiquitination of substrate proteins starts with the charging of the E1 enzyme in an ATP-dependent manner and leads to the formation of a thioester bond between the ubiquitin C terminus and the E1 active site cysteine. Next, ubiquitin is transferred to the E2 active site cysteine in a transthioesterification reaction. Then a RING E3 ligase binds both the E2~Ub thioester and the substrate and catalyses the attack of the primary amine on a lysine side chain or protein N terminus on the thioester. Adapted from [37].

To this date, over 600 E3 ligases are known in humans to specifically target a huge variety of substrates [44] which allows these enzymes to operate in many different cellular contexts, respond to a variety of signals, and .process a great number of substrate proteins [43]. E3 ligases can be grouped into three classes [45], characterised by the mechanism by which Ub is transferred from the E2 to the substrate and by conserved structural domains [37], [41]. RING (really interesting new gene)-type E3s bind both the substrate and the E2~Ub simultaneously and transfer Ub directly [37], [41]. RBR (RING-between-RING) E3s and HECT (homologous to the E6AP carboxyl terminus)–type E3s act in a two-step reaction, first transferring the Ub from the E2 active site to an active site cysteine in the E3 and in a second step from the E3 to the substrate [46], [47]. The family of RING E3 ligases constitutes the largest family of Ub ligases [43]. Since E3 ligases play such an important role, their activity needs to be regulated to avoid random ubiquitination. Often, E3 are kept in a latent state and are only fully activated by post translational modifications (PTMs) [43]. Another layer of

regulation is self-ubiquitination of E3. This can act as a turn-off switch via proteasomal degradation [48].

1.3.3 The proteasome

After substrate proteins have been labelled by ubiquitin, they are degraded into short peptides by the 26S proteasome in an ATP-dependent manner [40], [49], [50]. The 26S proteasome is a 2.5 MDa multi subunit protein complex and is comprised of a 20S core particle (CP) , where degradation occurs and 19S regulatory particles (RP) [40]. The barrel shaped interior of the 20S CP contains the active proteolytic sites of the 26S proteasome [51]. This prevents native and unfolded proteins to be degraded in an uncontrolled fashion [51]. RPs are usually located at the distal ends of the barrel. Here, ubiquitinated proteins are received, unfolded and translocated to the CP [51], [52].

1.3.4 Degrons

The question of how E3 ligases recognize their specific targets has led to the discovery of multiple degradation signals, coined degrons [53]. Degrons can generally be divided into two groups: inherent and acquired degrons. Inherent degrons are permanently present in proteins and can be specific amino acid sequences, or N- or C-terminal amino acids corresponding to the N-degron and the C-degron pathways. However, many inherent degrons consist of hydrophobic amino acid sequences which are normally buried in the protein core. If the protein fails to fold properly, those sequences are exposed, allowing for recognition by E3 ligases [54] [55], [56].

Acquired degrons are induced by post-translational modifications (PTMs) [54], [57]. These PTMs include phosphorylation, ligation of Small Ubiquitin-like Modifier (SUMOylation) and hydroxylation [54], [58].

1.4 GID complex

1.4.1 Discovery and structure

The GID (glucose induced degradation deficient) complex is a multi-subunit RING E3 ubiquitin ligase [59]. It was first discovered in the yeast *Saccharomyces cerevisiae* [60] where the complex is a key regulator in the metabolic shift from gluconeogenesis to glycolysis [61]. The mammalian homologue to the GID complex is called C-terminal to LisH (CTLH) complex [62]. In *S. cerevisiae*, the Gid complex consists of seven proteins GID1 (VID30), GID2, GID4 (VID24), GID5 (VID28), GID7, GID8 and GID9) which results a mass of 600 kDa [63].

The subunits GID2 and GID9 both contain Really Interesting New Gene (RING) finger domains and are responsible for the E3 activity of the GID complex [61], [62] in transferring ubiquitin directly from the E2 to the substrate [62].

The GID complex facilitates the polyubiquitination and subsequent proteasomal degradation of fructose-1,6-bispohosphatase (FBPase) [63]. This enzyme is needed for gluconeogenesis when yeast is grown on a non-fermentable carbon source [63]. When glucose is added and gluconeogenesis is not needed anymore, GID4 is synthesized, binds via GID7 to the GID complex and thus activates GID2 E3 ligase activity [63]. FBPase is then polyubiquitinated and degraded by the proteasomal system [63]. Phosphoenolpyruvate carboxykinase (PEPCK), another enzyme involved in gluconeogenesis, was also found to be a substrate of the GID complex in yeast [61].

In mammals, many GID complex counterparts can be found [88, 89]. When considering domain organisation and sequence identity, GID1 is similar to RanBP9, GID2 to the RING containing protein RMND5a, GID5 to ARMc8, GID7 to MKLN1, GID8 to TWA1 and GID9 to MAEA (see also Table 1.1) [63]–[65]. Figure 1.6. shows a schematic representation of both the subunits of the GID complex from yeast and their mammalian homologues.

Table 1 The GID complex and its mammalian homologous counterparts with accession numbers [63], [65]

S. cerevisiae		Homo sapiens	
GID subunit	Accession no.	Gid subunit	Accession no.
GID1	NP_011287.1	RANBP9, RANBP10	NM_005493
GID2	NP_010541.3	RMND5a/ RMND5b	NM_022780
GID4	NP_009663.1	GID4	NM_024052
GID5	NP_012247.3	ARMc8	NM_213654
GID7	NP_009891.1	MKLN1	NM_013225
GID8	NP_013854.1	TWA1	NM_017896
GID9	NP_012169.1	MAEA	NM_001017405.3

The mammalian homologue of the GID complex is also called the CTLH complex. In five of the subunits (RanB9, RMND5, MKLN1, TWA1, and MAEA) LisH (lissencephaly-1 homology) and CTLH (C-terminal to LisH) domains could be found in their central regions and are followed in all components but MKLN1 by a CRA (CT11-RanBP9) domain [61], [63], [66].
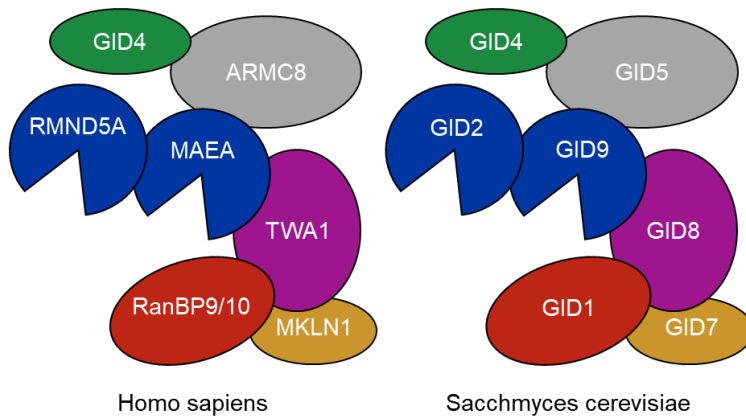
Figure 6 A schematic representation of the human and the yeast GID complex. Adapted from [59], [67]

In vitro ubiquitination assays of the mammalian CTLH complex showed E3 ligase activity which depends on RMND5a (GID2) and MAEA (GID9) [62]. The same could be shown for the *Xenopus laevis* orthologue of GID2 [68]. It has been suggested that RanBP9 and TWA1 are essential for complex stability [62]. Also it could be demonstrated that MKLN1 ubiquitination is dependent on RMND5a, which suggests that it is regulated by the CTLH complex which could mean that it may be part of an autoregulatory mechanism [62]. However, very little is known about the exact composition, activity and function of the mammalian GID complex and needs to be characterized further [69].

1.4.2 Substrates, substrate recognition, N-end rule

For the GID complex in yeast, several substrates are known (FBPase, PEPCK, malate dehydrogenase (c-MDH)) [70]. The ubiquitination and subsequent degradation depends on the two RING domain containing subunits GID2 and GID9 [70]. These two subunits seem to form the heterodimeric E3 ligase unit of the GID complex [70]. However, the GID complex is not active until GID4 attaches to the other six subunits [71]. GID1, GID2, GID5, GID7, GID8 and GID9 are constitutively expressed in yeast, no matter the growth conditions [71]. Upon the addition of glucose, GID4 appears within mere minutes and initiates the degradation process of the gluconeogenic enzymes and thus switching the cells from gluconeogenesis to glycolysis [61]. GID4 itself seems to be a rather unstable protein and its degradation depends also on the GID complex [61].

From this, it has been stipulated that GID4 acts as the substrate recognition component of the GID complex [72]. It is assumed that GID4 recognizes its substrates by a proline at position 1 or 2 of the N-terminus [72]. The substrate is then degraded via the Pro/N-degron pathway [73] (see Figure 1.7). Additionally to GID4, a new substrate recognition component, called GID10, was identified in *S. cerevisiae* [73]. Apparently, substrate specificities of GID4 and GID10 overlap but are not identical [73]. These two components also differ in their expression, while GID4 is expressed under normal growth conditions, GID10 seems to be expressed under starvation or osmotic stresses [73].
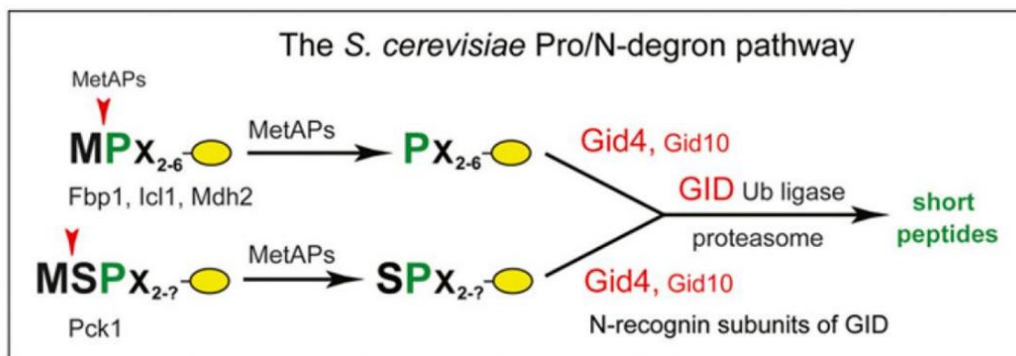
Figure 7 The Pro/N-degron pathway in *S. cerevisiae*. This schematic shows both the pathway's main N-recognin, GID4 and GID10, a stress-inducible minor recognin. It could be demonstrated that both the human and the yeast GID4 recognizes not only Nt-Pro, but also Nt-Ile, Nt-Leu, Nt-Val, and Nt-Phe. M=methionine, P=proline, S=serine, X=any amino acid, MetAPs=methionyl aminopeptidase. Adapted from [74].

However, it was reported that the human CTLH complex ubiquitinylates substrates which do not have an N-terminal proline [67], although a proline seems to be required for human GID4 to bind [69]. A possible explanation could exist in the discovery that the GID E3 ligase is not a singular complex but rather a family of E3 ligases with different substrate receptors [69]. This means that GID4 could be substituted by other GID subunits and in this way modulate substrate specificity [67], [69].

The understanding of the E3 ligase function and the roles of most components of the mammalian CTLH complex is still very limited [63]. It was suggested that ARMc8 regulates degradation of α-catenin and facilitates the interaction of hepatocyte growth factor-regulated tyrosin kinase substrate (HRS) with ubiquitinated proteins [88]. Yet, ARMc8 is not needed for the assembly of the CTLH complex [63]. MAEA was identified as a macrophage attachment protein of erythroblasts and is thought to play a role in nuclear extrusion in erythropoiesis [63]. MKLN1 and RanBP9 seem to form a complex which is involved in the regulation of cell morphology but it is unknown if this function occurs in context of TWA1, MAEA or RMND5A [63].

Recent studies suggest that proteins ubiquitinylated or regulated by the CTLH complex in mammalian cells include HBP1 (HMG box-containing protein 1), LMNB2 (lamin B2), PRKAA (the catalytic subunit of AMP-activated protein kinase (AMPK)), c-Raf (RAF proto-oncogene serine/threonine-protein kinase, also called RAF1), HDAC6 (histone deacetylase 6), and its own subunit MKLN1 [64], [75]. Also, there are indications that, like in yeast, the CTLH complex is involved in the regulation of glucose metabolism, although it appears to do so in a different way [89]. It was shown that the CTLH complex functions to inhibit glycolytic flux and is responsible for the ubiquitination of pyruvate kinase M1/2 (PKM) and L-lactate dehydrogenase A chain (LDHA) [64]. It has also been reported that a dysfunctional CTLH complex in *Caenorhabditis elegans* results in a significant life span extension [75].

2 Aim of the thesis

The aim of the thesis was to gain a better and more in depth understanding of the mammalian GID complex and the roles it plays in mammalian cells. A study published by Boldt *et al.* investigated the network of human proteins and complexes located at the primary cilium [76], placing the human GID complex at the basal body. This prompts the question if the GID complex is a functional part of the primary cilium and what roles the complex plays in cilia development, maintenance and signalling. To address these questions this work is split in three parts.

2.1 The role of the GID complex in cilia signalling

Using qPCR, the amount of relative mRNA levels of different Shh signalling markers need to be compared between the wild type cell line NIH-3T3 (WT) and a NIH-3T3 knock out cell line that no longer expresses RMND5a (Rmnd5a KO). This knockout leads to a dysfunctional GID complex and thus to its inactivity. Two different growth conditions should be analysed, i.e., starvation medium and starvation medium with an added stimulant of the Shh signalling pathway. Next, a series of immunofluorescence experiments ought to be performed with both cell lines to investigate any differences in the localisation of components of the Shh signalling pathway, also taking into account the two different growth conditions. In a next step, whole cell lysates of both cell types in both growth conditions should be separated into a cytoplasmic and a nuclear fraction and the relative amount of expressed proteins involved in Shh signalling need to be compared.

2.2 Localisation of different subunits of the GID complex

The location of various subunits of the GID complex relative to the primary cilium in mammalian cells ought to be determined. For this, a series of immunofluorescence experiments using NIH-3T3 WT cells in both cycling cells and starved cell must be performed.

2.3 Identifying novel GID4 interacting partners

To further elucidate the role the GID complex plays in mammalian cells it is crucial to investigate novel interacting partners of the substrate recognition factor GID4. To approach this aim, GID4 needs to be over expressed in HEK293 cells, whole cells lysates need to be analysed by mass spectrometry and compared to cells transfected with a vector control. In the next step, a co-immunoprecipitation (co-IP) with HEK293 cells expressing a Myc tagged GID4 ought to be performed and the eluates must be analysed by mass spectrometry to be compared to those of vector controls. Additionally, a BioID for proximity-dependent biotin identification should be performed to further establish putative novel GID4 interacting partners.

3 Materials and Methods

3.1 Materials

3.1.1 Chemicals

Table 2 – List of chemicals and respective distributor

Substance	Distributor
Agarose	Biozym
Ampicillin	Roth
Biotin	Roth
Boric acid	Roth
Bovine serum albumin	Roth
Bromphenol blue	Roth
CASYton	OMNI Life Science
4′,6-diamidino-2-phenylindole (DAPI)	Sigma-Aldrich
Dimethyl sulfoxide (DMSO)	Sigma-Aldrich
Disodium phosphate	Roth
Ethanol 99%	Roth
EDTA	Roth
EGTA	Roth
Glycerol	Roth
Glycine	Roth
HEPES	Roth
Isopropanol	Roth
Kanamycin	Roth
β-Mercaptoethanol	Sigma-Aldrich
Methanol	Roth
Milk powder	Roth
Monopotassium phosphate	Roth
Paraformaldehyde	Roth
Potassium chloride	Roth
Sodium chloride	Roth
Sodium dodecyl sulfate	Roth
Tetracycline	Sigma-Aldrich
Tetrasodium pyrophosphate	Roth
Tris	Roth,
Triton X-100	Roth
Tween 20	Roth

3.1.2 Composition of buffers

Table 3 – List of buffer compositions

Buffer	Substance	Concentration
Blocking solution		
	BSA	5 % (w/v) in PBS
Dilution buffer		
	Tris/Cl pH 7.5	10 mM
	NaCl	150 mM
	EDTA	0.5 mM
Laemmli buffer		
	Tris pH 6.8	0.5 M
	Glycerine	45 % (v/v)
	β-mercaptoethanol	12.5 % (v/v)
	Bromphenol blue	
Lysis buffer		
	HEPES pH 7.5	50 mM
	NaCl	150 mM
	EGTA	1 mM
	Triton X-100	1 %
	$Na_4P_2O_7$ x 10 H_2O	10 mM
	NaF	100 mM
Phosphate-buffered saline (PBS)		
	NaCl	137 mM
	KCl	2.7 mM
	Na_2HPO	8 mM
	KH_2PO_4	1.7 mM
	pH 7.4	
SDS-PAGE running buffer		
	Tris	25 mM
	Glycine	192 mM
	SDS	3.5 mM
Tris/borate/EDTA (TBE)		
	Tris	89 mM
	Boric acid	89 mM
	EDTA	2 mm

Table 3 – List of buffer compositions (continued)

Buffer	Substance	Concentration
Tris-buffered saline-Tween 20 (TBS-T)		
	Tris	20 mM
	KCl	6.7 µM
	NaCl	150 mM
	Tween 20	0.05 %
	pH 7.4	
Wash buffer I		
	Tris/Cl pH 7.5	10 mM
	NaCl	150 mM
	Nonidet™ P40 Substitute	0.05 %
	EDTA	0.5 mM
Wash buffer II		
	Tris/Cl pH 7.5	10 mM
	NaCl	250 mM
	Nonidet™ P40 Substitute	0.05 %
	EDTA	0.5 mM
Western blot transfer buffer		
	Tris	25 mM
	Glycin	192 mM Glycin
	Methanol	20 % (v/v)

3.1.3 Equipment used within this project

Table 4 – List of equipment and respective distributor

Equipment	Distributor
Autoclave	
Systec V-series	Systec
Cell culture	
CELLSTAR® Cell Culture Dishes 100 mm	Greiner Bio-One
CELLSTAR® Cell Culture Flasks (T25, T75)	Greiner Bio-One
CELLSTAR® Cell Culture Microplates (6, 12, 96 well)	Greiner Bio-One
CASY® TT Cell Counter and Analyser System	OMNI Life Science
CASY®cups	OMNI Life Science

Table 4 – List of equipment and respective distributor (continued)

Equipment	Distributor
Centrifuges	
Biofuge 15R	Heraeus Sepatech
Centrifuge 5425	Eppendorf
2K15	Sigma
Heraeus Biofuge Stratos	Thermo Electric Cooperation
Electrophoresis	
GelDoc	Intas Scientific
Incubator/ Thermoblock	
Heracell 150	Heraeus
I26 Incubator Shaker Series	New Brunswick Scienfitic
Thermomixer 5437	Eppendorf
Microscope	
Zeiss Axio Observer 7 with ApoTome.2	Carl Zeiss AG
TELAVAL 31	Carl Zeiss AG
Evos® fl	AMG
PCR Thermocycler	
Tpersonal Thermocycler	Biometra
Real-Time PCR	
LightCycler®480 II	Roche
LightCycler®480 Multiwell Plate 96, white	Roche
*Shake*r	
RM5	CAT
KM-2	Edmund Bühler
Spectrophotometer	
Nanodrop® Spectrophotometer ND-100	peQLab Biotechnology
Sterile hood	
Herasafe	Heraeus Instruments
Biological Safety Cabinet	Nuaire
Western Blot analyses	
Standard Power Pack P25	Biometra
XCell SureLock Mini-Cell Electrophoresis System	Thermo Fisher Scientific
Eco-Mini Blotting Chamber	Biometra
Novex™WedgeWell™ 10% Tris-Glycin Gel	Invitrogen
Chromatography Paper 3MM CHR	GE Healthcare Life science Whatman™

Table 4 – List of equipment and respective distributor (continued)

Equipment	Distributor
Western Blot analyses	
Amersham™Hybond™ P 0.45 PVDF Blotting Membrane	GE Healthcare Life science
ChemiDoc MP Imaging System	Bio-Rad
Others	
ClarioStar microplate reader	BMG Labtech
Vortex Genie 2	Scientific Industries
MicroPulsar™ electroporator	Bio-Rad
pH Meter pH 526	WTW
Water bath	Memmert
PIPETMAN (P2, P10, P20, P200, P1000)	Gilson

3.1.4 Primers

Table 5 – List of oligonucleotides, description and sequence

Oligonucleotide	Description	Sequence
Mm_Hprt_for	qPCR	GGGGCTGTACTGCTTAACCAG
Mm_Hprt_rev	qPCR	TCAGTCAACGGGGGACATAAA
Mm_Alas_for	qPCR	CTCCTCGAACCCTGTCCAC
Mm_Alas_rev	qPCR	GCCATCTGGGACTCGTCAG
Mm_Rmnd5a_for	qPCR	CAGCCAACGGCTTCTCAATG
Mm_Rmnd5a_rev	qPCR	GACAGACCAGATTCCTGGCA
Mm_Gli1_for	qPCR	GGTCTCGGGGTCTCAAACTG
Mm_Gli1_rev	qPCR	TGTAGTGCTGAGCAGGTGTG
Mm_Gli2_for	qPCR	GGGACTCTTTAGCCTCGCAG
Mm_Gli2_rev	qPCR	CCACAGGGTTGAGGTAGTCAT
Mm_Ptch1_for	qPCR	GTCCACTGTGGTCCATCCG
Mm_Ptch1_rev	qPCR	GACAAGGAGCCAGAGTCCAG
Hs_Gid4_EcoRI_for	PCR	CGAATTCTATGCCGGTCCGCACCGAGTGTCCC
Hs_Gid4_XhoI_rev	PCR	GCTCGAGTCACCGGAACTCATAGATGGGTGC
Hs_Gid4_prox_for	PCR	AATGCCGGTCCGCACCGA
Hs_Gid4_prox_C_rev	PCR	CCGGAATTCATAGATGGGTGC
Hs_Gid4_prox_N_rev	PCR	TCACCGGAATTCATAGATGGGT

3.1.5 Antibodies for western blot analysis and immunofluorescence

Table 6 – List of antibodies for western blot analysis and immunofluorescence, respective distributor and order number

Antibody	Distributor	Order number
β-actin	Sigma-Aldrich	A-5441
ARMc8	Santa Cruz Biotechnology	sc-365307
β-catenin	Cell Signaling Technology	9562
GAPDH	Sigma-Aldrich	8795
GFP	Chromotek	pabg1-20
GLI1	Santa Cruz Biotechnology	sc-515751
GLI2	Santa Cruz Biotechnology	sc-271786
GLI3	R&D Systems	AF3690
MKLN1	Santa Cruz Biotechnology	sc-398956
Myc-Tag (71D10) Rabbit mAb	Cell Signaling Technologies	2278
PTCH1	Santa Cruz Biotechnology	sc-518044
RMND5a	Atlas Antibodies	HPA046795
SUFU	Santa Cruz Biotechnology	sc-137014
Ac-Tubulin	Sigma-Aldrich	T6793
Ac-Tubulin	Cell Signaling Technology	5335
γ-Tubulin	Sigma-Aldrich	T6557
γ-Tubulin	Cell Signaling Technology	5886
TWA1	Novus Biologicals	NBP1-32596
Streptavidin-HRP	Thermo Fisher Scientific	21130
AlexaFluor™488 donkey anti rabbit IgG (H+L)	Invitrogen	A21206
AlexaFluor™546 goat anti mouse IgG (H+L)	Invitrogen	A11030
Anti-mouse IG, HRP-linked Antibodyg	Cell Signaling Technology	7076
Anti-rabbit IgG, HRP-linked Antibody	Cell Signaling Technology	7074

3.1.6 Vectors used for cloning

Table 7 – List of vectors and respective distributor

Vector	Source
pcDNA5-pDEST-BirA-Flag-C-term	Dr. Alessandro Ori, FLI Jena
pcDNA5-pDEST-BirA-Flag- N-term	Dr. Alessandro Ori, FLI Jena
pCS2+	AG Hollemann, Martin-Luther-University Halle-Wittenberg
pCS2+-Gid4-c-Myc	This work
pEGFP	AG Hollemann, Martin-Luther-University Halle-Wittenberg
pEGFP-Gid4	Eliza Karapetian, AG Pfirrmann, Martin-Luther-University Halle-Wittenberg
pOG44	Dr. Alessandro Ori, FLI Jena

3.1.7 Enzymes used for cloning

Table 8 – List of enzymes and respective distributor

Enzyme	Distributor
EcoRI-HF	New England Biolabs
Q5® High Fidelity DNA Polymerase	New England Biolabs
T4 ligase	New England Biolabs
XhoI-HF	New England Biolabs

3.1.8 Kits used within the project

Table 9 – List of kits and respective distributor

Kit	Distributor
Gateway™ LR Clonase™ II Enzyme mix	Thermo Fisher Scientific
GeneJET PCR Purification Kit	Thermo Fisher Scientific
GeneJET RNA Purification Kit	Thermo Fisher Scientific
HiScript II Q RT SuperMix for qPCR	Vazyme Biotech
Invitrogen™ SuperScript™ II Reverse Transcriptase	Thermo Fisher Scientific
Maxima SYBR Green/ROX qPCR Master Mix (2x)	Thermo Fisher Scientific
Myc-Trap for Immunoprecipitation (IP)	ChromoTek
pENTR™/D-TOPO™ Cloning Kit, with One Shot™ TOP10 Chemically Competent E. coli	Thermo Fisher Scientific
Pierce™ BCA Protein Assay Kit	Thermo Fisher Scientific

Table 9 – List of kits and respective distributor (continued)

Kit	Distributor
Q5® High-Fidelity DNA Polymerase	New England Biolabs
QIAprep Spin Midiprep Kit	Qiagen
Subcellular Protein Fractionation Kit for Cultured Cells	Thermo Fisher Scientific
SuperSignal™ West Femto Maximum Sensitivity Substrate	Thermo Fisher Scientific
ZymoPURE™ Plasmid Miniprep	Zymo Reseach

3.1.9 Standards

Table 10 – List of standards and respective distributor

Standard	Distributor
Gel Loading Dye Purple (6x)	New England Biolabs
GeneRuler 1kb	Thermo Fisher Scientific
PageRuler™ Prestained Protein Ladder	Thermo Fisher Scientific
PageRuler™ Plus Prestained Protein Ladder	Thermo Fisher Scientific

3.1.10 Cell lines used in this project

Table 11 – List of cell lines, description and respective distributor / origin

Cell line	Description	Distributor / Origin
HEK293 FlpIn TREx	Ensures rapid generation of stable cell lines and homogenous expression of a protein of interest from a Flp-In™ expression vector	Dr. Alessandro Ori, FLI Jena
HEK293T	Human Embryonic Kidney cells	ATCC
NIH-3T3 WT	Mouse fibroblasts, wild type	ATCC
NIH-3T3 Rmnd5a KO	Mouse fibroblasts, Rmnd5a knock out	AG Hollemann, Martin-Luther University Halle-Wittenberg

3.1.11 Medium compositions for Cell culture

Table 12 – List of medium composition for cell culture and respective distributor

Medium	Composition	Distributor
Gibco™ DMEM, high glucose	Contains high glucose (4.5 g/l), no L-glutamin, no sodium pyruvate	Thermo Fisher Scientific
Gibco™ DMEM, high glucose, starvation medium	Gibco™ DMEM, high glucose, supplemented with 0.5 % FBS	Thermo Fisher Scientific, modified
Gibco™ DMEM, SHH inducing medium	Gibco™ DMEM, high glucose, supplemented with 0.5 % FBS and 100 nM SAG	Thermo Fisher Scientific, modified
Gibco™ Opti-MEM™	Reduced Serum Medium	Thermo Fisher Scientific

3.1.12 Cell culture reagents and media supplements

Table 13 – List of cell culture reagents, media supplements and respective distributor

Supplement / Reagent	Distributor
Biotin	Merck
cOmplete™, Mini Protease Inhibitor Cocktail	Roche
Compound C (Dorsomorphin)	Merck
Gibco ™ Blasticidin S HCl	Thermo Fisher Scientific
Gibco™ Sodium Pyruvate (100 mM)	Thermo Fisher Scientific
Gibco™ Trypsin-EDTA (0.05%)	Thermo Fisher Scientific
Hygromycin B	Thermo Fisher Scientific
Invitrogen™ Lipofectamine™ RNAiMAX Transfection Reagent	Thermo Fisher Scientific
Lipofectamine™ 2000 Transfection Reagent	Thermo Fisher Scientific
Prolong™ Gold antifade reagent	Invitrogen
SAG (Smoothened Agonist)	Merck
Tetracyclin	Merck
Torin	InvivoGen

3.1.13 Competent bacteria for cloning

Table 14 – List of competent bacteria used for cloning and respective distributor / origin

Bacterial strain		Distributor / Origin
E. coli DH5α		AG Posern, Martin-Luther-University Halle-Wittenberg
E. coli XL1 blue		Stratagene
One Shot™ TOP10 Chemically Competent E. coli		Thermo Fisher Scientific

3.1.14 Data bases and software

Table 15 – List of data bases, software and respective distributor

Software	Distributor
BLAST	NCBI
CLUSTAL W	EBI
ExPASY	SIB
Image Lab 6.1	BioRad
ImageJ	National Institutes of Health, USA
Microsoft Excel	Microsoft
SigmaPlot	SystatSoftware Inc.
ZEN 2.3 (blue edition)	Carl Zeiss AG

3.2 Methods

3.2.1 Molecular Biology

3.2.1.1 Agarose gel electrophoresis

Agarose gel electrophoresis is used to separate DNA fragments by size.

Agarose gels were prepared by dissolving 1 % agarose in 1 x Tris/borate/EDTA (TBE) by heating. Ethidium bromide (EtBr) was added to a concentration of 0.2 µg. DNA solutions were mixed with 6x Gel Loading Dye Purple (New England Biolabs) and applied to the gel. A DNA ladder mix containing DNA fragments of known length (GeneRuler 1kb, Thermo Fisher Scientific) was applied for size comparison. An electrical force between 100 and 120 V was applied to the gel for separation for at least 30 min. Finally, the gel was analysed under ultraviolet (UV) light by means of the intercalating dye EtBr. Images were taken using the GelDoc system (Intas) to document the separation pattern.

3.2.1.2 Polymerase Chain Reaction

Using the polymerase chain reaction (PCR), specific fragments of deoxyribonucleic acid (DNA) can be amplified. Those fragments are determined by established oligonucleotides (primers). Primers can also be used to insert recognition sites for restriction enzymes.

Table 16 – PCR programme and master mix Gid4-c-Myc

Component	V [µl]	PCR programme		
5xQ5 Reaction Buffer	5	Temperature [°C]	Time [min]	Cycles
dNTP mix	1	98	0:30	
Primer forward	2.5	98	0:30	35
Primer reverse	2.5	67	0:30	
Template	0.5 – 3.0 (100 ng)	72	0:30	
Q5 Polymerase	0.5	72	2:00	
ddH2O	ad. 50	4	hold	

Table 17 – PCR programme and master mix proximity labelling Gid4

Component	V [µl]	PCR programme		
5xQ5 Reaction Buffer	5	Temperature [°C]	Time [min]	Cycles
dNTP mix	1	98	0:30	
Primer forward	2.5	98	0:30	35
Primer reverse	2.5	67	0:30	
Template	0.5 – 3.0 (100 ng)	72	0:30	
Q5 Polymerase	0.5	72	2:00	
ddH2O	ad. 50	4	hold	

3.2.1.3 PCR product clean up

PCR product clean up was performed using the GeneJET PCR Purification kit (Thermo Fisher Scientific) according to the manufacturer's instructions. PCR products were eluted in 30 µl H_2O.

3.2.1.4 Restriction digest

After amplification and clean up of the fragments required for cloning (described in 3.2.1.2 and in 3.2.1.3) PCR products were subjected to restriction digest. For the cloning of Gid4 into the pCS2+ vector, EcoRI-HF and XhoI-HF (New England Biolabs) were used. The digest was performed according to the manufacturer's instructions. The entire PCR product (30 µl) and 3 µg of vector were used for the restriction digest. After the digest was completed, samples were loaded on an agarose gel to check for a complete restriction digest. In preparation for the ligation of the digested fragments and vector, all components were cleaned as described above in 3.2.1.3

3.2.1.5 Ligation of DNA fragments

Ligation of the previously digested PCR fragments and vector was performed using T4 ligase (New England Biolabs) according to the manufacturer's instructions. 100 ng of the linearised vector was used for the ligation reaction. The ligation reaction was incubated over night at 4°C. Afterwards, transformation of *E. coli* was performed as described in 3.2.1.8.

3.2.1.6 pENTR™ directional TOPO cloning

The pENTR™ directional TOPO cloning system allows the ligation of a blunt end PCR product into the pENTR™/D-TOPO vector. For the proximity labelling of Gid4, two different versions of the BirA-Gid4 construct were generated, one C-terminal and one N-terminal version. For the N-terminal version, the forward primer starts with the first base of the gene of interest and the reverse primer ends with the last base. For the C-terminal version, the forward primer is the same as for the N-terminal version but the reverse primer ends with the last base before the STOP codon, i.e., there is no STOP codon in the amplified DNA fragment. After the PCR (see 3.2.1.1) was performed, the DNA fragments were cleaned up (3.2.1.3) and cloned into the pENTR™/D-TOPO vector using the pENTR™/D-TOPO™ Cloning Kit, with One Shot™ TOP10 Chemically Competent *E. coli* (Thermo Fisher Scientific) according to the manufacturer's instructions.

3.2.1.7 Gateway Cloning

Expression vectors facilitating the inducible expression of BirA-Gid4 were constructed using the Gateway™ LR Clonase™ II Enzyme mix (Thermo Fisher Scientific). For this purpose, 300 ng of the prior constructed and purified pENTR™/D-TOPO-Gid4 plasmids were mixed with 300 ng of pcDNA5-pDEST-BirA-Flag-C-term or pcDNA5-pDEST-BirA-Flag-N-term vector. The subsequent procedure followed the manufacturer's instructions.

3.2.1.8 Transformation of E. coli with Plasmid DNA

Transformation of E. coli was performed either by heat shock transformation or by electroporation.

For heat shock transformation, 50 µl of chemically competent *E. coli* were gently mixed with the ligation product and incubated for 30 min on ice. After heat shocking the bacteria for 45 sec at 42°C the suspension was stored on ice for 2 min before adding 500 µl of pre-warmed antibiotic-free lysogeny broth (LB). The bacteria were grown for 1 h at 37°C in a thermo mixer while shaking. After that 100 µl of the bacterial suspension was plated onto LB-Agar-plates containing either kanamycin or ampicillin. Plates were incubated at 37°C over night.

For electroporation 50 µl of electrocompetent *E. coli* XL1 blue cells were gently mixed with the ligation product or up to 100 ng plasmid and incubated for 5 mins on ice. The mixture was then transferred to a precooled 1 mm electroporation cuvette. The cuvette was placed to an electroporator and pulsed once with 500 V for 8 msec. 500 µl pre-warmed antibiotic-free LB medium was added to the bacterial solution and the whole mixture was incubated for 1 h at 37°C in a thermo mixer while shaking. After that 100 µl of the bacterial suspension was plated onto LB-Agar-plates containing either Kanamycin or Ampicillin. Concentration Plates were incubated at 37°C over night.

3.2.1.8 DNA sequencing

Sequencing was performed by Microsynth SeqLab GmbH (Göttingen).

Sequences were analysed using CLUSTALW at EBI, BLAST at NCBI and ExPASy.

3.2.1.9 Plasmid purification

Plasmids were purified using either the ZymoPURE™ Plasmid Miniprep kit (Zymo Reseach) or the QIAprep Spin Midiprep Kit (Qiagen) according to the manufacturer's instructions. DNA was eluted using 50 µl H_2O for minipreps and 500 µl H_2O for midipreps.

3.2.1.10 RNA isolation from cultured cells

Ribonucleic acid (RNA) was isolated using the GeneJET RNA Purification Kit (Thermo Fisher Scientific) according to the manufacturer's instructions. RNA was eluted using 30 µl H_2O.

3.2.1.11 cDNA Synthesis

1,5 µg RNA was reverse transcribed into complementary DNA (cDNA) by using either the SuperScript® II Reverse Transcriptase Kit-System (Invitrogen) or by using HiScript II Q RT SuperMix for qPCR (Vazyme Biotech).

3.2.1.12 Quantitative PCR (qPCR)

Levels of messenger RNA (mRNA) for different genes of the SHH pathway in both NIH-3T3 wild type (WT) and NIH-3T3 Rmnd5a knock out (KO) cells were investigated using qPCR.

A 10 µl qPCR reaction set up contained 10 ng cDNA, 5 µl 1 × Maxima SYBR Green/ROX qPCR Master Mix (Thermo Fisher Scientific), 0.3 µM forward primer, and 0.3 µM reverse primer (**Table 5**). A qPCR run on Roche LightCycler 480 II consisted of an UDG pre-treatment for 2 min at 50°C, an initial hot start for 10 min at 95°C, followed by 40 cycles with a denaturation step of 15 s at 95°C and an annealing/extension step of 60 s at 60°C. Afterwards, a melt curve was recorded. Each measurement was repeated three times, and each sample was analysed in triplicate with hypoxanthine phosphoribosyltransferase (hprt) and 5-aminolevulinate synthase (alas) as an internal control. Results are presented as mean ± SEM. Relative expression was determined using the Abs Quant/2nd Derivative Max analysis method, given as Mean ± SEM, statistically analysed by t-test and measured by two-tailed P-value.

3.2.1.13 Determination of concentration of nucleic acids

Nucleic acid concentrations were determined by NanoDrop instrument measuring UV absorption at 260 nm (A_{260}) in 1,5 µl of a loaded sample. An absorption of 1 at 260 nm equals a concentration of 50 µg/ ml for dsDNA and 40 ng/ µl for ssRNA. A ratio of A_{260}/ A_{280} above 1.8 was indicative for pure DNA and ~2.0 for pure RNA preparation.

3.2.2 Cell culture techniques

3.2.2.1 Maintenance of NIH-3T3 cells

NIH-3T3 WT and NIH-3T3 Rmnd5a KO cells were cultivated in DMEM high glucose medium, supplemented with 1 mM sodium pyruvate and 10% FCS. The cell lines were maintained as adherent monolayers in 10 cm culturing dishes and incubated at 37°C in a humidified atmosphere with 5 % CO_2. Every 2 – 3 days the cultivation medium was exchanged and when the cells reached 80 – 90 % confluency, they were passaged at ratios from 1:10 to 1:15 into new culturing dishes. For passaging, cells were washed with pre-warmed phosphate buffered saline (PBS) and detached using Trypsine-EDTA. The reaction was stopped by addition of DMEM high glucose and the cells were seeded into new culturing dishes or plates, depending on the experimental setup.

3.2.2.2 Maintenance of HEK293 cells

HEK293T and HEK293 FlpIn TREx cells were cultivated in DMEM high glucose medium, supplemented with sodium pyruvate and 10% FCS The cell lines were maintained as adherent monolayers in 10 cm culturing dishes and incubated at 37°C in a humidified atmosphere with 5 % CO_2. Every 2 -3 days the cell medium was exchanged and when the cells reached 80 –

90 % confluency, they were passaged at ratios from 1:10 to 1:15 into new culturing dishes. For passaging, cells were washed with pre-warmed phosphate buffered saline (PBS) and detached using Trypsine-EDTA. The reaction was stopped by addition of DMEM high glucose and the cells were seeded into new culturing dishes or plates, depending on the experimental setup. The generated cells lines HEK293 FlpIn TREx BirA-Gid4 C-terminal and HEK293 FlpIn TREx BirA-Gid4 N-terminal were cultivated in DMEM high glucose medium supplemented with sodium pyruvate, 10 % FCS, 15 µg/ml Blasticidin and 100 µg/ml HygromycinB. Otherwise, they were treated as HEK293 FlpIn TREx cells.

3.2.2.3 Cell counting
Cells were counted prior to seeding using a CASY® TT Cell Counter (OMNI Life Science) together with CASY® ton buffer. Before counting, cells were centrifuged at 500 x g for 3 mins, the supernatant was aspirated and cells were resuspended in 5 ml pre-warmed DMEM. 100 µl of the cell solution was diluted with 9900 µl CASY®ton buffer and the number of vital cells in the cell solution was determined.

3.2.2.4 Transient transfection of NIH-3T3 / HEK293 cells
Transient transfection of HEK293 cells was performed using Lipofectamine 2000™. HEK293 cells were seeded with $1,5 \times 10^5$ cells/ml in different plates/dishes, depending on the experimental setup. Per ml culturing medium 1 µg plasmid DNA was diluted in 50 µl OptiMEM and mixed well. For every 1 µg plasmid DNA 3 µl of Lipofectamine 2000™ were mixed with 50 µl OptiMEM. After that, the diluted DNA and the diluted Lipofectamine 2000™ were combined, mixed and incubated for 5 min at room temperature (rt). Meanwhile, the cultivation medium from 70 – 80% confluent cells were removed, cells were washed with PBS and fresh cultivation medium was added. Transfection complexes were then added in a drop wise manner. Cells were incubated for 24 h and further analysed.

3.2.2.5 Stable transfection of HEK293 FlpIn TREx cells
Stable transfection of HEK293 FlpIn TREx cells was performed as described in 3.2.2.4. Cells were transfected with either pcDNA5-pDEST-BirA-Flag-C-term or pcDNA5-pDEST-BirA-Flag-N-term. 24 h after transfection the culturing medium was aspirated and cells were washed with PBS. Fresh culturing medium containing 15 µg/ml Blasticidin and 100 µg/ml HygromycinB was added to select for cells that have incorporated the plasmid. Cells were monitored by microscopy until after a decline in cell number and vitality, parameters recovered and were equal to non- transfected HEK293 FlpIn TREx cells. Once stable cell lines were established, cells were prepared for long term storage as described in 3.2.2.8.

3.2.2.6 Starvation and induction of ciliogenesis in NIH-3T3 cells

To induce ciliogenesis in NIH-3T3 WT and NIH-3T3 Rmnd5a KO cells, cells at 70 – 80 % confluency were washed three times with pre-warmed PBS and subsequently incubated with starvation medium, i.e., DMEM high glucose supplemented with 0.5 % FCS. Cells were then incubated for 24 h.

3.2.2.7 Induction of SHH signalling in NIH-3T3 cells

To induce SHH signalling in NIH-3T3 WT and NIH-3T3 Rmnd5a KO cells, cells at 70 – 80 % confluency were washed three times with pre-warmed PBS and subsequently incubated with SHH-inducing medium, i.e., DMEM high glucose supplemented with 0,5 % FCS and 100 nM Smoothened Agonist (SAG). Cells were incubated for 24 h.

3.2.2.8 Cryopreservation of HEK293 FlpIn TREx cells

For long term storage, cells were grown in a monolayer 75 cm^2 culture flask until a confluency between 80 – 90% was reached. Cells were then washed with pre-warmed PBS, trypsinised and resuspended in cultivation medium. After that, cells were centrifuged for 3 mins at 500 x g and the supernatant was removed. Cells were then resuspended in 6 ml freeze medium, consisting of 90 % high glucose DMEM supplemented with sodium pyruvate and 10 % FCS and 10 % DMSO. 1 ml each was transferred to cryo vials and the tubes were placed in a Mr. Frosty™ Freezing Container (Thermo Fisher Scientific). The freezing container was placed in a -80°C freezer overnight and subsequently, the tubes were moved to a -150°C freezer for long term storage.

3.2.3 Protein biochemistry

3.2.3.1 Generation of whole cell lysates

Cell lines were grown either in 10 cm culturing dishes or in 6-well plates, depending on the experimental setup. For harvest, plates or dishes were placed on ice and the culturing medium was removed. Cells were washed with ice cold PBS and Lysis buffer was added, 60 µl per well for the 6 well plate and 500 µl for 10 cm dishes. Cells were scraped off using a cell scraper and the lysate was transferred in a pre-cooled tube and incubated on ice for 30 mins. After that, cell lysates were centrifuged for 10 mins at 13 000 x g and 4°C. After centrifugation, the supernatant was removed, the protein concentration was determined and the samples were mixed with Laemmi buffer.

3.2.3.2 Determination of protein concentration in whole cell lysates

To determine the protein concentration in whole cell lysates, a bicinchoninic acid assay (BCA, Thermo Fisher Scientific) was performed, according to the manufacturer's instructions. The

colorimetric readout was performed using the ClarioStar (BMG Labtech) microplate reader. Protein concentrations were calculated based on the generated standard curve using Microsoft Excel.

3.2.3.3 SDS-PAGE

With the use of sodium dodecyl sulphate–polyacrylamide gel electrophoresis (SDS-PAGE) denatured proteins can be separated according to their molecular mass. For separation, precast 10% Novex Tris-Glycine Gels were used (dimensions 8 cm x 8 cm,1.0 mm thick). Samples were diluted 1:5 in 5 x Laemmli buffer, heated for 5 mins at 95°C and the indicated amounts of sample were loaded on the gel. As a marker for protein mass, PageRuler™ Prestained Protein Ladder or PageRuler™ Plus Prestained Protein Ladder (Thermo Fisher Scientific) were used. Electrophoresis was run at 120 – 160 V for up to 90 min in 1x SDS running buffer.

3.2.3.4 Western blotting

To transfer separated proteins from the SDS PA gels to PVDF membranes, a wet blotting method was used. PVDF membranes were activated for 5 mins in 100% methanol at rt. The blotting was conducted in blotting buffer (**Table 3**) at 200 mA for 1h 10 min. After the transfer was complete, membranes were blocked in blocking solution (**Table 3**) for 30 min at rt. Membranes were then washed three times for 5 min in Tris buffered saline Tween20 (TBS-T). After washing membranes were incubated with respective primary antibodies (Table 2.5) and indicated dilutions overnight at 4 °C. On the next day, membranes were washed three times for 5 min in TBS-T followed by incubation with a horseradish peroxidase (HRP)-coupled secondary antibody for 1 h at rt. Next, membranes were washed three times for 5 mins in TBS-T. Detection was performed using SuperSignal™ West Femto Maximum Sensitivity Substrate (Thermo Fisher Scientific) and images were obtained using a ChemiDoc MP Imaging System (Bio-Rad Laboratories). Images were saved as 300 dpi tiff images. Densitometry was performed with the ImageJ software using the rectangular area selection tool. Background signals were subtracted, and relative protein levels were compared with the loading control (Glyceraldehyde-3-phosphate dehydrogenase (GAPDH)).

3.2.3.5 Immunoprecipitation

Immunoprecipitation of Myc-tagged proteins was performed using the ChromoTek Myc-Trap® system (ChromoTek) according to the manufacturer's instructions. Briefly, HEK293T cells were seeded into 10 cm culturing dishes with a density of 1 x 10^5 cells/ml. After 24 h, cells were transfected with either pCS2+-Gid4-c-Myc or pCS2+ vector control (VC) as described in 3.2.2.4. After incubation for 24h, whole cell lysates were generated using 200 µl Lysis buffer as described in 3.2.3.1. Cell lysates were mixed with 300 µl Dilution buffer and 50 µl of the

mixture was removed for western blot analysis. Next, the diluted lysate was added to equilibrated beads and incubated for 1 h at 4°C using an end-over-end rotator. After incubation, beads were washed once with 500 µl Wash Buffer I, once with 500 µl Wash Buffer II and once again with 500 µl Wash Buffer I. Lastly, bound proteins were eluted using Peptide elution buffer, containing 0.1 mg/ml Myc peptide in Dilution buffer. After elution, samples were stored at -80°C and sent to Alessandro Ori's lab in Jena for mass spectrometry analyses.

3.2.3.6 Subcellular Protein Fractionation

Cytosolic extracts were obtained using the Subcellular Protein Fractionation Kit for Cultured Cells (Thermo Fisher Scientific) according to the manufacturer's instructions. Briefly, cells were harvested and washed with ice-cold PBS. The cell pellets were suspended in ice-cold CEB buffer, incubated for 10 min at 4°C and centrifuged for 5 minutes at 500 x g. The supernatant contained the cytoplasmic extract (CE). The CE was then mixed with 5x Laemmli buffer and incubated for 5 min at 95°C.

3.2.3.7 Immunofluorescence

For immunofluorescence analysis, NIH-3T3 WT and NIH-3T3 Rmnd5a KO cells were seeded on coverslips in 12-well plates and grown for 24 h under standard conditions. 0.3×10^5 cells were seeded per well. Depending on the experimental setup, cells were either fixed and permeabilized after 24 h or subjected to induction of ciliogenesis (see 3.2.2.6) or induction of SHH signalling pathway (see 3.2.2.7). After incubation, cells were fixed and permeabilized by either one of the two following methods, depending on the compatibility of the primary antibodies.

(a) Cells were washed one with PBS prior to fixation in 4 % paraformaldehyde (PFA) in PBS for 15 min at rt. Next, cells were permeabilized by adding PBS containing 0.2 % (v/v) Triton X-100 for 10 min at rt.

(b) Cells were washed once with PBS and subsequently fixed in -20°C cold methanol for 5 min. Afterwards, cells were washed three times for 5 min in PBS.

After fixation cells were blocked for 30 min at rt in blocking solution (Table 3.2). Next, coverslips were incubated with indicated primary antibodies at rt for 2 h. Primary antibodies were diluted 1:100 in blocking solution. Afterwards, coverslips were washed three times for 10 min in PBS and then fluorescently labelled secondary antibodies were diluted 1:250 in blocking solution, 4′,6-diamidino-2-phenylindole (DAPI) was added and the solution was applied for 1 h at rt. After incubation, coverslips were washed three times for 10 min in PBS, then dipped into water to remove remaining salts and once into ethanol for dehydration. Prolong™ Gold antifade reagent (Thermo Fisher Scientific) was used to fix the coverslip onto a microscope glass slide. Images were taken with Zeiss Axio Observer 7 using ApoTome2.

Intensity of fluorescence was determined using ImageJ software using the freeform selection tool. Background signals were subtracted, and relative fluorescence levels were compared with the fluorescence levels of n-acetylated tubulin for primary cilia and DAPI for nuclei. The corrected total cell fluorescence (CTCF) was calculated using the following formula: CTCF = Integrated Density – (Area of selected cell x Mean fluorescence of background readings). The CTFC [primary cilium/nucleus] was then divided by the CTFC [n-acetylated tubulin/DAPI] to quantify the level of fluorescence intensity.

3.2.3.8 BioID for proximity-dependent biotin identification

To identify novel interaction partners of Gid4 in mammalian cells, BioID for proximity-dependent biotin identification was used as described in [77]. Briefly, the gene coding for Gid4 was fused to the gene coding for BirA, an *Escherichia coli* (*E. coli*) biotin protein ligase as described in 3.2.1.6 and 3.2.1.7. Two different variants were generated, a C-terminal fusion variant and an N-terminal fusion variant. After cloning, stable cell lines for the expression of both fusion variants were generated as described in 3.2.2.5. Expression of the fusion protein was induced by adding 1 µg/ml tetracycline to the cells and incubating for 48 h. Next, 50 µM biotin was added and cells were incubated for 24 hours. After that, medium was removed and cells were washed with PBS and trypsinised. Cells were then pelleted by centrifugation at 500 x g for 3 min. Afterwards, cell pellets were washed three times with ice-cold PBS. After every addition of PBS, cells were centrifuged for 3 min at 500 x g and 4°C. When the last wash step was performed, the PBS was aspirated completely and cell pellets were snap frozen in liquid nitrogen and stored at -20°C. All subsequent steps including mass spectrometry were performed at Dr Alessandro Ori's lab at the Fritz Lipman Institute in Jena.

For each experiment, 2 x 10^6 snap-frozen cells were used. Pellets were thawed on ice and resuspended in 4.75 ml *lysis buffer* (50mM Tris pH 7.5; 150mM; 1mM EDTA; 1mM EGTA; 1% (v/v) Triton X-100, 1 mg/ml aprotinin; 0.5 mg/ml leupeptin; 250U Turbonuclease (MoBiTec GmbH, 0,1% (w/v) SDS). The samples were incubated for 1 in a rotator at 15rpm and 4°C to aid the lysis. Next, samples were briefly sonicated (Bioruptor Plus) for 5 cycles (30 s ON/30 s OFF) at high setting and subsequently centrifuged for 30 min at 20,817 g and 4 °C to remove any debris. Streptavidin coated Sepharose beads (Merck) were previously acetylated by two successive treatments with 10mM Sulfo-NHS-Acetate (Thermo Fisher Scientific) for 30 min at rt. To quench the reaction, the beads were first incubated with 1M Tris pH 7,5 (1:10 v/v), next washed with 1xPBS and then centrifuged at 2,000 g for 1 min at rt. The beads were washed three times in total.

In the next step, the cleared sample lysates were transferred to new tubes and 50µl of acetylated beads were added to this. The mixture was incubated for 3 h in the rotator at 15rpm and 4°C, followed by centrifugation at 2000 x g for 5 min at 4°C. From each sample, 4.5 ml of the supernatant was removed and the remaining sample with the beads at the bottom was

transferred to a Pierce Spin Column Snap Cap column (Thermo Fisher Scientific, 69725). Additionally, the tubes were rinsed with lysis buffer and this was added to the Pierce Spin Column Snap Cap column as well. Next, the beads were first washed on the column with lysis buffer and then washed three times with freshly prepared 50 mM Amonium Bicarboante (AmBic), pH 8.3. Afterwards, the bottom of the column was closed with a plug and the beads were transferred to fresh 2 ml tubes, using 3 x 300µl 50 mM AmBic, pH 8.3. The samples were then centrifuged for 5 min at 2,000 g and 4°C, so that the content of each tube could be removed until around 200 µl of the liquid (including the bead) remained at the bottom. Next, 1 µg of LysC (Wako pure chemical Industries) was added and incubated at 37°C for 16 h while shaking at 500 rpm.

After that, the samples were centrifuged for 5 min at 2,000 g and rt and the content of the tubes were transferred to Pierce Spin Column Snap Cap columns (Thermo Fisher Scientific). To elute the digested peptides, 150 µl of freshly made 50 mM ammonium bicarbonate was added to the columns twice. To remove any biotinylated peptides still bound to the beads, 150 µl of 80% ACN and 20% TFA was added, briefly mixed, and eluted. This step was performed twice and the elutions were merged. To the AmBic elutions 0.5 µg of trypsin was added and digest continued for additional 3h at 500rpm and 37°C. Digested AmBic elutions were then dried down in a vacuum concentrator and resuspended in 200 µl solvent A (0.05 % (v/v) formic acid prepared with milliQ (Merck, CDU FBI001)). This was followed by sonication in a Bioruptor Plus (5 cycles with 1 min ON and 30 s OFF with high intensity at 20 °C) and after that samples were acidified with 10 % (v/v) trifluoracetic acid (Biosolve) ensuring pH <3.

ACN elutions were dried down in a vacuum concentrator, not to completeness but until roughly 50 µl were left. Next, 50µl of 200 mM HEPES pH 8.0 was added and pH of the samples were checked to ensure required pH 7-9. Following this, 0.5 µg of trypsin was added to ACN elutions and digest continued for additional 3h at 500 rpm and 37°C. Samples were acidified with 10 % (v/v) trifluoracetic acid (Biosolve) ensuring pH <3.

After this, both elutions were treated in the same way and were desalted using Macro Spin Column C18 columns, dried down, dissolved in solution containing 5 % (v/v) acetonitrile (Biosolve), and 0.1 % (v/v) formic acid and spiked with iRT kit peptides (Biognosys, Zurich, Switzerland) prior to analysis by LC-MS/MS.

LC-MS/MS based on Data Independent Acquisition (DIA)
Peptides (approx. 1 µg) were separated using a nanoAcquity UPLC M-Class system (Waters Milford, USA) with a trapping (nanoAcquity Symmetry C18, 5 µm, 180 µm x 20 mm) and an analytical column (nanoAcquity BEH C18, 1.7 µm, 75 µm x 250 mm). The outlet of the analytical column was coupled directly to a Q-exactive HF-X (Thermo Fisher, Waltham, MA, USA) using the Proxeon nanospray source. Solvent A was water, 0.1% formic acid and solvent B was acetonitrile, 0.1 % formic acid. The samples (approx. 1 µg) were loaded onto the

trapping column with a constant flow of solvent A at 5 µl/min. Trapping time was 6 min. Peptides were eluted via the analytical column with a constant flow of 0.3 µl/min. During the elution step, the percentage of solvent B increased in a non-linear fashion from 0 % to 40 % in 90 min. Total runtime was 115 min, including clean-up and column re-equilibration. The peptides were introduced into the MS via a Pico-Tip Emitter 360 µm OD x 20 µm ID; 10 µm tip and a spray voltage of 2.2 kV was applied. The capillary temperature was set at 300 °C. The radio frequency (RF) ion funnel was set to 40 %. The conditions were as follows: Full scan MS spectra with mass range 350-1650 m/z were acquired in profile mode in the Orbitrap with resolution of 120,000 FWHM. The default charge state was set to 3+. The filling time was set at maximum of 60 ms with limitation of 3 x 106 ions. DIA scans were acquired with 34 mass window segments of differing widths across the MS1 mass range. HCD fragmentation (stepped normalized collision energy; 25.5, 27, 30 %) was applied and MS/MS spectra were acquired with a resolution of 30,000 FWHM with a fixed first mass of 200 m/z after accumulation of 3 x 106 ions or after filling time of 40 ms (whichever occurred first). Data were acquired in profile mode. For data acquisition and processing of the raw data Xcalibur 4.0 and Tune version 2.9 (both Thermo Fisher) were employed.

Data processing

DIA runs were analysed in directDIA mode using Spectronaut Pulsar (v10/11, Biognosys, Zurich, Switzerland). The data were searched against species specific protein databases (Uniprot Homo sapiens, reviewed entry only, release 2016_01) with a list of common contaminants appended. The data were searched with the following modifications: carbamidomethyl (C) as fixed modification, and oxidation (M), acetyl (protein N-term) and biotin (K) as variable modifications. A maximum of 3 missed cleavages was allowed. The search was set to 1 % false discovery rate (FDR) at both protein and peptide levels. DIA data were then uploaded and searched against this spectral library using Spectronaut Professional (v.11) and default settings. Relative quantification was performed in Spectronaut for each pairwise comparison using the replicate samples from each condition using default settings, except: Major Group Quantity = Sum peptide quantity; Major Group Top N = OFF; Minor Group Quantity = Sum precursor quantity; Minor Group Top N = OFF; Data Filtering = Q value sparse; Normalization Strategy = Local normalization; Row Selection = Q value complete. The data (candidate tables) and protein quantity data reports were then exported and further data analyses and visualization were performed with R (v.3.6.3) and R studio server (v. 1.2.5042) using in-house pipelines and scripts.

3.2.3.8 Statistical analysis

Statistic values were calculated using a t-test analysis or chi-square test with the GraphPad Prism 9 software as described. Data include values from at least three replicate experiments.

4 Results

4.1 Shh signalling

A work by Boldt et al. [76] placed the GID complex at the basal body of the primary cilium using a proteomics approach. This led to the question if the GID complex is a functional part of the primary cilium and if it is, what roles does it play. To investigate these questions, experiments were performed comparing two cell lines, NIH-3T3 WT and NIH-3T3 Rmnd5a KO. The KO cell line was generated previously by CRISPR-Cas9 mediated knock out of the gene for Rmnd5a [75]. Rmnd5a carries a RING domain and is thus essential for the E3 ligase activity of the GID complex (described in detail above). Loss of this subunit leads to inactivity of the GID complex [67].

The ciliary membrane is rich in receptors and thus the cilium plays an important role in various cell signalling pathways [2], one of these being the Shh signalling pathway (discussed in detail above). Rohatgi et al. showed that defects in the primary cilium correlate with aberrant Shh signalling [78] which means that the Shh pathway is a well suited tool to investigate potential functions of the GID complex at the primary cilia. To activate the Shh pathway in cell culture, Smoothed Agonist (SAG) can be used.

To investigate if the GID complex plays a role in Shh signalling the relative mRNA levels of Gli1 and Ptch1 were determined, two genes that are regulated by Shh signalling. For this, NIH-3T3 WT and Rmnd5a KO cells were seeded in 6-well plates and serum starved for 24 h using starvation medium (see 3.2.2.6) to induce ciliogenesis. Additionally, to one well of each cell line 100 nM SAG was added to activate Shh signalling. Next, RNA was isolated and purified using the GeneJET RNA Purification Kit (Thermo Fisher Scientific) according to the manufacturer's instructions. After that, cDNA was generated using the SuperScript® II Reverse Transcriptase kit system (Invitrogen) according to the manufacturer's instructions (see 3.2.1.11). For each qPCR reaction, a 10 µl reaction set up containing 10 ng cDNA, 5 µl 1 × Maxima SYBR Green/ROX qPCR Master Mix (Thermo Fisher Scientific), 0.3 µM forward primer, and 0.3 µM reverse primer (see Table 3.4 and 3.2.1.12) were combined and mixed carefully. Every sample was analysed in triplicates. The qPCR runs were performed using a Roche LightCycler 480 II Each run consisted of an UDG pre-treatment for 2 min at 50°C, an initial hot start for 10 min at 95°C, followed by 40 cycles with a denaturation step of 15 s at 95°C and an annealing/extension step of 60 s at 60°C. Afterwards, a melt curve was recorded for every sample. Each measurement was repeated three times, and each sample was analysed in triplicate with hypoxanthine phosphoribosyltransferase (hprt) and 5-aminolevulinate synthase (alas) as an internal control. Relative levels of gene expression were determined using the Abs Quant/2nd Derivative Max analysis method and statistically analysed by t-test and measured by two-tailed P-value. The results are given as Mean ± SEM. **Figure 8** shows the relative mRNA levels of *Gli1* and *Ptch1*.
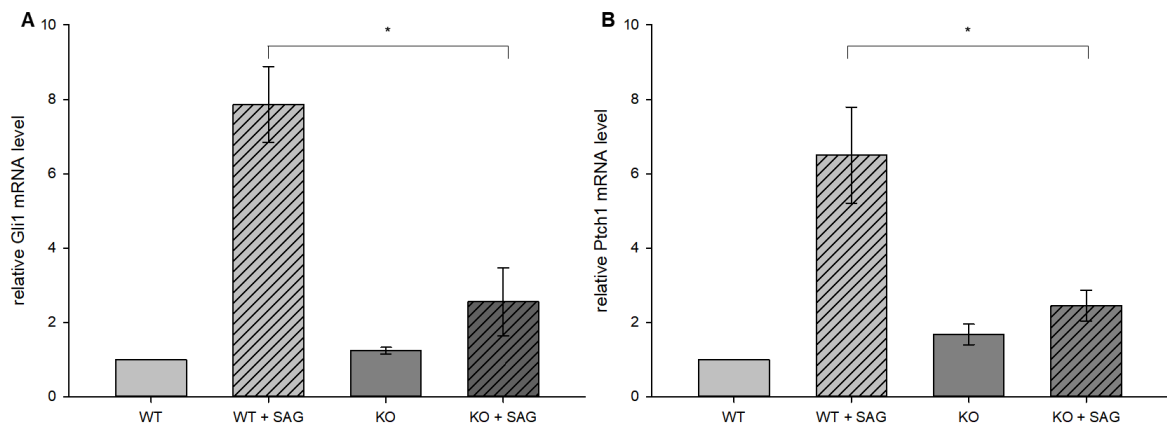
Figure 8 Rmnd5a KO cells show significantly lower relative mRNA levels of two Shh signalling markers.
Results from qPCR experiments show that the relative amount of *Gli1* (**A**) and *Ptch1* (**B**) mRNA is increased upon the addition of SAG to the growth medium in both NIH-3T3 WT and Rmnd5a KO cells. The relative mRNA levels of both markers are significantly lower in Rmnd5a KO cells compared to WT cells. Cells were grown in either starvation or Shh inducing medium and RNA was isolated using the GeneJET RNA Purification Kit (Thermo Fisher Scientific). qPCR was performed as described above. Unpaired t-test n = 3, *, $P < 0.05$.

The results of the qPCR analysis show an increase in the relative amounts of both *Gli1* and Ptch1 in both cell lines after the induction of the Shh signalling pathway with SAG. However, Rmnd5a KO cell lines show a significantly lower upregulation of *Gli1* and *Ptch1* after the addition of SAG. These results indicate that the GID complex might play an important role at the primary cilium and might be involved in Shh signalling.

The question which arose from these results was if the formation of primary cilia in Rmnd5a KO cells were affected. For this, NIH-3T3 WT and Rmnd5a KO cells were grown on coverslips and incubated with starvation medium for 24 h to induce ciliogenesis. Additionally, to one half of the coverslips of each cell line 100 nM SAG was added to activate Shh signalling. Cells were fixed using 4 % PFA and incubated first with antibodies against acetylated tubulin (ac-tubulin, 1:200, Sigma-Aldrich, mouse) and next with AlexaFluor™ 546 goat anti mouse IgG (H+L) (1:250, Invitrogen, red) and DAPI (300 nM, blue) to make the axoneme and the nucleus visible. Images of 30 ciliated cells per condition and cell line were taken, using a Zeiss Axio Observer 7 with ApoTome.2. Relative cilia length was determined using ImageJ software. No significant differences in cilia length could be observed between the cell lines or the conditions analysed (**Figure 9**).
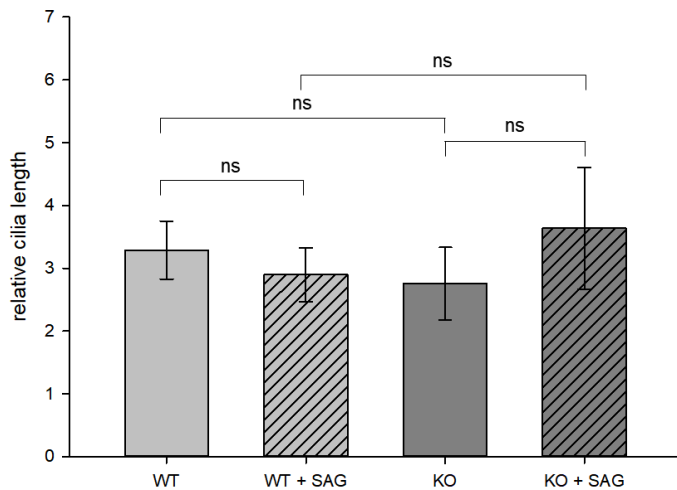
Figure 9 Relative cilia length is not significantly influenced by Rmnd5a knock out or induction of Shh signalling. NIH-3T3 and NIH-3T3 Rmnd5a KO cells were grown on coverslips with starvation medium, serum to induce the formation of primary cilia and Shh signalling was induced by adding 100 nM SAG. Cells were then fixed with 4 % PFA and stained with anti ac-tubulin antibodies to visualise the cilia. Images of 30 cilia for each condition were taken using a Zeiss Axio Observer 7 with ApoTome2. Relative cilia length was measured using ImageJ Software. Unpaired t-test n = 30 (WT), n = 30 (KO), ns = not significant.

Next, the number of ciliated cells for both cell lines were determined. For this, the same samples as for the measurement of relative ciliary length was used. For each cell lines, 500 cells were looked at and ciliated and non-ciliated cells were counted. For 67.3 % of scrutinised NIH-3T3 WT cells a primary cilium could be observed. For Rmnd5a KO cells this number was only at 42.0 %. The lower number of ciliated cells in Rmnd5a KO cells could be one of the reasons for the lowered expression of the Shh signalling markers *Gli1* and *Ptch1*.

To investigate the connection between the SHH signalling pathway and the GID complex further, a series of IF were performed. The aim was to look for differences in the localisation of different components of the Shh signalling pathway in the two cell lines, NIH-3T3 WT and NIH-3T3 Rmnd5a KO. IF were performed as described above (see 3.2.3.7). Both WT and KO cells were seeded on coverslips and incubated for 24 h with starvation medium (3.2.2.6) to induce ciliogenesis. Cells were fixed with 4 % PFA and stained with DAPI and antibodies against various components of the Shh signalling pathway, listed in **Table 18** and ac-tubulin. Images were taken with a Zeiss Axio Observer 7 with ApoTome.2.

Table 18 Antibodies used to investigate the localisation of various components of the Shh signalling pathway.

Primary antibody	Secondary antibody	Colour
Anti GLI1, 1:200, Santa Cruz Biotechnology, mouse	AlexaFluor™ 546 goat anti mouse IgG (H+L), 1:250, Invitrogen	Red
Anti GLI2, 1:200, Santa Cruz Biotechnology, mouse	AlexaFluor™ 546 goat anti mouse IgG (H+L), 1:250, Invitrogen	Red
Anti GLI3. 1:100, R&D Systems, rabbit	AlexaFluor™ 488 donkey anti rabbit IgG (H+L), 1:250, Invitrogen	Green
Anti PTCH1, 1:100, Santa Crus Biotechnology, mouse	AlexaFluor™ 546 goat anti mouse IgG (H+L), 1:250, Invitrogen	Red
Anti SUFU, 1:100. Santa Cruz Biotechnologies, mouse	AlexaFluor™ 546 goat anti mouse IgG (H+L), 1:250, Invitrogen	Red
Anti ac-tubulin, 1:200, Cell Signaling Technologies, rabbit	AlexaFluor™ 488 donkey anti rabbit IgG (H+L), 1:250, Invitrogen	Green
Anti ac-tubulin, 1:200, Sigma-Aldrich, mouse	AlexaFluor™ 546 goat anti mouse IgG (H+L), 1:250, Invitrogen	Red

The first component under investigation was GLI1. Representative images are shown in in **Figure 10 A**. It can be observed that both WT and KO cells show a co-localization of GLI1 and ac-tubulin (**Figure 10 A**). This indicates that GLI1 localises to the axoneme in both cell types. Also, GLI1 signals could be detected in the nuclei of both cell lines. Experiments previously performed (Figure 4.1) showed reduced mRNA levels for *Gli1* in KO cells so the relative GLI1 fluorescence was quantified for both the axoneme and the nucleus and compared between WT and Rmnd5a KO cells as described above (see 3.2.3.7). Using ImageJ, relative fluorescence levels of GLI1 were compared with the fluorescence levels of n-acetylated tubulin for primary cilia and DAPI for nuclei. Figure 8. shows that GLI1 fluorescence is significantly reduced in nuclei in KO cells (**C**) but not changed in primary cilia (**B**). For quantification, 30 cells of each cell type were analysed and results are given as Mean ± SEM.
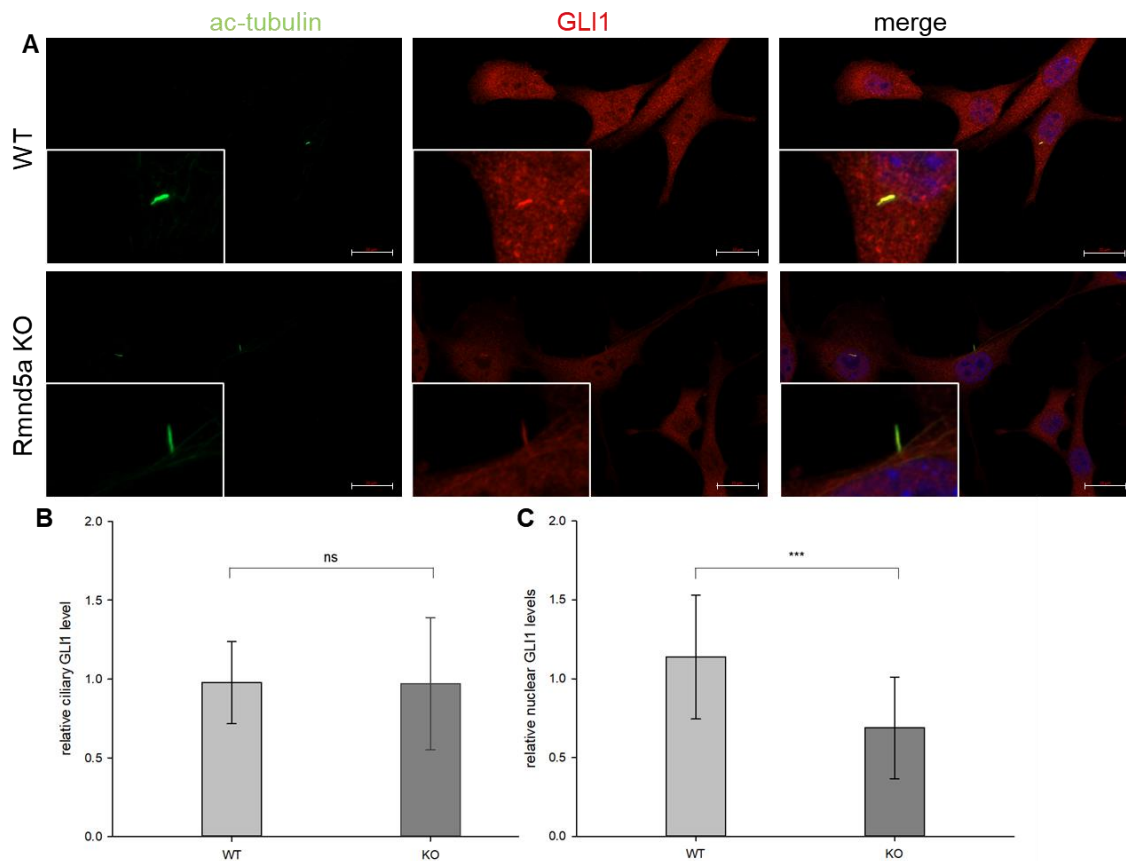
Figure 10 GLI1 localises to the primary cilium in both WT and Rmnd5a KO cells. A: GLI1 shows no obvious differences in localisation between WT and Rmnd5a KO cells. In both cases GLI1 can be detected in both the primary cilium and the nucleus. Cells were seeded on coverslips, incubated for 24 h with starvation medium and then fixed using 4 % PFA. Staining was performed using DAPI (blue) and antibodies against GLI1 (red) and ac-tubulin (green). Representative images are shown. White bars indicate a size of 20 μm. To quantify the relative GLI1 levels in **B** the primary cilia and **C** the nucleus the intensity of GLI1 fluorescence was determined using ImageJ software. The area of interest was selected using the freeform selection tool, background signals were subtracted, and relative fluorescence levels were compared with the fluorescence levels of n-acetylated tubulin for primary cilia and DAPI for nuclei. Unpaired t-test n = 30 (WT), n = 30 (KO). ***, P< 0.001, ns = not significant.

Next, the localisation and fluorescence of GLI2 was investigated. Both IF and fluorescence quantification were performed as described for GLI1 with the addition of a second growth condition for each cell type. For this, cells were grown in Shh signalling inducing medium, containing 100 nM SAG (Table 3.12) for 24h and fixed with 4 % PFA (strv+SAG). Representative images shown in **Figure 11** show that GLI2 locates to the primary cilium under all investigated conditions.
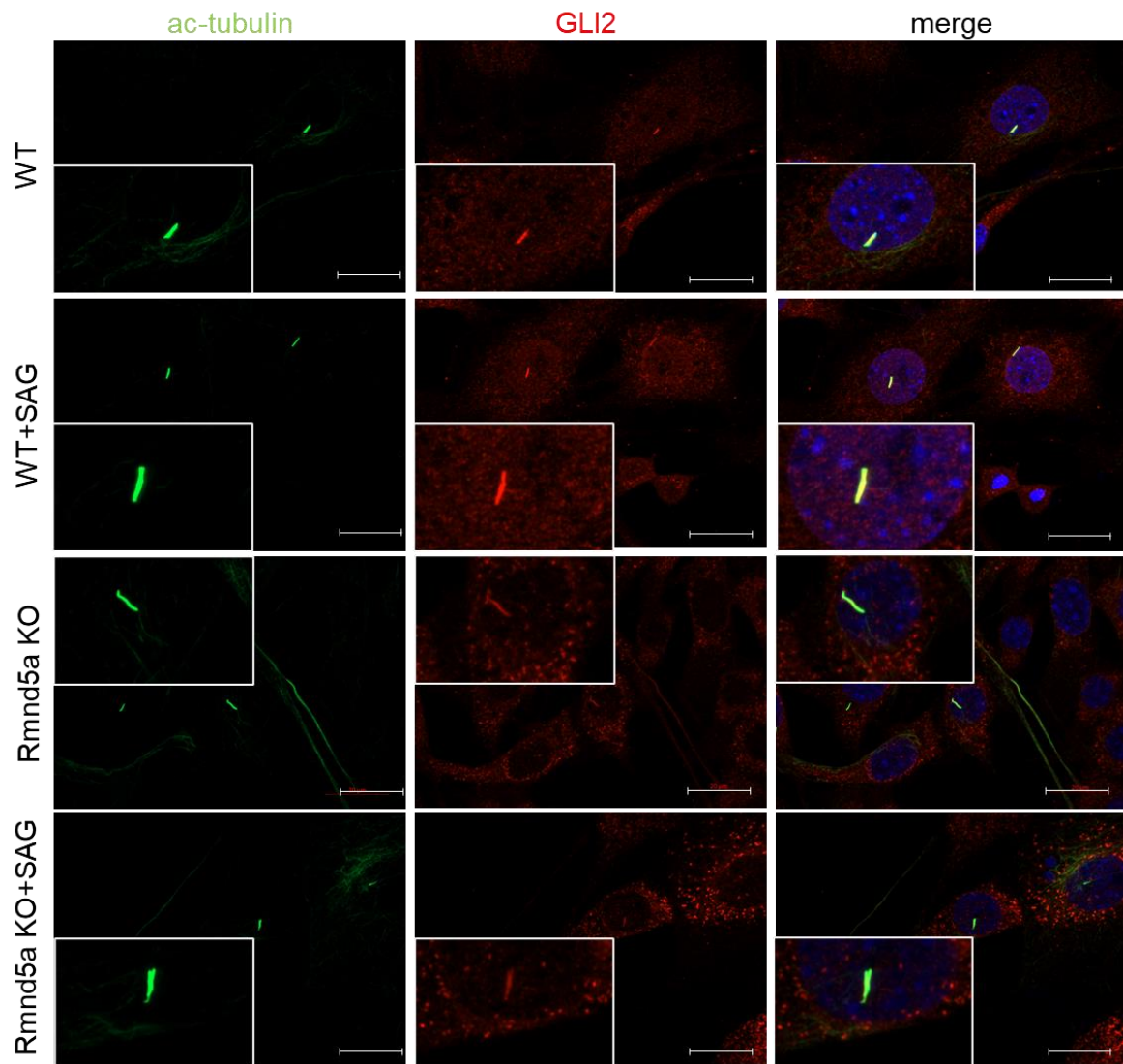
Figure 11 Detectable amounts of GLI2 appear to be lower in Rmnd5a KO cells than in WT cells. Shh signalling pathway component GLI2 localises to both the primary cilium and the nucleus in WT and Rmnd5a KO cells. The detectable amounts of GLI2 fluorescence appear to be lower in KO cells than in WT cells. Cells were seeded on coverslips, incubated for 24 h with starvation (strv) medium or Shh inducing medium (strv+SAG) and then fixed using 4 % PFA. Staining was performed using DAPI (blue) and antibodies against GLI2 (red) and ac-tubulin (green). Representative images are shown. White bars indicate a size of 20 µm.

However, quantification of the relative fluorescence showed that the amount of GLI2 fluorescence was significantly lowered in Rmnd5a KO cells in the primary cilium compared to WT cells (**Figure 12 A**). This could be observed for both the non-Shh induced cells (strv) and Shh induced cells (strv+SAG). **Figure 12 B** shows the relative nuclear GLI2 levels. Similar to the axonemal levels, GLI2 fluorescence was significantly reduced in Rmnd5a KO cells under both tested conditions. For quantification, 30 cells of each cell type were analysed and results are given as Mean ± SEM.
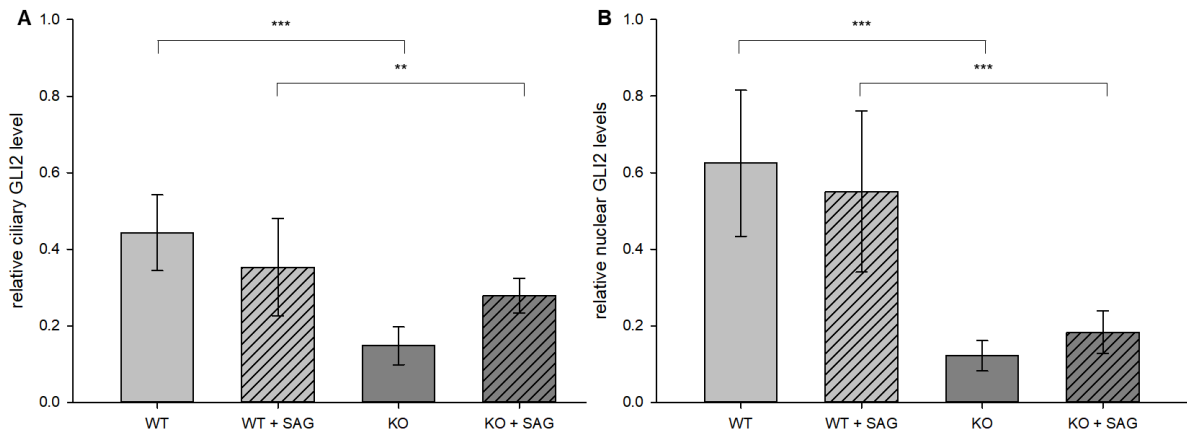
Figure 12 Relative GLI2 levels are significantly lowered in Rmnd5a KO cells compared to WT cells. Quantification of relative GLI2 levels in WT and Rmnd5a cells showed a significant decrease of GLI2 levels in both the primary cilia (**A**) and the nucleus (**B**) in Rmnd5a KO cells for both conditions, i.e., strv and strv+SAG. To quantify the relative GLI2 levels, ImageJ software was used. The area of interest was selected using the freeform selection tool, background signals were subtracted, and relative fluorescence levels were compared with the fluorescence levels of n-acetylated tubulin for primary cilia and DAPI for nuclei. Unpaired t-test n = 30 (WT), n = 30 (KO). *** = P< 0.001, ** = P<0.01.

These results indicate an overall lower detectable amount of GLI2 in Rmnd5a KO cells compared to WT cells. To verify this observation, western blot analysis of the cytoplasmatic and the nuclear fraction of both cell lines was performed. For this, both WT and KO cells were seeded in 6-well plates and grown in either starvation medium (see 3.2.2.6) or Shh inducing medium (see 3.2.27) for 24 h. Next, whole cell lysates of WT and KO cells were generated as described above (see 3.2.3.1). Afterwards, lysates were separated into cytoplasmic and nucleic fractions using the Subcellular Protein Fractionation Kit for Cultured Cells (Thermo Fisher Scientific) according to the manufacturer's instructions. Samples were loaded on a polyacrylamide gel and subsequently blotted to a PVDF membrane (see 3.2.3.4). After incubation with antibodies against GLI2 (1:1.000, Santa Cruz Biotechnologies, mouse), GAPDH (1:5.000, Sigma-Aldrich, mouse) as a cytoplasmic marker and β-Catenin as a marker for the nucleus, membranes were developed using a ChemiDoc MP Imaging System (Bio-Rad Laboratories). Relative protein levels were calculated using GAPDH as loading control for the cytoplasmic fractions and β-Catenin for the nucleic fractions. The experiment was performed four times and the results are shown in **Figure 13**. It can be observed that significantly higher levels of GLI2 were detected in the cytoplasm compared to the nucleus. Also, there seems to be no significant difference between either the two cell lines (WT, KO) tested or the two growth conditions (strv, strv+SAG).
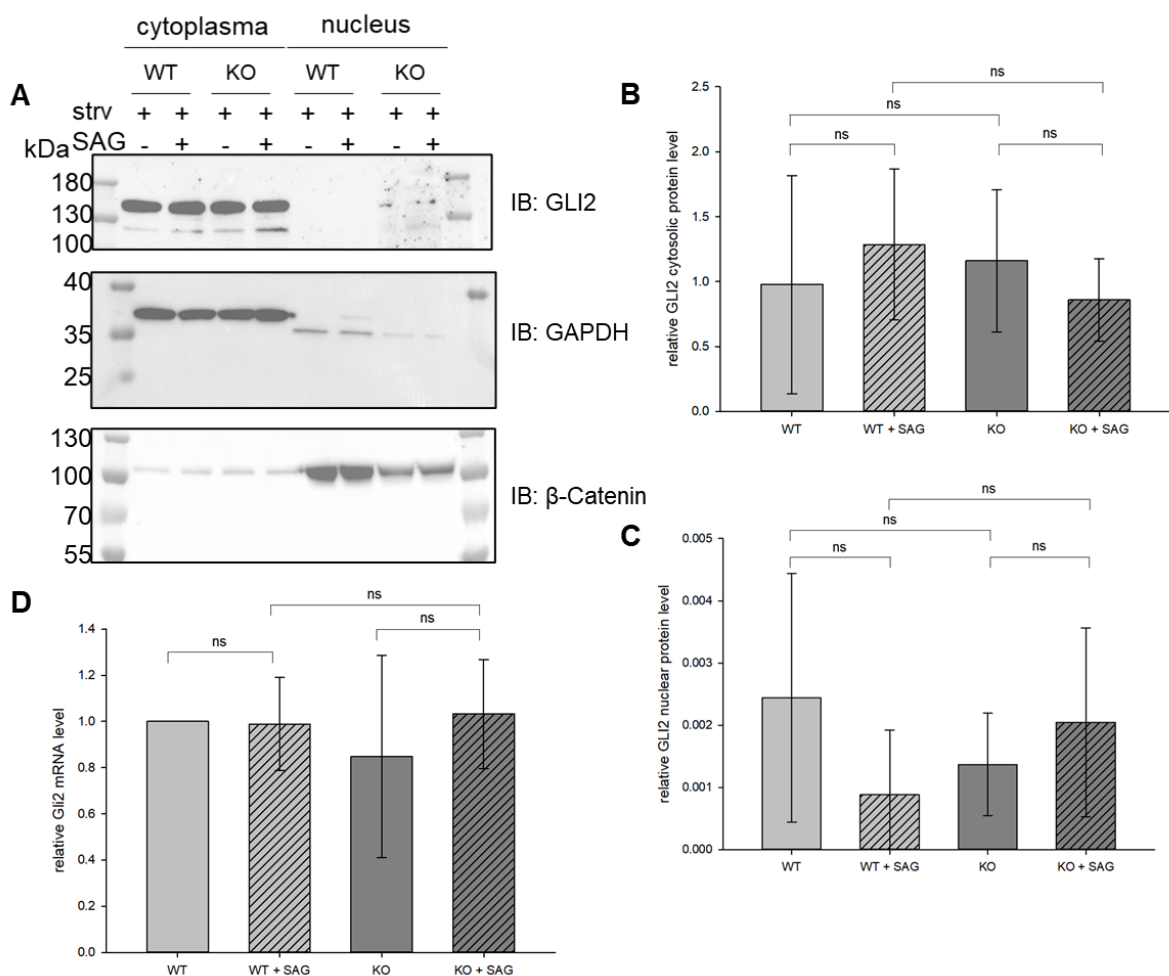
Figure 13 No significant differences in GLI2 protein and Gli2 mRNA levels could be detected between WT and Rmnd5a KO cells. A, C: Western blot analysis of WT and Rmnd5a KO cells show no differences in the amount of detectable GLI2 protein. Cells were grown in either starvation or Shh inducing medium and whole cell lysates were separated to yield cytoplasmic and nuclear cell extracts using the Subcellular Protein Fractionation Kit for Cultured Cells (Thermo Fisher Scientific). **A** monoclonal GLI2 antibody (Santa Cruz Biotechnology, 1:1000) followed by a secondary HRP-coupled antibody (Cell Signaling Technologies 1:10.000) was used. As loading control a GAPDH blot for the cytoplasmic fraction and a β-Catenin blot for the nuclear fraction (**A**) is shown, developed using an anti GAPDH antibody (Sigma-Aldrich 1:5.000) or an anti-β-Catenin antibody (Cell Signaling Technologies 1:1000) followed by a secondary HRP-coupled antibody (Cell Signaling Technologies 1:10.000). **B, D**: Quantification of the western blot analysis showed no significant differences in the protein level of GLI2 in WT and Rmnd5a KO cells or between starvation or Shh inducing conditions. Quantification was performed using the ImageJ software using the rectangular area selection tool. Background signals were subtracted, and relative protein levels were compared with the loading control. Unpaired t-test n = 4 (WT), n = 4 (KO) ns = not significant. E: qPCR results showed no difference in relative Gli2 mRNA levels between WT and Rmnd5a KO for either starvation or Shh inducing conditions. Cells were grown in either starvation or Shh inducing medium and RNA was isolated using the GeneJET RNA Purification Kit (Thermo Fisher Scientific). qPCR was performed as described above. Unpaired t-test n = 4 (WT), n = 4 (KO), ns = not significant.

Relative *Gli2* mRNA levels were also investigated. For this, NIH-3T3 WT and Rmnd5a KO cells were seeded in 6-well plates and serum starved for 24 h using starvation medium (see 4.2.2.6) to induce ciliogenesis. Additionally, to one well of each cell line 100 nM SAG was added to activate Shh signalling. Next, RNA was isolated and purified using the GeneJET RNA Purification Kit (Thermo Fisher Scientific) according to the manufacturer's instructions. After that, cDNA was generated using the SuperScript® II Reverse Transcriptase kit system

(Invitrogen) according to the manufacturer's instructions. For each qPCR reaction, a 10 µl reaction set up containing 10 ng cDNA, 5 µl 1 × Maxima SYBR Green/ROX qPCR Master Mix (Thermo Fisher Scientific), 0.3 µM forward primer, and 0.3 µM reverse primer (see Table 3.4) were combined and mixed carefully. Every sample was analysed in triplicates. The qPCR runs were performed using a Roche LightCycler 480 II Each run consisted of an UDG pre-treatment for 2 min at 50°C, an initial hot start for 10 min at 95°C, followed by 40 cycles with a denaturation step of 15 s at 95°C and an annealing/extension step of 60 s at 60°C. Afterwards, a melt curve was recorded for every sample. Each measurement was repeated three times, and each sample was analysed in triplicate with hypoxanthine phosphoribosyltransferase (hprt) and 5-aminolevulinate synthase (alas) as an internal control. Relative levels of gene expression were determined using the Abs Quant/2nd Derivative Max analysis method and statistically analysed by t-test and measured by two-tailed P-value. The results are given as Mean ± SEM. The results shown in **Figure 13 D** display no significant differences in *Gli2* mRNA levels between the two cell lines or the growth conditions tested.

The localisation of GLI3 was investigated next. IF were performed as described for GLI1 with the difference that signals for ac-tubulin are shown in red (α-ac-tubulin antibody, 1:200, Cell Signaling Technologies) and signals for GLI3 are shown in green (α-GLI3 antibody, 1:50, R&D Systems). **Figure 14** shows representative images of the localisation of GLI3. It can be observed that GLI3, similar to GLI1 and GLI2, localises to the primary cilia in both NIH-3T3 WT and KO cells.
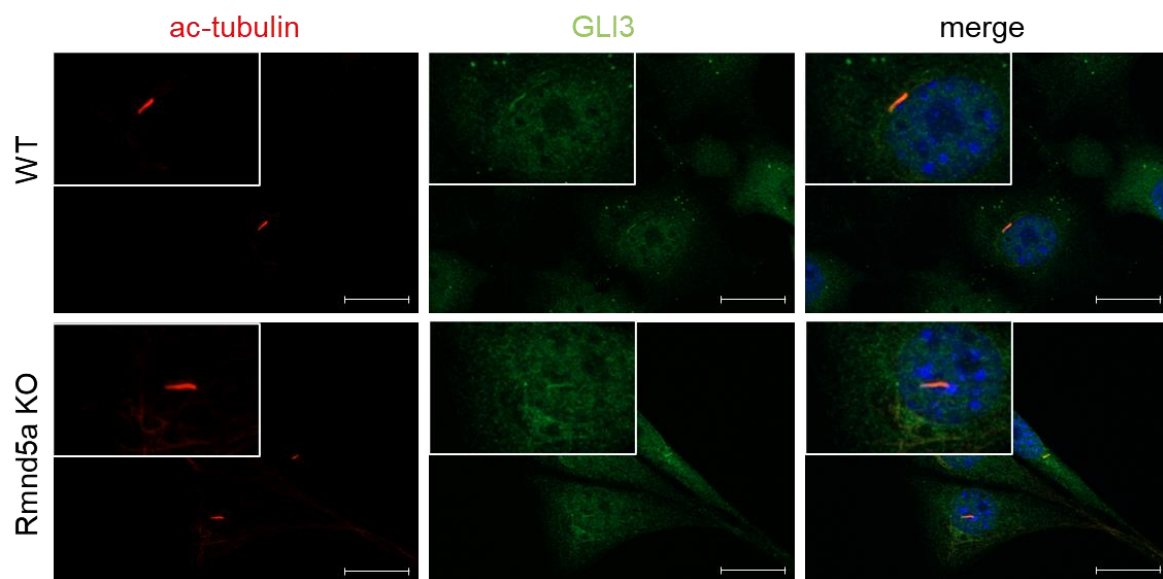
Figure 14 GLI3 localises to the primary cilium in both WT and Rmnd5a KO cells. In both WT and Rmnd5a KO cells, GLI3 signals could be detected in the primary cilia. Cells were seeded on coverslips, incubated for 24 h with starvation medium and then fixed using 4 % PFA. Staining was performed using DAPI (blue) and antibodies against GLI3 (green) and ac-tubulin (red). Representative images are shown. White bars indicate a size of 20 µm.

The next experiment investigated the localisation of the Shh signalling pathway component PTCH1. Previous experiments showed a significant decrease in the relative mRNA levels of *Ptch1* in Rmnd5a KO cells compared to WT cells (**Figure 8**). To investigate the localisation of PTCH1 relative to the primary cilia, immunofluorescence was used as described for GLI1 above. **Figure 15 A** shows a clear localisation of PTCH1 to the axoneme in both NIH-3T3 WT and Rmnd5a KO cells.

Quantification of the relative ciliary PTCH1 levels, performed as described for GLI1, showed a significant decrease in Rmnd5a KO cells compared to WT cells (**Figure 15 B**). F These results are in accordance with the findings from the qPCR experiments (**Figure 15 B**). For each cell line, 15 cells were measured and the results are given as Mean ± SEM.
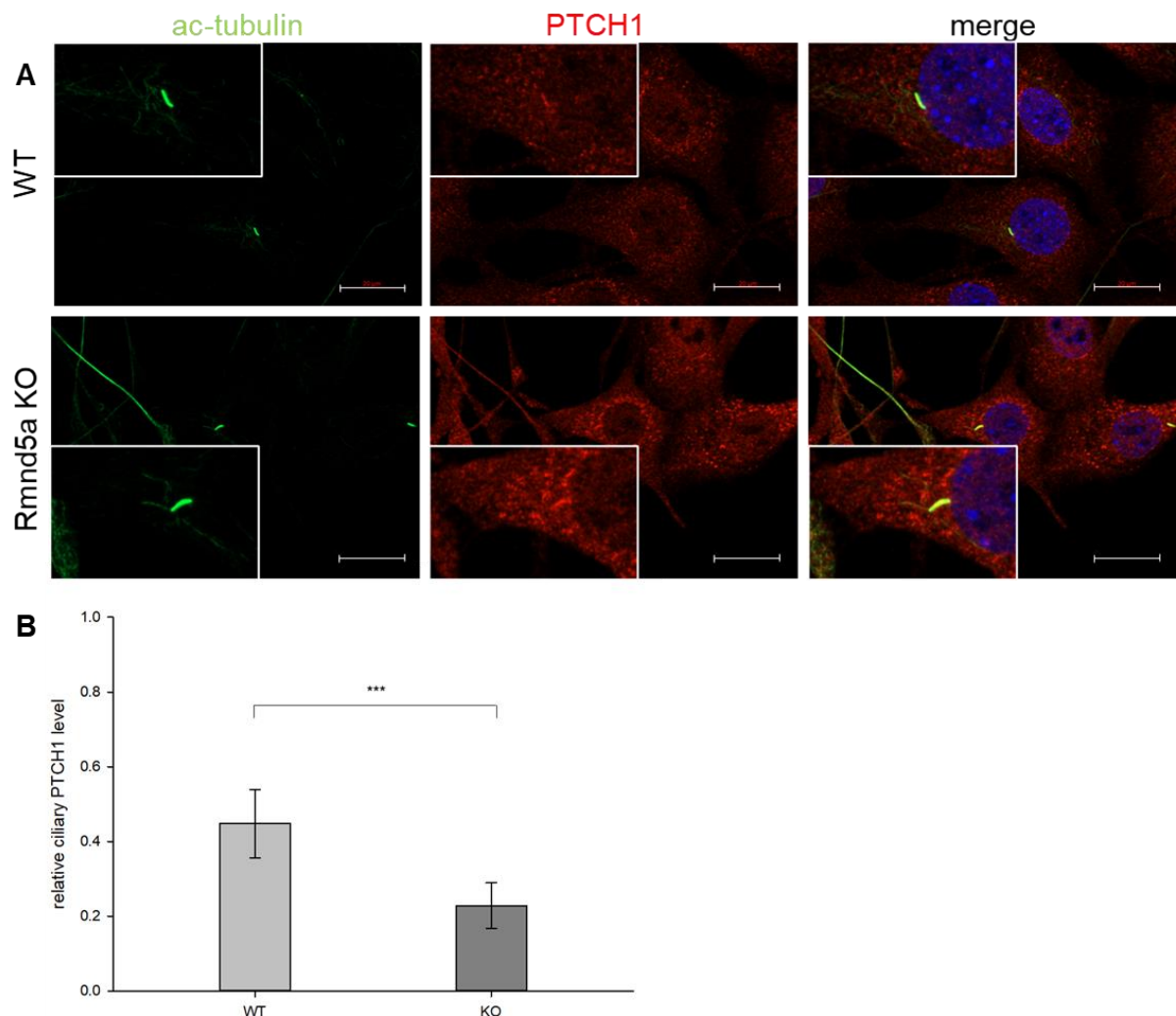
Figure 15 Relative PTCH1 levels are significantly reduced in primary cilia in Rmnd5a KO cells. **A:** In both WT and Rmnd5a KO cells, PTCH1 localises to the primary cilia and no obvious differences in localisation can be observed. Cells were seeded on coverslips, incubated for 24 h with starvation medium and then fixed using 4 % PFA. Staining was performed using DAPI (blue) and antibodies against PTCH1 (red) and ac-tubulin (green). Representative images are shown. White bars indicate a size of 20 µm. **B:** Quantification of relative ciliary PTCH1 levels showed a significant reduction in PTCH1 levels in Rmnd5a KO compared to WT. To quantify the relative PTCH1 levels, ImageJ software was used. The area of interest was selected using the freeform selection tool, background signals were subtracted, and relative fluorescence levels were compared with the fluorescence levels of n-acetylated tubulin for primary cilia and DAPI for nuclei. Unpaired t-test n = 15 (WT), n = 15 (KO). *** = P< 0.001.

The localisation and fluorescence of SUFU were investigated next. Both immunofluorescence and fluorescence quantification were performed as described for GLI1. The results are shown in **Figure 16 A**. SUFU clearly localizes to the primary cilium in both WT and Rmnd5a KO cells. However, the quantification of the fluorescence shows no significant differences between WT and KO cells **Figure 16 B**.
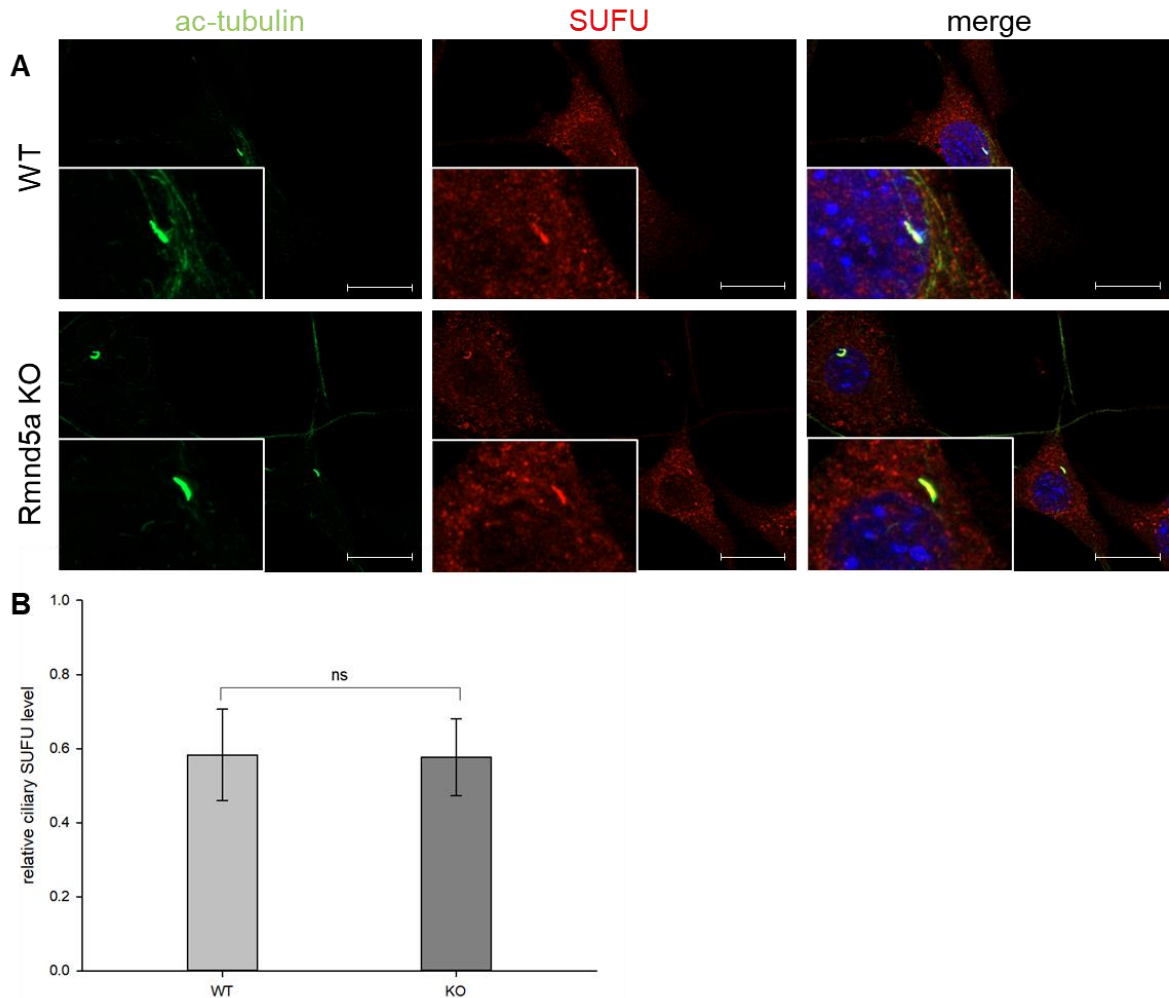
Figure 16 No differences in SUFU localisation and relative ciliary SUFU levels could be observed.
A: In both WT and Rmnd5a KO cells, SUFU localises to the primary cilia and no obvious differences in localisation can be observed. Cells were seeded on coverslips, incubated for 24 h with starvation medium and then fixed using 4 % PFA. Staining was performed using DAPI (blue) and antibodies against SUFU (red) and ac-tubulin (green). Representative images are shown. White bars indicate a size of 20 µm. **B:** Quantification of relative ciliary SUFU levels showed no significant differences in SUFU levels in Rmnd5a KO compared to WT. To quantify the relative PSUFU levels, ImageJ software was used. The area of interest was selected using the freeform selection tool, background signals were subtracted, and relative fluorescence levels were compared with the fluorescence levels of n-acetylated tubulin for primary cilia and DAPI for nuclei. Unpaired t-test n = 15 (WT), n = 15 (KO). ns = not significant.

4.2 Gid subunits and the primary cilium

To investigate the localisation of various components of the GID complex relative to the primary cilia, immunofluorescence was used. In a first experiment, a GID4-GFP fusion protein was used to determine the localisation of GID4. For this, NIH-3T3 WT and NIH-3T3 Rmnd5a KO

cells were transfected with a vector containing a GID4-GFP fusion protein and a vector control, containing only GFP (VC). Before transfection, cells were maintained as described above. To determine the number of vital cells, cells were trypsinised, centrifuged at 500 x g for 3 min and the supernatant was aspirated. Cells were resuspended in 5 ml pre-warmed DMEM and 100 µl of the cell solution was diluted with 9900 µl CASY®ton buffer. The number of vital cells in the solution was determined using a CASY® TT Cell Counter (OMNI Life Science).

Both cell types were seeded on coverslips placed in 12 well plates with a density of 0,5 x 10^5 cells per well and incubated in cultivation medium over night at 37°C and 5 % CO_2. On the next day, 1 µg plasmid DNA was diluted in 50 µl OptiMEM per well and mixed well. At the same time, 3 µl Lipofectamine 2000™ were mixed with 50 µl OptiMEM for each well. Both mixtures were combined and incubated for 5 min at rt. During the incubation time, culturing medium was removed from the wells, cells were washed with 1 x PBS and 1 ml pre-warmed DMEM was added to each well. Then, the transfection mixture was added in a drop wise manner and cells were incubated for 24 h at 37°C and 5 % CO_2. Cells were incubated for 24 h at 37°C and 5 % CO_2. After incubation, the medium was aspirated, cells were washed and fixed with 4 % PFA. Next, the coverslips were first incubated with anti-ac-tubulin (1:200, Sigma-Aldrich, mouse) antibodies as primary antibodies and then with AlexaFluor™ 546 goat anti mouse IgG (H+L) (1:250, Invitrogen, depicted in red) and DAPI (300 nM, blue). Images were taken using a Zeiss Axio Observer 7 with ApoTome.2. It was observed that no GFP fluorescence could be detected in the cells transfected with the vector expressing the GID4-GFP fusion protein. In the cells expressing only GFP, a clear signal could be observed.

The experiment was repeated as described above, but additionally to incubating the fixed cells with anti-ac-tubulin (1:200, Sigma-Aldrich, mouse) antibodies as primary antibodies, anti-GFP antibodies (1:200, Cell Signaling Technologies, rabbit) were used. As secondary antibodies, AlexaFluor™ 546 goat anti mouse IgG (H+L) (1:250, Invitrogen, red), AlexaFluor™ 488 donkey anti rabbit IgG (H+L) (1:250, Invitrogen, green) and DAPI (300 nM, blue) were used. Images were taken using a Zeiss Axio Observer 7 with ApoTome.2 and representative images are shown in **Figure 17**.

Fixed and stained cells were counted and the percentage of cells with both detectable GFP signals and primary cilia were quantified. **Figure 18** shows that 24% of the cells expressing the vector control (CTRL) are forming primary cilia. However, the percentage of cells expressing the GID4-GFP fusion protein and showing cilia is significantly reduced to 10%.
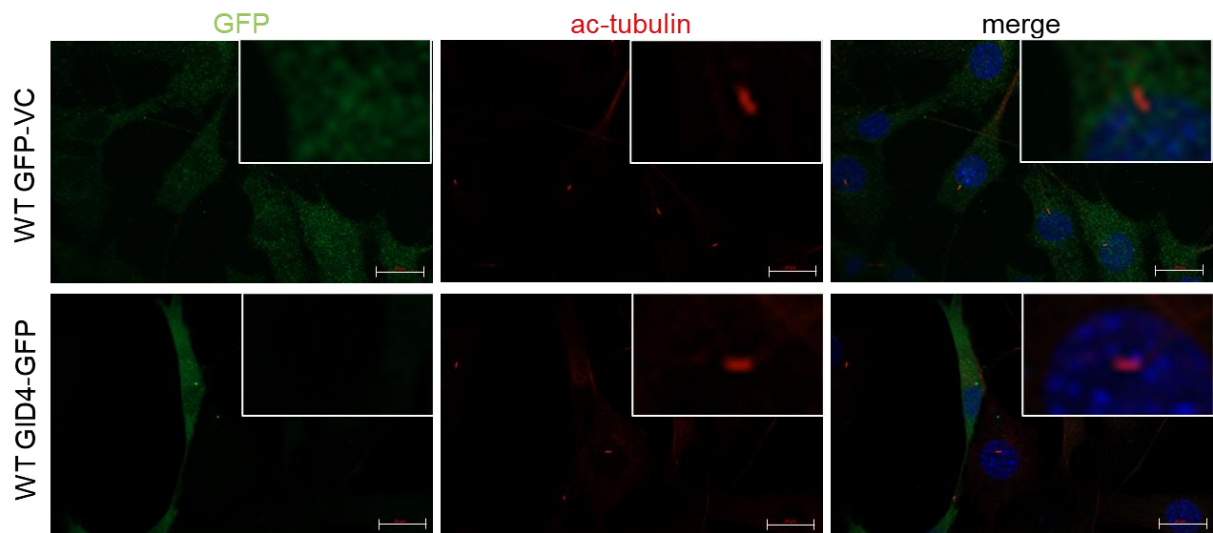
Figure 17 Comparison of GFP expression between NIH-3T3 WT and NIH-3T3 Rmnd5a KO cells and GID4-GFP and GFP-VC. NIH-3T3 WT and Rmnd5a KO cells were seeded on coverslips and transfected with plasmids for the expression of either GFP vector control (VC), or GID4-GFP. After incubation for 24 h, cells fixed with 4 % PFA and stained with antibodies against GFP (green) and ac-tubulin (red) and DAPI (blue). Representative images are shown. White bars indicate a size of 20 µm
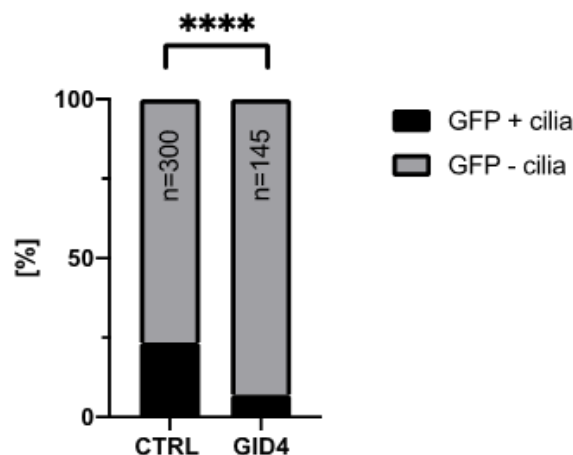
Figure 18 Overexpression of GID4 results in a significant reduction of ciliated cells.
NIH-3T3 WT cells show a decrease in detectable cilia formation when transfected with pEGFP-Gid4, compared to transfection with pEGFP vector control (CTRL). Cells were seeded on coverslips and transfected with either GFP CTRL or GID4-GFP. After incubation for 24 h, cells fixed with 4 % PFA and stained with antibodies against GFP (green) and ac-tubulin (red) and DAPI (blue). The experiment was performed three times and 100 cells for each condition and experiments were analysed. Unpaired t-test. **** = P< 0.0001.

In the following experiments, antibodies against four different subunits of the GID complex, i.e., ARMc8, MKLN1, RMND5A and TWA1 were used to elucidate the localisation of these subunits. First, the localisation of the four subunits during normal growth conditions should be investigated. For this, cells were seeded on coverslips and incubated in cultivation medium for 24 h. Afterwards they were either fixed with 4 % PFA or 100 % methanol as described above (see 3.2.3.7). Cells fixed with methanol were incubated with either anti-TWA1 (1:100, Novus Biologicals, rabbit) and anti γ-tubulin (1:250, Sigma-Aldrich, mouse) antibodies or anti-RMND5a (1:100, Atlas Antibodies, rabbit) and anti-γ-tubulin (1: 1:250, Sigma-Aldrich, mouse)

antibodies. Anti-γ-tubulin antibodies are used to visualise the centrioles, the structure from which the primary cilium originates (see introduction 1.1.1). As secondary antibodies AlexaFluor™ 546 goat anti mouse IgG (H+L) (1:250, Invitrogen, red), AlexaFluor™ 488 donkey anti rabbit IgG (H+L) (1:250, Invitrogen, green) and DAPI (300 nM, blue) were used. PFA-fixed cells were incubated with either anti-MKLN1 (1:100, Santa Cruz Biotechnology, mouse) and anti γ-tubulin (1:200, Cell Signaling Technologies, rabbit) antibodies or anti-ARMc8 (1:100, Santa Cruz Biotechnology, mouse) and anti-γ-tubulin antibodies (1:200, Cell Signaling Technologies, rabbit). As secondary antibodies, antibodies AlexaFluor™ 546 goat anti mouse IgG (H+L) (1:250, Invitrogen, depicted in green), AlexaFluor™ 488 donkey anti rabbit IgG (H+L) (1:250, Invitrogen, depicted in red) and DAPI (300 nM, blue) were used. Images were taken using a Zeiss Axio Observer 7 with ApoTome.2. Representative images are shown in **Figure 19**. It can be clearly observed that both TWA1 and RMND5a colocalize with γ-tubulin. For TWA1 31 cells were looked at and 87,1 % showed a co localisation with γ-tubulin. 29 cells were analysed for RMND5a and 82,8 % co localised with γ-tubulin. For MKLN1 and ARMc8, fluorescence could be detected but no colocalization with γ-tubulin could be observed in any of the 30 or 28 cells investigated respectively.
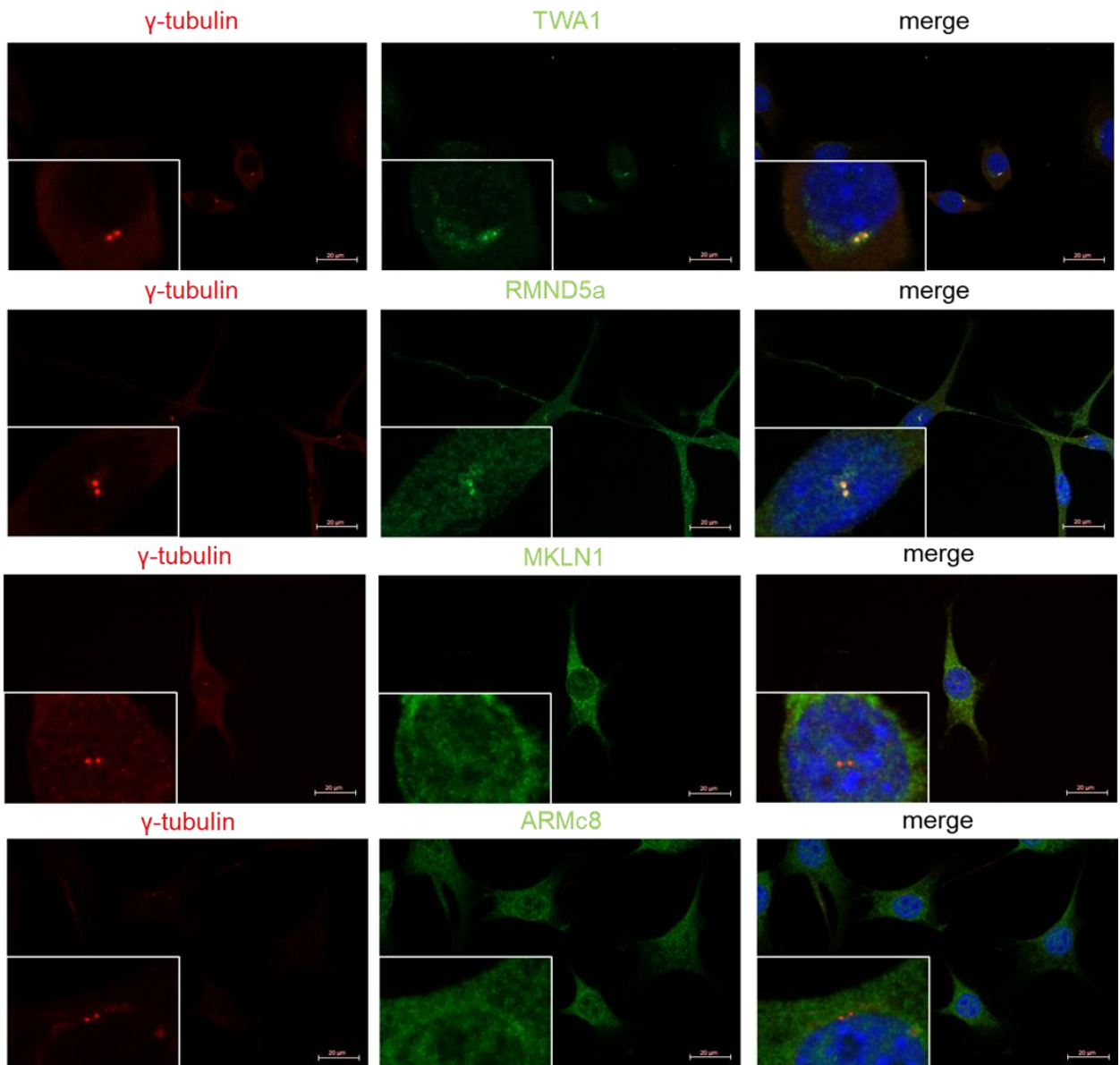
Figure 19 Subunits of the mammalian GID complex co-localise with centrioles. NIH-3T3 WT cells were seeded on coverslips and fixed with either 100 % Methanol (for TWA1 and anti RMND5a staining) or 4 % PFA (for MKLN1 and ARMc8 staining). Staining was performed using DAPI (blue) and antibodies against γ-tubulin (red) and various subunits of the GID complex (TWA1, RMND5a, MKLN1, ARMc8, green). Representative images are shown. White bars indicate a size of 20 µm. Cells with γ-Tubulin co-localization: TWA1, 87,1%, n=31; RMND5A, 82,8%, n=29; ARMC8, 0%, n=30; MKLN1, 0%, n=28.

Next, localisation of TWA1, RMND5a, MKLN1 and ARMc8 relative to the primary cilium should be analysed. For this, cells were grown on coverslips and incubated in starvation medium (see 3.2.26) for 24 h. Afterwards they were either fixed with 4 % PFA or 100 % methanol as described above (see 3.2.3.7). Cells fixed with methanol were incubated with either anti-TWA1 (1:100, Novus Biologicals, rabbit) and anti-ac-tubulin (1:200, Sigma-Aldrich, mouse) antibodies or anti-RMND5a (1:100, Atlas Antibodies, rabbit) and anti-ac-tubulin antibodies (1:200, Sigma-Aldrich, mouse). As secondary antibodies AlexaFluor™ 546 goat anti mouse IgG (H+L) (1:250, Invitrogen, red), AlexaFluor™ 488 donkey anti rabbit IgG (H+L) (1:250, Invitrogen, green) and DAPI (300 nM, blue) were used. PFA-fixed cells were incubated with either anti-MKLN1 (1:100,

Santa Cruz Biotechnology, mouse) and anti ac-tubulin (1:200, Cell Signaling Technologies, rabbit) antibodies or anti-ARMc8 (1:100, Santa Cruz Biotechnology, mouse) and anti-ac-tubulin antibodies. As secondary antibodies, antibodies AlexaFluor™ 546 goat anti mouse IgG (H+L) (1:250, Invitrogen, depicted in green), AlexaFluor™ 488 donkey anti rabbit IgG (H+L) (1:250, Invitrogen, depicted in red) and DAPI (300 nM, blue) were used. Anti-ac-tubulin antibodies are used to visualise the axoneme, i.e., the primary cilia as described above (see Figure 1.1). Images were taken using a Zeiss Axio Observer 7 with ApoTome.2. Representative images are shown in **Figure 20**.
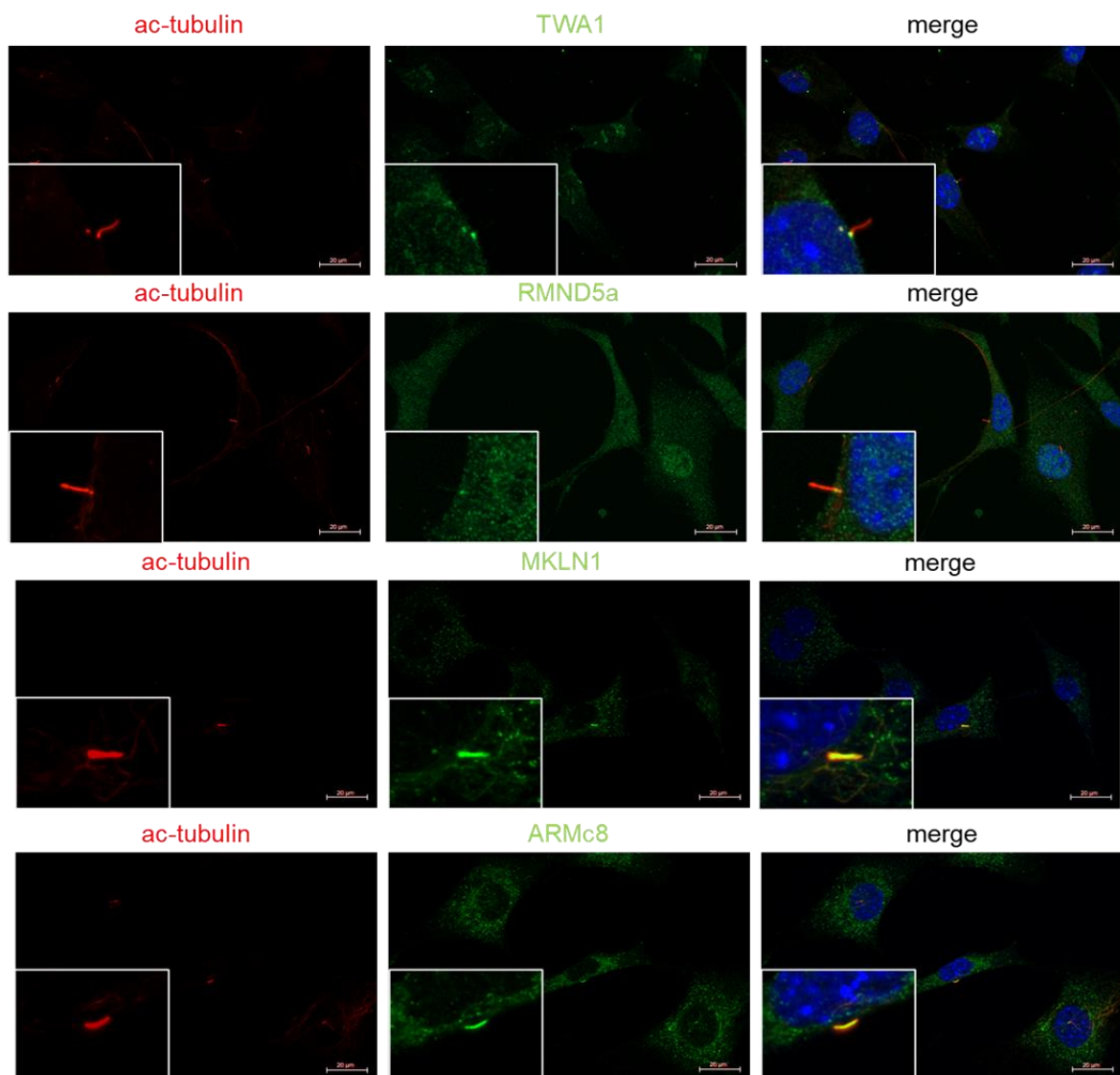
Figure 20 Subunits of the mammalian GID complex co-localise with the primary cilium. NIH-3T3 WT cells were seeded on coverslips and incubated with starvation medium for 24 h. Cells were fixed with either 100 % Methanol (for TWA1 and anti RMND5a staining) or 4 % PFA (for MKLN1 and ARMc8 staining). Staining was performed using DAPI (blue) and antibodies against ac-tubulin (red) and various subunits of the GID complex (TWA1, RMND5a, MKLN1, ARMc8, green). Representative images are shown. White bars indicate a size of 20 µm. Percentage of cells with ac-Tubulin co-localization: TWA1, 75,9%, n=29; RMND5A, 60,7%, n=28; ARMC8, 96,3%, n=27; MKLN1, 93,1%, n=29.

It can be observed that both TWA1 and RMND5a localise proximal to the axoneme with a partial overlap. For TWA1, 29 cells were analysed and 75,9 % showed a co localisation with

γ-Tubulin. For RMND5a 60,7 % of the 28 cells investigated cells showed a co localisation with γ-tubulin. MKLN1 and ARMc8 co localise with ac-tubulin, i.e., the primary cilium. For MKLN1 93,1 % of the 29 investigated cells showed a co localisation with ac-tubulin and for ARMc8 96,3 % of the 27 analysed cells showed a co localisation.

4.3 Identifying novel Gid4 interacting partners

4.3.1 Over expression of Gid4 in HEK293 cells

The subunit GID4 is thought to be a substrate recognition factor of the GID complex. In yeast, several substrates have been found for GID4, but this is not the case for the mammalian GID complex homologue. To identify human GID4 interaction partners, the Gid4 gene was cloned into a pCS2+ expression vector. First, Gid4 was amplified from cDNA using PCR as described in 3.2.1.1. After verifying the successful amplification of Gid4 using agarose gel electrophoresis (see 3.2.1.2), the PCR product was cleaned up (see 3.2.1.3) to prepare for restriction digest. For this, both the empty vector and the cleaned PCR product were digested with as described above (see 3.2.1.4). The entire PCR product (30 µl) and 3 µg of the vector were digested using the restriction enzymes EcoRI and XhoI. After incubation at 37°C for 1 h, the samples were checked for complete digest using agarose gel electrophoresis (see 3.2.1.2). Afterwards, samples were cleaned up and then ligation was performed using T4 ligase (New England Biolabs) as described above (see 3.2.1.5). The entire digested PCR product and 100 ng of the digested vector were used for ligation. After incubation at 4°C overnight, transformation of electrocompetent *E. coli* was performed as described above (see 3.2.1.8). Transformed bacterial suspension was plated on LB-agar plates containing ampicillin and incubated at 37°C overnight. On the next day, colonies were picked and 4 ml LB medium containing ampicillin was inoculated with one colony each. After incubation at 37°C overnight, plasmids were purified using ZymoPURE™ Plasmid Miniprep kit (Zymo Reseach) as described in 3.2.1.9. The concentration of purified plasmids was determined (see 2.2.1.13) and samples were then sent for sequencing (see 3.2.1.14). Samples were checked for correct sequences using the CLUSTAL W alignment tool. Plasmids containing the correct sequence was again transformed in *E. coli* as described above and the bacterial suspension was transferred to 100 ml LB medium, containing ampicillin. The solution was incubated over night at 37°C. The next day, plasmids were purified using the QIAprep Spin Midiprep Kit (Qiagen) as described above (see 3.2.1.9).

For transient transfection with pCS2+-Gid4-c-Myc (Gid4-c-Myc) and pCS2+ (vector control, VC), HEK293 cells were used. Cells were maintained as described above (see 3.2.2.2). Before seeding HEK293 cells for transient transfection, cells were trypsinised, centrifuged at 500 x g for 3 min and the supernatant was aspirated. Cells were resuspended in 5 ml pre-warmed DMEM and 100 µl of the cell solution was diluted with 9900 µl CASY®ton buffer. The number of vital cells in the solution was determined using a CASY® TT Cell Counter (OMNI Life

Science). Cells were then seeded in 10 cm dishes with a density of 1,5 x 10^5 cells/ml with 10 ml pre-warmed DMEM culturing medium and incubated over night at 37°C and 5 % CO$_2$. On the next day, 10 µg plasmid DNA was diluted in 500 µl OptiMEM and mixed well. At the same time, 30 µl Lipofectamine 2000™ were mixed with 500 µl OptiMEM. Both mixtures were combined and incubated for 5 min at rt. During the incubation time, culturing medium was removed from the dishes, cells were washed with 1 x PBS and 10 ml pre-warmed DMEM was added to each dish. Then, the transfection mixture was added in a drop wise manner and cells were incubated for 24 h at 37°C and 5 % CO$_2$.

After incubation, cells were harvested and whole cell lysates were prepared as described in 3.2.3.1. For this, dishes were placed on ice and the culturing medium was aspirated. Cells were washed with ice cold PBS and 500 µl of lysis buffer was added to each dish. Cells were scraped off using a cell scraper and the lysates were transferred to pre-cooled tubes and kept on ice for 30 mins. After that, samples were centrifuged for 10 mins at 4°C and 13000 x g. After centrifugation, the supernatant was transferred to a fresh pre-cooled tube. Next, the protein concentration of each lysate was determined, using a BCA assay as described in 3.2.3.2. 20 µg of each sample was mixed with 5 x Laemmli buffer and incubated for 10 min at 95°C to prepare for SDS-PAGE and western blotting. The remaining lysate was stored at -80°C and sent to Alessandro Ori's lab in Jena for mass spectrometry analysis.

To verify the expression of transfected Gid-4-c-Myc, SDS-PAGE and western blot were performed. For this, the prepared samples were loaded on a precast 10% Novex Tris-Glycine Gel, together with PageRuler™ Prestained Protein Ladder as a marker for size. Electrophoresis was run at 120 – 160 V for up to 90 min in 1x SDS running buffer. Next, the separated proteins from the SDS PA gels were transferred to PVDF membranes. After blotting, membranes were blocked with 5 % milk powder, membranes were incubated with anti-c-Myc antibodies, diluted 1:1000 in 5 % BSA in TBS-T, at 4°C overnight. On the next day, membranes were incubated with an anti-mouse-HRP-coupled secondary antibody for 1 h at rt. After incubation, detection was performed using SuperSignal™ West Femto Maximum Sensitivity Substrate (Thermo Fisher Scientific) and images were obtained using a ChemiDoc MP Imaging System (Bio-Rad Laboratories).

From the results shown in **Figure 21** can be concluded that transfection and expression of Gid4-c-Myc was successful and the prepared lysates can be further analysed using mass spectrometry.
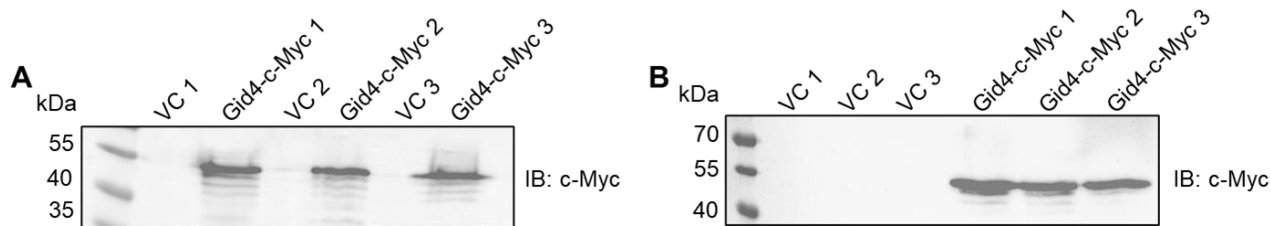
Figure 21 Western blot analysis confirming the expression of Gid4-c-Myc in HEK293 cells.
A: Expression of GID4-c-Myc was verified for lysates prepared for mass spectrometry analysis. **B:** Expression of GID4-c-Myc was verified for lysates prepared for Immunoprecipitation and subsequent mass spectrometry analysis. HEK293 cells were transfected with pCS2+-Gid4-c-Myc and PCS2+ VC using Lipofectamine™ 2000 (Thermo Fisher Scientific). 24 h after transfection, whole cell lysates were generated and 20 µg of each lysate was loaded on a Novex™WedgeWell™ 10% Tris-Glycin Gel (Thermo Fisher Scientific). Detection was performed using a Myc-tag antibody (Cell Signaling Technology, 1:1.000) and a secondary anti-rabbit-HRP (Cell Signaling Technology 1:10.000) antibody. VC: vector control

It was found that 68 proteins were significantly down regulated upon over expression of Gid4 compared to the empty vector control. This number of hits needed to be narrowed down further, so in the next experiment, IP with Gid4-c-Myc was performed.

4.3.2 IP with Gid4 in HEK293 cells

To narrow down the hits from the over expression of Gid4 in HEK293 cells, a similar approach was used. Again, Gid4-c-Myc was transiently expressed in HEK293 cells and whole cell lysates were prepared as described above. As before, samples of each lysate were prepared for western blot analysis and SDS PAGE and western blotting were performed to verify the expression of Gid4-c-Myc. Again, the transfection and expression were successful as can be observed in **Figure 21**.

With the remaining lysates an IP was performed as described above in 3.2.3.4. For this, the ChromoTek Myc-Trap® system (ChromoTek) was used according to the manufacturer's instructions. Small recombinant antibody fragments are covalently bound to the surface of agarose beads. These antibody fragments recognize the Myc-tag sequence of the fusion protein Gid4-c-Myc so that the tagged protein and possible interacting factors can be isolated from cell lysates. To elute bound proteins, 0.1 mg/ml Myc peptide was used. After elution, samples were stored at -80°C and sent to Alessandro Ori's lab in Jena for mass spectrometry analysis. Here, 1342 proteins were found to be significantly up regulated in the samples with Gid4 overexpression compared to the empty vector control.

To find potential interacting partners of Gid4, the data from both the Gid4 over expression experiment and the GID4 IP were compared.
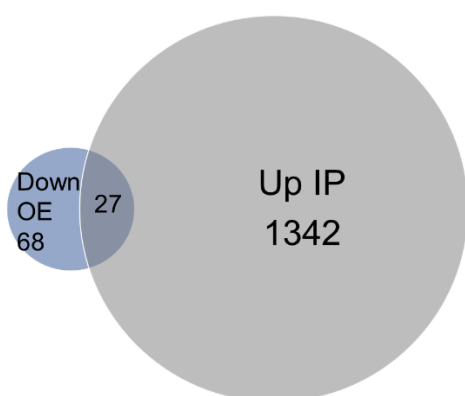
Figure 22 27 proteins are both down regulated in the over expression of GID4-c-Myc and up regulated in the GID4-c-Myc IP.

This resulted in 27 putative Gid4 interacting partners, shown as a Venn diagram in **Figure 22** and listed in **Table 19**.

Table 19 Overlapping hits from Gid4 over expression and IP.

Hit no.	Gene name	Protein name	Subcellular location
1	NNT	NAD(P) transhydrogenase, mitochondrial	mitochondrial membrane
2	NDUFA9	NADH dehydrogenase [ubiquinone] 1 alpha subcomplex subunit 9, mitochondrial	mitochondrial membrane
3	NDUFS1	NADH-ubiquinone oxidoreductase 75 kDa subunit, mitochondrial	mitochondrial membrane
4	NDUFS3	NADH dehydrogenase [ubiquinone] iron-sulfur protein 3, mitochondrial	mitochondrial membrane
5	VDAC1	Voltage-dependent anion-selective channel protein 1	mitochondrial membrane
6	VDAC2	Voltage-dependent anion-selective channel protein 2	mitochondrial membrane
7	SLC25A13	Calcium-binding mitochondrial carrier protein Aralar2	mitochondrial membrane
8	PGAM5	Serine/threonine-protein phosphatase PGAM5, mitochondrial	mitochondrial membrane
9	PHB2	Prohibitin-2	mitochondrial membrane
10	ALDH18A1	Delta-1-pyrroline-5-carboxylate synthase	mitochondrial membrane
11	NR3C1	Glucocorticoid receptor	mitochondrion
12	UHRF1	E3 ubiquitin-protein ligase	nucleus
13	TIAL1	Nucleolysin TIAR	lysosome, cytoplasm
14	FERMT2	Fermitin family homolog 2	cytoplasm, nucleus
15	PHAX	Phosphorylated adapter RNA export protein	cytoplasm, nucleus
16	TRA2B	Transformer-2 protein homolog beta	nucleus

Table 19 Overlapping hits from Gid4 over expression and IP (continued).

Hit no.	Gene name	Protein name	Subcellular location
17	RPL7L1	60S ribosomal protein L7-like 1	cytosolic large ribosomal subunit
18	SLC16A1	Monocarboxylate transporter 1	plasma membrane
19	G6PD	Glucose-6-phosphate 1-dehydrogenase	cytosol
20	GTPBP10	GTP-binding protein 10	nucleolus
21	APMAP	Adipocyte plasma membrane-associated protein	membrane
22	RPN2	Dolichyl-diphosphooligosaccharide--protein glycosyltransferase subunit 2	endoplasmic reticulum (ER)
23	VAPA	Vesicle-associated membrane protein-23associated protein A	plasma membrane, ER membrane
24	FSCN1	Fascin	cytosol, cytoskeleton
25	PGM3	Phosphoacetylglucosamine mutase	cytosol
26	CSNK1A1	Casein kinase I isoform alpha	cytosol, cytoskeleton
27	TECR	Very-long-chain enoyl-CoA reductase	ER membrane

To narrow down the number of putative GID4 interacting partners even further, a biotinylation assay was performed.

4.3.3 BioID for proximity-dependent biotin identification

For this approach the E. coli biotin protein ligase BirA is fused to a targeting protein. When this construct is expressed in cells, proteins in close proximity to the target protein are selectively biotinylated. After cell lysis and protein denaturation, biotinylated proteins can be isolated and analysed using mass spectrometry [100].

Here, two different variants of the fusion protein were created an N-terminal variant and a C-terminal variant. Cloning of Gid4 into pcDNA5-pDEST-BirA-Flag-C-term and pcDNA5-pDEST-BirA-Flag-N-term was performed using the Gateway™ LR Clonase™ II Enzyme mix (Thermo Fisher Scientific) as described above 3.2.1.7. Next, stable cell lines for the expression of both fusion variants were generated as described in 3.2.2.6. For this, HEK293 FlpIn TREx cells were used to ensure a rapid generation of stable cell lines as well as high-level expression of the fusion constructs. To induce the expression of the fusion proteins, cells were incubated with 1 µg/ml tetracycline for 48 h. Next, 50 µM biotin was added and cells were incubated for 24 h. After that, cells were harvested and processed further.

To verify the expression of the fusion proteins and the subsequent biotinylation, western blot analysis was used. For this, 1.5×10^5 cells/ml were seeded in 6 well plates with 3 ml per well. For both cell lines, three different setups were done. First, cells were not treated with either tetracycline nor biotin, second, cells were treated with tetracycline only and third, cells were treated with both tetracycline and biotin. After harvesting the cells, whole cell lysates were prepared and samples for SDS-PAGE and western blotting were generated as described

above 3.2.3.1. After SDS-PAGE and western blotting were performed, membranes were incubated with streptavidin-HRP, diluted 1:10000 and anti-GAPDH antibody, diluted 1:5000. It can be observed in **Figure 23** that after adding biotin to the cells, lysates from both cell lines showed a notable increase in the detectable amount of biotinylated proteins.
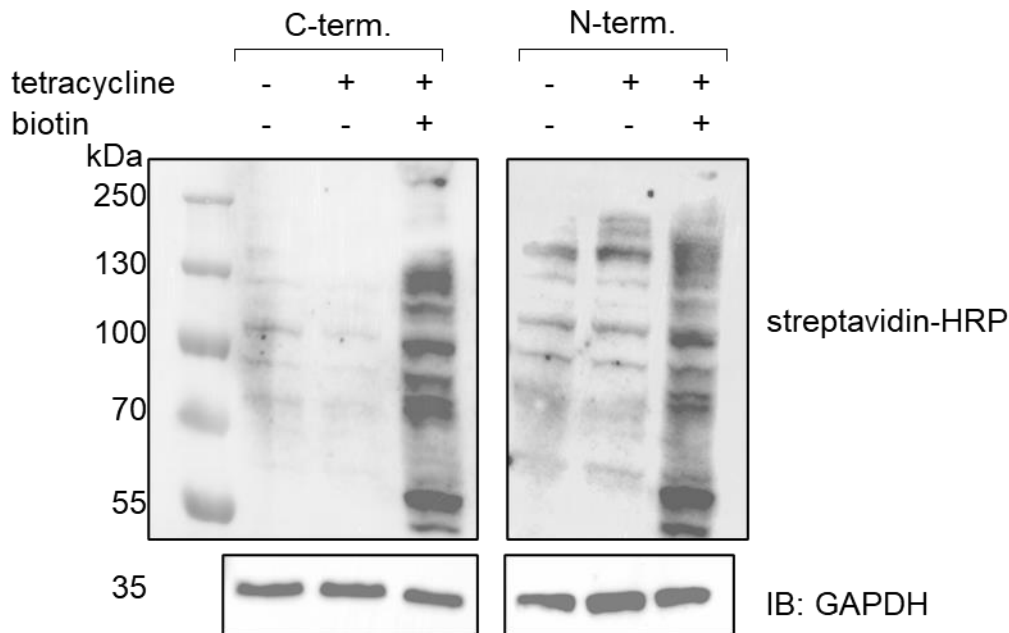
Figure 23 HEK293-BirA-Gid4-C-term and HEK293-BirA-Gid4-N-term show a notable increase in the detectable amount of biotinylated protein after induction with tetracycline.
Western blot analysis was performed to verify the expression of the fusion protein BirA-GID4 and subsequent biotynilation. Both generated cell lines, HEK293-BirA-Gid4-C-term and HEK293-BirA-Gid4-N-term were incubated with or without 1 µg/ml tetracyclin in normal growth medium as indicated. After 48 h 50 µM biotin was added as indicated above and cells were incubated for 24 h. Whole cell lysates were generated and 20 µg protein of each sample was loaded onto a Novex™WedgeWell™ 10% Tris-Glycin Gel (Thermo Fisher Scientific). Detection was performed using streptavidin-HRP (Thermo Fisher Scientific, 1:10.000). As loading control, a GAPDH blot is shown, developed using a anti GAPDH antibody (Sigma-Aldrich 1:5.000) followed by a secondary HRP-coupled antibody (Cell Signaling Technologies 1:10.000).

To generate samples for mass spectrometry analysis, cells were seeded with a density of 1 x 10^7 cells. For both cell lines, two conditions each were prepared. First, only biotin was added to the cells and second, both biotin and tetracycline were added to the cells. For each cell line and condition, five independent experiments using different passages of cells were performed. Cells were harvested and processed as described in 3.2.3.8. After processing, cell pellets were sent to Dr Alessandro Ori's lab at the Fritz Lipman Institute in Jena were all subsequent steps including mass spectrometry and data processing were performed.

For the final analysis only data generated with the N-terminal construct were used due to the better quality of this data set compared to the data received from the C-terminal construct.

The mass spectrometry analysis could identify all GID complex subunits in the pull down. Also, the following subunits of AMP-activated protein kinase (AMPK) could be detected: PRKAA1, PRKAA2, PRKAB1 and PRKAG1. Comparing the list of potential GID4 interacting partners

after the BioID experiment with the putative GID4 interacting partners suggested by the overexpression experiment and the immunoprecipitation study (**Table 19**) revealed a total of four proteins presents on both lists: PGAM5, NR3C1, FERMT2 and PHAX.

Next, all potential GID4 interacting partners revealed by the BioID experiment were compared to the SYSCILIA gold standard (SCGSv1) of known ciliary components [79] to specifically look for putative novel GID4 interacting partners connected to primary cilia. This resulted in a list of 152 proteins. These proteins were then checked for N-terminal prolines. Ten of the 152 proteins contain a proline at position 2, 3, 4 or 5, listed in **Table 20**.

Table 20 Ciliary proteins found in the BioID experiment with N-terminal prolines at position 2-5.

Hit no.	Gene name	Protein name	Position of N-terminal proline
1	KIF3A	Kinesin-like protein KIF3A	2
2	LRRC49	Leucine-rich repeat-containing protein 49	3
3	PEBP1	Phosphatidylethanolamine-binding protein 1	2
4	RPGRIP1L	Protein fantom	4
5	STIL	SCL-interrupting locus protein	3
6	STK3	Serine/threonine-protein kinase 3	4 and 5
7	STK39	STE20/SPS1-related proline-alanine-rich protein kinase	4
8	SYNE2	Nesprin-2	5
9	WDR60	Cytoplasmic dynein 2 intermediate chain 1	3
10	WDR62	WD repeat-containing protein 62	3

5. Discussion

5.1 Shh signalling is influenced by the GID complex

The ciliary membrane is enriched in proteins involved in many different signalling pathways [80]. One of the most well-known pathways involving the primary cilium is the Sonic Hedgehog signalling pathway [81]. When the Shh pathway is not activated by a ligand, the transcription factors GLI2 and GLI3 interact with suppressor of fused (SUFU) and are transported to the cytoplasm [82]. GLI2 and GLI3 are then partially degraded by the proteasome and the generated repressors formed translocate into the nucleus and inhibit the expression of Shh target genes [83]. Upon activation of the Shh pathway, the processing of GLI2 and GLI3 to the repressor forms is blocked and full-length GLI proteins are turned into GLI activators [84].

A study by Boldt et al [76] placed the GID complex at the basal body of the primary cilia. This led to the hypothesis that the GID complex might be involved in the regulation of Shh signalling. In this work, the molecular mechanisms underlying this relationship were investigated.

Figure 8 shows a significant reduction of relative mRNA levels of two key components of the Shh signalling pathway, *Gli1* and *Ptch1* in NIH-3T3 Rmnd5a KO cells after treatment with SAG compared to WT cells. NIH-3T3 Rmnd5a KO cells have a dysfunctional GID complex due to the CRISPR-Cas9 mediated knock out of the key component Rmnd5a (Gid2) [75].

This result points towards a defect in Shh signalling in GID-deficient cells. The activation of the transcription of important target genes of this pathway, i.e., *Gli1* and *Ptch1*, appears to be impaired in these cells. Still, the SAG activation of Shh signalling appears at least partially functional in both WT and KO cells, a higher relative amount of both *Gli1* and *Ptch1* mRNA after Shh induction could be observed. It was thus concluded that the GID complex influences the Shh signalling pathway downstream of the G protein-coupled receptor Smoothened (SMO) since SAG acts as an activator of SMO. Additionally, it was concluded that the absence of a functioning GID complex alters the expression of Shh target genes and thus impacts the proper Shh induced transcriptional response.

To further investigate the underlying reason for this phenomenon, primary cilia in WT and KO cells were analysed and their length and the percentage of ciliated cells was measured. While no significant difference in cilia length was measured (**Figure 9**) it was observed that only 42.0% of analysed KO cells compared to 67.3 % of WT cells formed a primary cilium. It is thus possible that the difference in the overall number of ciliated cells explains the lower amount of detectable mRNA in a sample. Yet, this difference in

the number of ciliated cells and thus primary cilia cannot explain the significant differences in *Gli1* and *Ptch1* expression satisfactorily.

Previous studies from AG Pfirrmann showed that cilia of Rmnd5a KO cells are significantly longer compared to WT cells [75]. This previous study, however, measured twice as many primary cilia compared to this study [75], providing the possible explanation for the different results. Moreover, measuring and evaluating primary cilia poses many challenges and are prone to error. Since cilia are protruding organelles extending into the extracellular space, they are likely to be present in random orientation within the microscopic plane, which is the main cause for inaccurate measuring [85]. Additionally, a possible human selection bias cannot be ruled out [85]. Saggesse *et al.* suggest a method to reconstruct each cilium to improve the accuracy of cilia measurement [86]. However, this method is time consuming and requires specific software and expertise for image processing [85]. A novel approach using artificial intelligence (Ai) programmes was described by Bansal *et al* in an effort to overcome the labour intensive, error and bias prone methos currently in use [87]. The authors predict that Ai-based approaches will likely emerge as a standard to achieve less biased and more reproducible results from image acquisition and analysis [87].

Whether primary cilia with dysfunctional Shh signalling are elongated or shortened seems to depend on both the cell type and the reason for the dysfunction. Canterini *et al.* associated the dysregulation of Shh signalling with shorter primary cilia in Npc1-deficient mouse brains [88]. In NIH-3T3 cells treated with Aβ peptides cilia were also shortened and Shh signalling impaired [89]. In contrast, a study by Kanamaru *et al.* demonstrated that over extension of the distal segment of primary cilia decrease Shh activation in NIH-3T3 cells [90]. Shin *et al.* demonstrated that in an Ick-mutant mouse model, cilia impaired in Shh signalling are significantly elongated [91].

Ciliogenesis is also regulated by autophagy, a process used by cells to degrade proteins and organelles [92]. It was shown in HK2 cells that high levels of autophagy result in elongated cilia and inhibition of autophagy decreases cilia length [93], [94]. The interplay between autophagy and primary cilia seems to be even more intricate as two different studies could demonstrate that autophagy is also regulated by primary cilia [95], [96].

To gain a better understanding of the interplay between the Shh pathway and the GID complex, the localisation of different components of the SHH pathway was investigated. As shown in **Figure 10 A**, GLI1 localises to the primary cilium and the nucleus with no apparent differences in the localisation of GLI1 in both cell lines. Measuring and calculating the intensity of relative fluorescence in the cilia and the nucleus similarly showed no significant differences for the cilia (**Figure 10 B**), however, significantly lower signals in the nucleus of Rmnd5a KO cells could be observed (**Figure 10 C**). In a very

similar fashion GLI2 also localises to both primary cilia and nuclei in both cell lines and both tested conditions (**Figure 11**). Strikingly, the amounts of GLI2 in both cilia and nuclei are significantly reduced in Rmnd5a KO cells. This led to the hypothesis that overall GLI2 levels are reduced in Rmnd5a KO cells possibly due to a decrease in *Gli2* expression in KO cells. However, no difference in relative total protein levels was observed between WT and Rmnd5a KO cells in either the cytoplasm nor the nucleus **(Figure 13 B, C)**. Transcriptional defects can also be excluded as the underlying reason for this observation because no significant differences in relative *Gli2* mRNA levels were measured for both cell lines (**Figure 13 D**). As a logical consequence, the different protein concentrations in the primary cilium and the nucleus that were observed in KO cells cannot be explained by a reduction of the overall protein and more likely can be explained by either a defect in protein im- or export from the cilium into the nucleus. Interestingly, relative ciliary PTCH1 levels also differed significantly between the two cell lines (**Figure 8**). However, this observation is not unique to all ciliary proteins that were tested, e.g., SUFU localises to both the axoneme and the nucleus in both WT and KO cells with no significant disparity in relative ciliary amounts of SUFU (**Figure 16**).

It was previously reported that the three GLI proteins (GLI1, GLI2 and GLI3) localise to the distal tip of the primary cilium when Shh signalling is not active [34] as well as upon activation of the Shh signalling pathway [97]–[102]. Other studies showed that GLI2 and GLI3 are present in the entire cilia when Shh signalling is turned off [103]–[106] underlining the importance of the IFT from the basal body of the cilia to the ciliary tip and back. The study by Emechebe *et al.* from 2016 reported that GLI3 localisation upon induction of Shh signalling with the use of SAG did not change but remained over the entire cilia [105].

This work, however, could not show an accumulation of any of the three GLI proteins at the ciliary tip (**Figure 10, 11, 14**) upon activation of Shh signalling using SAG. Still, SAG treatment of both cell lines led to an upregulation of relative mRNA levels of two target genes of the Shh signalling pathway, *Gli1* and *Ptch1* **(Figure 8)** and thus demonstrate a robust activation of the Shh signalling pathway.

Previous experiments performed in the AG Pfirrmann show that Rmnd5a KO cells are still able to perform GLI3 processing and that SAG induction of the Shh signalling pathway resulted in the removal of the GLI3 repressor form (GLI3-R), albeit on a much lower level than in WT cells with an unaffected GLI3 full length (GLI3-FL) to GLI3-R ratio [107].

It can be concluded from these experiments that cells with a dysfunctional GID complex can still regulate the processing of remaining GLI3 proteins. However, the resulting transcriptional signal seems to be too weak and not able to amplify the transcriptional response. Also, these findings suggest that the ciliary proteasome, which was shown to

be required for GLI3 processing [108], is still fully activated by the transition zone-located protein retinitis pigmentosa GTPase regulator-interacting protein 1-like (RPGRIP1L).

Given the evidence, it is probable that the transport of the GLI proteins to the nucleus is in some way corrupted in Rmnd5a KO cells. GLI proteins contain both a nuclear localisation signal (NLS) and a nuclear export signal (NES) which are crucial for the shuttling of these proteins in and out of the nucleus [109]. For a proper function of the Shh signalling pathway, it is essential to keep an ideal balance between GLI protein repressor and activator forms in the nucleus [110]. To date, the process of maintaining this fine balance is not thoroughly understood [110]. The transport of proteins into the nucleus is facilitated by nuclear pore complexes (NPCs) via active carrier-mediated transport [109], [111]. For this, Importin α first binds the cargo protein and then the newly formed complex binds to Importin β. Next, this heterotrimeric complex is shuttled into the nucleus, mediated by the RanGDP-RanGTP gradient [109], [111]. Once inside the nucleus, the complex dissociates and the cargo protein is released [109], [111].

The control of NLS function in GLI proteins is likely to be mediated by phosphorylation [109]. GLI1 can be phosphorylated at a threonine residue, Thr374, located next to the first basic cluster of the NLS by protein kinase A (PKA) [112]. This sequence is conserved among the GLI proteins, as well as in the *Drosophila* homologue Ci [112]. Phosphorylation within or close to classic NLSs is often associated with cytoplasmic protein localisation as it decreases the affinity of cargo to importin α [113].

Zic1 and Zic2 have also been reported to influence the nuclear accumulation of the GLI proteins [109]. Zic proteins interact with GLI proteins physically through their zinc finger domains and an increase in nuclear localisation in transfected cells could be shown [114]–[117].

On the other hand, the exportin Xpo7 was shown to interact with both GLI2 and SUFU to actively transport GLI2 out of the nucleus and in this way influence Shh signalling [110]. However, evidence suggests that Xpo7 does not interact with GLI1, but Xpo1 seems to be necessary for the nuclear export of Gli1 [110]. Depleting cells of Xpo7 increases the activity of Shh signalling [110].

Another way to regulate nuclear translocation of GLI proteins is through SUFU [118]. Knock down of SUFU in both cultured cells and mice leads to a constitutively active Shh signalling pathway [118]. Also, *Sufu* is a known tumour suppressor gene in humans [118]. How exactly SUFU regulates Shh signalling is discussed controversially [110]. There is evidence that it binds to the N-terminal domains of GLI1 and GLI2, thus competing with the binding of Importin α and Importin β [110], [119]. However, other studies suggest that SUFU localises to the nucleus together with GLI proteins and recruits transcriptional co-repressors to GLI-occupied chromatin loci [110], [120].

Additionally, it has been suggested that SUFU is involved in fine-tuning the Xop7-dependent nuclear export of GLI2 and GLI3 [110].

Considering the many different ways of regulating the import and export of the GLI proteins in and out of the nucleus, it is very well possible that the GID complex is somehow involved in one of these processes. It is evident from the significant reduction of GLI1 and GLI2 levels in the nucleus (**Figure 10 – 12**) that the GID complex negatively influences the translocation of GLI proteins to the nucleus. The exact mechanism can only be speculated on. It is clear, however, that the delicate balance of transcription factors in the nucleus is disrupted in cells with a dysfunctional GID complex resulting in aberrant Shh signalling which might be an explanation for the observed reduction in *Ptch1* and *Gli1* expression (**Figure 8**). In this respect, subunits of the GID-complex were described to function as a nucleocytoplasmic mediator of cell morphology [121].

The concentration of GLI2 was measured by western blot analysis performed with nuclear and cytosolic fractions (**Figure 13**) as well as by using fluorescence microscopy and subsequent quantification. While, the overall levels of detected proteins were too low for western blot quantification, GLI2 levels in different subcellular compartments including the nucleus and the axoneme were robustly and reproducibly quantified. Another hypothesis that explains the significant reduction of GLI2 in the axoneme and the nucleus points towards a selective regulation mechanism of ciliary Shh protein homeostasis mediated by the GID complex. This is likely due to defects in protein transport to the primary cilium or even in the transport within the cilium by means of the IFT system.

PTCH1 is located in the primary cilia [78] and responsible for the signal transduction from the cilia to the cytoplasm. In the inactive state of Shh signalling, PTCH1 binds to SMO thus inhibiting this protein and keeping the subsequent signalling turned off. Upon activation of Shh signalling, a ligand (SAG was used in this work) binds to PTCH1, inhibiting its activity and relieving the suppressed SMO and consequently promoting further signalling steps [84]. Therefore, it can be concluded that the reduction of PTCH1 in Rmnd5a KO cells is a possible explanation for a weaker Shh response.

SUFU is a major negative regulator of Shh signalling. When the pathway is turned off, SUFU binds to GLI proteins. It is thought that this prevents their translocation to the nucleus and thus inhibits Shh signalling [122]–[125]. This inhibition seems to be essential for the regulation of the pathway, since it was shown previously that cells deficient in SUFU have a ligand-independent, highly activated Shh pathway [125]–[127]. Since no differences in either localisation or relative amount of SUFU was observed, it can be concluded that the regulating functions of this protein are independent of the GID complex.

Previous findings from AG Pfirrmann and colleagues showed that knock down of *Rmnd5a* in the African claw frog *Xenopus laevis* impacts Shh signalling and results in several phenotypes reminiscent of ciliopathies [107] and that subunits of the GID complex also localize to basal bodies *in vivo*. These observations strengthen the hypothesis that the GID complex is involved in Shh signalling at the primary cilia.

Ciliopathies are a group of disorders involving malfunction of primary cilia [128] and manifest with a wide variety of symptoms [129]. Blocking *rmnd5a* transcription in *X. laevis* led to developmental alterations, including structural brain anomalies and severe eye anomalies. Especially the observed changes in the forebrain seem to be the result of Shh signalling dependent patterning events [107]. This effect, together with the perceived severe defects in craniofacial development [107] are reminiscent with the classic triad of Meckel syndrome that includes cystic renal disease, polydactyly, and a central nervous system malformation [130]. A further study linking the GID complex to ciliopathies is a case study from 2012 by Vogel *et al*. The authors observed a partial duplication of the *RMND5A* gene in a patient with a giant occipital encephalocele and craniofacial anomalies [131]. The defects observed in both *X. laevis* upon knock down of *rmnd5a* and the patient described by Vogel *et al*. resemble those observed in patients with Meckel-Gruber syndrome. From this, it can be hypothesised that the observed Meckel-Gruber-like phenotypes might result from defects in cilia-dependent signalling processes, like Shh signalling, which in turn might be caused by a dysfunctional GID complex. Considering the fact that disrupting the proper function of the GID complex in *X. laevis* leads to ciliopathy-like phenotypes, it might be possible that GID subunits are possible candidate genes for human ciliopathies stemming from defects in Shh signalling.

In conclusion, all components of the Shh signalling pathway investigated in this work were present in both NIH-3T3 WT and Rmnd5a KO cells. No difference regarding the localisation could be observed when both cell types were compared. However, two factors, *Gli1* and *Ptch1*, showed significantly lower mRNA levels in cells with a dysfunctional GID complex. GLI2 and PTCH1 protein levels were also significantly decreased in primary cilia in KO cells.

These results give rise to the hypothesis that the significant reduction of these components of the Shh signalling pathway in the primary cilium is the underlying reason for aberrant Shh signal transduction in cells with a dysfunctional GID complex. Also, these findings suggest a strong relation between the GID complex and primary cilia. It can be hypothesised that the GID complex is indeed involved in the regulation of some ciliary signalling processes like the Shh signalling pathway.

5.2 The role of the GID complex at the primary cilium

The GID complex is a multi-subunit RING E3 ubiquitin ligase [59], first discovered in the yeast *Saccharomyces cerevisiae* [60] where the complex is involved in the shift from gluconeogenesis to glycolysis [61]. Yet, little is known about the mammalian homologue [69], also known as the CTLH-complex [62].

To further investigate the relationship between the GID complex and the primary cilia, experiments were conducted to elucidate the localisation of four different subunits of the complex, i.e., ARMC8, MKLN1, RMND5a and TWA1. All four subunits are located at the primary cilium (**Figure 20**) and additionally, two of these subunits, TWA1 and RMND5a, associate with the centrioles in cycling cells (**Figure 19**). This further strengthens the hypothesis that the GID complex is not only involved in Shh signalling at the primary cilium but plays a much broader role in the regulation of ciliogenesis.

Although several subunits of the GID complex localise to the primary cilium, it cannot be concluded that the GID complex is exclusively located at this cell organelle. It can be speculated that only a subset of GID complex variants in this work called the 'ciliary' GID complex, functions at the primary cilium and that there are many distinct roles this complex plays at various locations of the mammalian cell.

This study shows that both TWA1 and RMND5a only partially co-localise with the centrioles. Possibly, these GID complex components localise with specific sub structures of the centrioles. The centrioles are surrounded by centriolar satellites, small, highly dynamic non-membranous structures [132]. These structures have been reported to be involved in many cellular processes, including ciliogenesis and autophagy [133]. Gheiratmand et al. used BioID analysis to investigate the centriolar satellite proteome and indeed, MKLN1 was found among potential associated proteins of this structure [134], hinting at a potential interaction of at least parts of the GID complex with centriolar satellite proteins. Most centriolar satellite components undergo assembly and disassembly in a cell cycle-dependent manner [132]. Since this structure is highly dynamic, the localisation of many components is not defined to the centrosome, but they can also be found at the basal body, around the nucleus or dispersed in the cytoplasm [132]. How exactly centriolar satellites are involved in the formation and function of primary cilia is complex [132]. It was shown that the recruitment of the BBSome is linked to these structures and five members of the BBSome (BBS2, BBS4, BBS7, BBS8 and BBS9) were found to be part of centriolar satellites [135]. During cilia formation, centriolar satellites were also shown to move negative regulators of ciliogenesis away from the basal body, e.g., the E3 Ubiquitin ligase Mindbomb 1 [136]. It is probable that other E3 ligases are involved in this process and that the GID complex is indeed one of them. Additionally, the Shh signalling pathway is also connected to centriolar satellites. It was reported that cells that still form cilia but are deficient in centriolar satellites have reduced

amounts of SMO in the cilia and thus preventing a proper function of Shh signalling [4], [137]–[139].

The fact that the two subunits of the GID complex MKLN1 and ARMC8 were found only at the axoneme (**Figure 20**) might indicate that the ciliary GID complex is not very stable or exists with different subunit compositions in different organelles. It is possible that the complex is assembled and disassembled according to distinct cellular cues and conditions. It is likely that different components get transported to the ciliary tip and it cannot be ruled out that they show activity in the axoneme. The images taken using immunofluorescence are only snapshots of what is happening in the cells. Other approaches need to be taken to elucidate dynamic events happening in the cilia.

One hypothesis that can be stipulated regarding the role of the GID complex at the primary cilium is that it plays an important role in the vesicle transport to this organelle. Since cilia have no means of synthesising their own proteins, everything needs to be transported to these organelles by using vesicles [140]. Proteins are then transported and distributed in the cilia by the IFT [141]. Consequently, proteins that are no longer needed are removed from the cilia by the same system [141].

A work by Gerhardt *et al.* discovered that several components of the proteasomal system are localised at the primary cilium and dubbed this the 'ciliary proteasome' [108]. The group also found out that proteasomal activity at the primary cilium depends on RPRIP1LI and they could showed that it interacts with Psmd2 at the ciliary TZ [108]. Psmd2 is a part of the 19S subunit of the proteasome [142] which is responsible for the recognition of ubiquitinated proteins [143].

Considering that the GID complex acts as a E3 ligase [59] and marks proteins for degradation by the proteasomal system [61], [62] and its location at the primary cilia leads to the hypothesis that the GID complex is involved in ubiquitinating and thus facilitates the degradation of specific ciliary proteins and consequently alters protein homeostasis. Maintaining protein homeostasis in the primary cilium is crucial for a functioning Shh signalling pathway. This is achieved by a strict regulation of entry and exit of proteins, as well as degradation of proteins at the ciliary base [144]. The differences in Shh signalling between WT and KO cells described in this work can possibly be attributed to disturbances in the said protein homeostasis of primary cilia. It was also previously shown that the ciliary proteasome is essential for GLI3 processing [145]. This is in agreement with the hypothesis that the GID complex is involved in the proper functioning of the Shh signalling pathway.

From the subcellular localisation studies performed in this work, it can be concluded that the GID complex localises to the primary cilia. There are strong indications that the ciliary GID complex is involved in regulating the protein homeostasis in these organelles.

To investigate the possible interaction of the GID complex and other ciliary proteins, e.g., regulators of ciliogenesis, experiments were performed to identify novel interacting partners of GID4. It has been proposed that GID4 is the substrate binding component of the GID complex [72] and was therefore chosen for further experiments. Also, it was shown in this work that overexpression of a GID4-GFP fusion protein interferes with ciliogenesis in both NIH-3T3 WT and Rmnd5a KO cells (see 5.2).

So far, not many substrates of GID4 are known in mammalian cells [63]. Examples of suggested targets for ubiquitination and regulation by the mammalian GID complex include HBP1, LMNB2, PRKAA and its own subunit MKLN1 (see also 1.4.2) [64], [75].

Upon overexpression of a GID4-GFP fusion protein only a small percentage of cells showed signals for both the primary cilium and the fusion protein (**Figure 17 and 18**). This suggests that overexpression of GID4 negatively influences ciliogenesis. In fact, the ectopic expression of Gid4 in *S. cerevisiae* is sufficient to induce substrate degradation independent of its natural inductors [61]. It is thus likely that this function is evolutionary conserved and that overexpression of GID4 induces the degradation of substrates independent of its inducers. In an attempt to identify such substrates that explain a lack of ciliogenesis, we performed several mass spectrometry based experiments to identify GID4 interacting proteins but also to find proteins that are reduced by GID4 overexpression.

In a first approach, GID4 was overexpressed in HEK293 cells and whole cell lysates were analysed using mass spectrometry at Alessandro Ori's lab at the FLI in Jena, yielding 68 proteins which were down regulated. In other experiments GID4 interacting partners were identified using co-immunoprecipitation and subsequent mass spectrometry analysis. By combining both datasets, 27 candidate proteins were identified that both interacted with GID4 and were downregulated by GID4 overexpression (**Table 19**).

Interestingly, eleven out of these 27 proteins are located in the mitochondria or the mitochondrial membrane and five are involved in oxidative phosphorylation and play a part in the regulation of energy homeostasis. AMP-activated protein kinase (AMPK) is a well-known regulator of energy metabolism and autophagy [146] and was previously described as a substrate of the GID-complex [75]. Autophagy ensures that damaged molecules and cellular components are recycled and their building parts are available for the cell again [147]. This is especially important under nutrient stress [147]. Other important function of AMPK are the control of the number of mitochondria per cell and the regulation of factors involved in mitophagy [146]. Mitophagy is a specialised form of autophagy and responsible for the removal of damaged mitochondria thus ensuring

proper cellular functions [148]. A dysfunctional GID complex leads to aberrant levels of AMPK activity [75] which influences mitochondrial biogenesis. It is thus tempting to speculate that the amount of mitochondrial proteins detected using mass spectrometry could be a result of AMPK activity, however it remains enigmatic how GID4 interacts with these components.

Another interesting potential GID interacting partner is the voltage-dependent anion channel 1 (VDAC1) protein. This proteins is involved in the regulation of mitophagy and apoptosis [149]. However, none of these proteins contain a proline at the N-terminus and with that do not fall under the N-end rule, established by the Varshavsky lab for the GID complex in *S. cerevisiae* [72], [73]. This rule states that GID4 as the substrate recognition component of the GID complex recognizes its substrates by a proline at position 1 or 2 of the N-terminus [72]. The existence for an N-end rule in mammalian cells similar to the one found in *S. cerevisiae* is still under debate and previously described substrates of the mammalian GID complex do not contain an N-terminal proline, e.g., HBP1, LMNB2, PRKAA and MKLN1 [67]. However, a recent study discovered a high similarity between the substrate-binding pockets of yeast and human GID4. The authors claim that although those two proteins share only an amino acid sequence identity of about 30%, almost all the residues composing the substrate-binding pocket are strictly conserved [150]. The authors were also able to report crystal structures of human GID4 in complex with various Pro/N-degrons further strengthening the hypothesis that the N-end rule might also be valid for the mammalian GID complex [150]. Taken together, these studies show that more work is needed to elucidate the mechanism by which the mammalian GID complex binds its targets.

To further identify possible new substrates, a BioID assay was performed with GID4 as bait. This assay could detect all subunits of the GID complex and several subunits of AMPK demonstrating the quality of this experiment and further supporting that the GID complex targets AMPK for degradation.

Four out of the 27 candidate proteins established by overexpression and immunoprecipitation are also present in the BioID dataset, namely, FERMT2, PGAM5, PHAX and NR3C1. The remaining 19 proteins listed in **Table 19** were not confirmed by the BioID experiments and are thus less likely to be novel GID4 interacting partners and should not be considered for further investigation.

However, none of these four candidate genes is reported to be localised to the primary cilium. Two proteins, PGAM5 and NR3C1 are localised to the mitochondria and the other two PHAX and FERMT2 localise to the cytoplasm and the nucleus.

Interestingly, PHAX (phosphorylated adaptor for RNA export) is involved in the export of U snRNA from the nucleus which is mediated by XOP1 [151]. XOP1 was shown to be also involved in the export of GLI1 out of the nucleus [110].

The list of GID4 interacting proteins was compared with a known database of ciliary proteins. The BioID assay resulted in 152 possible GID4 interacting partners with a connection to the primary cilium. Interestingly, none of these proteins has a proline at the N-terminus. Listed in **Table 20** are ten proteins with prolines in the N-terminal region, ranging from a proline at position two to position five. The consensus sequence for recognition by the GID complex in *S. cerevisiae* does allow for a proline to be at position one or two, but no other prolines are thought to be recognized [74]. However, as discussed above, it is not clear if these rules also apply to the mammalian GID-complex. A study by Chrustowicz *et al*. identified numerous peptides with non-Pro N-termini that bind to human GID4 with a high affinity using phage display screening [152]. From this, the authors concluded that substrates of the GID complex are not only recognized by their N-terminal residue, but that the pattern of downstream amino acids also plays a crucial role. The authors hypothesised that the degron binding is only a part of substrate targeting, followed by ubiquitination and degradation of the GID complex. It seems that both the pairing of a degron and the configuration of the GID complex in either a simplistic monovalent format or in a multivalent chelator assembly are key to the successful recognition of some of the substrates of the complex [152].

It might be reasonable to compare only the data from the GID 4 co-IP and the BioID and not considering the data of the GID4 over expression. This approach might lead to a slightly different set of potential substrates of the GID complex as in both experiments additional steps to extract only proteins binding to GID4 were performed. On the other hand, omitting the data from the over expression might lead to the oversight of proteins that only bind to GID4 for a short moment and do not form an interaction solid enough to be captured by pull-down techniques. To ensure all interactions are recorded during these experiments, a strategy to cross-link protein-protein interactions might be used.

As of today, it is still unknown how exactly the human GID complex recognises its substrates. The hypotheses discussed in this work show clearly, that more research needs to be done to identify novel GID4 interacting partners and thus new substates of the GID complex. Here, a list of 10 candidate proteins is proposed (Table 4.3) but a lot more needs to be done to investigate these putative GID4 interacting partners further.

6 Summary

The primary cilium is involved in many signalling pathways in mammalian cells, as well as in the development and function of most organs in the human body. It acts as a signalling hub for many important pathways, including the Hedgehog signalling pathway (Hh) which plays a key role during the organogenesis of almost all organs. One of the three described Hh proteins, Sonic hedgehog (Shh) can be activated via the canonical signalling route, involving proteins of the GLI family, which localise to the primary cilium. If the proper assembly or function of this organelle is disrupted, severe conditions, known as ciliopathies, can be the consequence. Primary cilia are rooted to the basal body, a structure derived from centrioles.

A study by Boldt et al. located the mammalian homologue to the GID (glucose induced degradation deficient) complex in close proximity to this structure. The GID complex was first discovered in *Saccharomyces cerevisiae* where it is a key regulator in the metabolic shift from gluconeogenesis to glycolysis. However, little is known about the mammalian GID complex and the roles it plays, especially regarding primary cilia.

The investigations conducted int this work led to the hypothesis that the human GID complex plays an important role in the regulation of Shh signalling. In cells with a dysfunctional GID complex, relative mRNA levels of two key components of the Shh pathway, *Gli1* and *Ptch1*, were significantly reduced. Further investigation led to the result that the localisation of all investigated components of the Shh signalling pathway did not differ between the WT and the KO cell lines. However, differences in the relative amount of GLI1, GLI2 and PTCH1 were observed.

In subsequent experiments it was shown that four components of the GID complex, ARMc8, MKLN1, RMND5a, and TWA1, are located to the primary cilium. This further underlines the existence of an important relationship between these organelles and the GID complex.

This work could also suggest putative novel interacting partners for GID4, the subunit of the GID complex responsible for substrate recognition. However, these potential interacting partners need further investigation and verification.

In summary, this thesis underscores the interplay between the primary cilia and the GID complex in mammalian cells. It could be demonstrated that cells deficient in the GID complex have a modified Shh signalling pathway. Additionally, four subunits of the GID complex were shown to localise to the primary cilia, further strengthening the hypothesis of an intricate relationship between these two players. Lastly, putative novel interacting partners for GID4 could be proposed.

7 References

[1] I. Sánchez and B. D. Dynlacht, 'Cilium assembly and disassembly', *Nat Cell Biol*, vol. 18, no. 7, pp. 711–717, Jul. 2016, doi: 10.1038/ncb3370.

[2] Q. Lu *et al.*, 'Early steps in primary cilium assembly require EHD1/EHD3-dependent ciliary vesicle formation', *Nat Cell Biol*, vol. 17, no. 3, pp. 228–240, Mar. 2015, doi: 10.1038/ncb3109.

[3] M. Fliegauf, T. Benzing, and H. Omran, 'When cilia go bad: cilia defects and ciliopathies', *Nat Rev Mol Cell Biol*, vol. 8, no. 11, pp. 880–893, Nov. 2007, doi: 10.1038/nrm2278.

[4] G. Wheway, L. Nazlamova, and J. T. Hancock, 'Signaling through the Primary Cilium', *Front. Cell Dev. Biol.*, vol. 6, p. 8, Feb. 2018, doi: 10.3389/fcell.2018.00008.

[5] S. Kim and B. D. Dynlacht, 'Assembling a primary cilium', *Current Opinion in Cell Biology*, vol. 25, no. 4, pp. 506–511, Aug. 2013, doi: 10.1016/j.ceb.2013.04.011.

[6] A. M. Fry, M. J. Leaper, and R. Bayliss, 'The primary cilium: Guardian of organ development and homeostasis', *Organogenesis*, vol. 10, no. 1, pp. 62–68, Jan. 2014, doi: 10.4161/org.28910.

[7] H. Ishikawa and W. F. Marshall, 'Intraflagellar Transport and Ciliary Dynamics', *Cold Spring Harb Perspect Biol*, vol. 9, no. 3, p. a021998, Mar. 2017, doi: 10.1101/cshperspect.a021998.

[8] R. Pala, N. Alomari, and S. Nauli, 'Primary Cilium-Dependent Signaling Mechanisms', *IJMS*, vol. 18, no. 11, p. 2272, Oct. 2017, doi: 10.3390/ijms18112272.

[9] Joukov and De Nicolo, 'The Centrosome and the Primary Cilium: The Yin and Yang of a Hybrid Organelle', *Cells*, vol. 8, no. 7, p. 701, Jul. 2019, doi: 10.3390/cells8070701.

[10] M. Mirvis, T. Stearns, and W. James Nelson, 'Cilium structure, assembly, and disassembly regulated by the cytoskeleton', *Biochemical Journal*, vol. 475, no. 14, pp. 2329–2353, Jul. 2018, doi: 10.1042/BCJ20170453.

[11] D. Takao and K. J. Verhey, 'Gated entry into the ciliary compartment', *Cell. Mol. Life Sci.*, vol. 73, no. 1, pp. 119–127, Jan. 2016, doi: 10.1007/s00018-015-2058-0.

[12] F. R. Garcia-Gonzalo and J. F. Reiter, 'Scoring a backstage pass: Mechanisms of ciliogenesis and ciliary access', *Journal of Cell Biology*, vol. 197, no. 6, pp. 697–709, Jun. 2012, doi: 10.1083/jcb.201111146.

[13] F. R. Garcia-Gonzalo and J. F. Reiter, 'Open Sesame: How Transition Fibers and the Transition Zone Control Ciliary Composition', *Cold Spring Harb Perspect Biol*, vol. 9, no. 2, p. a028134, Feb. 2017, doi: 10.1101/cshperspect.a028134.

[14] H. Ishikawa and W. F. Marshall, 'Ciliogenesis: building the cell's antenna', *Nat Rev Mol Cell Biol*, vol. 12, no. 4, pp. 222–234, Apr. 2011, doi: 10.1038/nrm3085.

[15] J. Gonçalves and L. Pelletier, 'The Ciliary Transition Zone: Finding the Pieces and Assembling the Gate', *Molecules and Cells*, vol. 40, no. 4, pp. 243–253, Apr. 2017, doi: 10.14348/molcells.2017.0054.

[16] K. F. Lechtreck, 'IFT–Cargo Interactions and Protein Transport in Cilia', *Trends in Biochemical Sciences*, vol. 40, no. 12, pp. 765–778, Dec. 2015, doi: 10.1016/j.tibs.2015.09.003.

[17] S. Webb, A. G. Mukhopadhyay, and A. J. Roberts, 'Intraflagellar transport trains and motors: Insights from structure', *Seminars in Cell & Developmental Biology*, vol. 107, pp. 82–90, Nov. 2020, doi: 10.1016/j.semcdb.2020.05.021.

[18] J. L. Wingfield, K.-F. Lechtreck, and E. Lorentzen, 'Trafficking of ciliary membrane proteins by the intraflagellar transport/BBSome machinery', *Essays in Biochemistry*, vol. 62, no. 6, pp. 753–763, Dec. 2018, doi: 10.1042/EBC20180030.

[19] M. Taschner and E. Lorentzen, 'The Intraflagellar Transport Machinery', *Cold Spring Harb Perspect Biol*, vol. 8, no. 10, p. a028092, Oct. 2016, doi: 10.1101/cshperspect.a028092.

[20] C. Nüsslein-Volhard and E. Wieschaus, 'Mutations affecting segment number and polarity in Drosophila', *Nature*, vol. 287, no. 5785, pp. 795–801, Oct. 1980, doi: 10.1038/287795a0.

[21] G. B. Carballo, J. R. Honorato, G. P. F. de Lopes, and T. C. L. de S. e Spohr, 'A highlight on Sonic hedgehog pathway', *Cell Commun Signal*, vol. 16, no. 1, p. 11, Dec. 2018, doi: 10.1186/s12964-018-0220-7.

[22] M. Wijgerde, M. Ooms, J. W. Hoogerbrugge, and J. A. Grootegoed, 'Hedgehog Signaling in Mouse Ovary: Indian Hedgehog and Desert Hedgehog from Granulosa Cells Induce Target Gene Expression in Developing Theca Cells', *Endocrinology*, vol. 146, no. 8, pp. 3558–3566, Aug. 2005, doi: 10.1210/en.2005-0311.

[23] H. H.-C. Yao, 'Desert Hedgehog/Patched 1 signaling specifies fetal Leydig cell fate in testis organogenesis', *Genes & Development*, vol. 16, no. 11, pp. 1433–1440, Jun. 2002, doi: 10.1101/gad.981202.

[24] M. J. Bitgood, L. Shen, and A. P. McMahon, 'Sertoli cell signaling by Desert hedgehog regulates the male germline', *Current Biology*, vol. 6, no. 3, pp. 298–304, Mar. 1996, doi: 10.1016/S0960-9822(02)00480-3.

[25] T. Rimkus, R. Carpenter, S. Qasem, M. Chan, and H.-W. Lo, 'Targeting the Sonic Hedgehog Signaling Pathway: Review of Smoothened and GLI Inhibitors', *Cancers*, vol. 8, no. 2, p. 22, Feb. 2016, doi: 10.3390/cancers8020022.

[26] Z. Choudhry *et al.*, 'Sonic hedgehog signalling pathway: a complex network', *ANS*, vol. 21, no. 1, Jan. 2014, doi: 10.5214/ans.0972.7531.210109.

[27] P. B. Desai, M. W. Stuck, B. Lv, and G. J. Pazour, 'Ubiquitin links smoothened to intraflagellar transport to regulate Hedgehog signaling', *Journal of Cell Biology*, vol. 219, no. 7, p. e201912104, Jul. 2020, doi: 10.1083/jcb.201912104.

[28] N. Denef, D. Neubüser, L. Perez, and S. M. Cohen, 'Hedgehog Induces Opposite Changes in Turnover and Subcellular Localization of Patched and Smoothened', *Cell*, vol. 102, no. 4, pp. 521–531, Aug. 2000, doi: 10.1016/S0092-8674(00)00056-8.

[29] A. Ruiz i Altaba, 'Catching a Gli-mpse of Hedgehog', *Cell*, vol. 90, no. 2, pp. 193–196, Jul. 1997, doi: 10.1016/S0092-8674(00)80325-6.

[30] H. Sasaki, 'Gli2 as a mediator of Shh signaling', p. 10.

[31] J. Kim, M. Kato, and P. A. Beachy, 'Gli2 trafficking links Hedgehog-dependent activation of Smoothened in the primary cilium to transcriptional activation in the nucleus', *Proceedings of the National Academy of Sciences*, vol. 106, no. 51, pp. 21666–21671, Dec. 2009, doi: 10.1073/pnas.0912180106.

[32] E. K. Schrader, K. G. Harstad, R. A. Holmgren, and A. MatouscHEK, 'A Three-part Signal Governs Differential Processing of Gli1 and Gli3 Proteins by the Proteasome', *Journal of Biological Chemistry*, vol. 286, no. 45, pp. 39051–39058, Nov. 2011, doi: 10.1074/jbc.M111.274993.

[33] G. Canettieri *et al.*, 'Histone deacetylase and Cullin3–RENKCTD11 ubiquitin ligase interplay regulates Hedgehog signalling through Gli acetylation', *Nat Cell Biol*, vol. 12, no. 2, pp. 132–142, Feb. 2010, doi: 10.1038/ncb2013.

[34] C. J. Haycraft, B. Banizs, Y. Aydin-Son, Q. Zhang, E. J. Michaud, and B. K. Yoder, 'Gli2 and Gli3 Localize to Cilia and Require the Intraflagellar Transport Protein Polaris for Processing and Function', *PLoS Genet*, vol. 1, no. 4, pp. 480–488, 2005.

[35] A. Hershko, 'THE UBIQUITIN SYSTEM', p. 57, 1998.

[36] D. Komander and M. Rape, 'The Ubiquitin Code', *Annu. Rev. Biochem.*, vol. 81, no. 1, pp. 203–229, Jul. 2012, doi: 10.1146/annurev-biochem-060310-170328.

[37] C. E. Berndsen and C. Wolberger, 'New insights into ubiquitin E3 ligase mechanism', *Nat Struct Mol Biol*, vol. 21, no. 4, pp. 301–307, Apr. 2014, doi: 10.1038/nsmb.2780.

[38] S. Vijay-kumar, C. E. Bugg, and W. J. Cook, 'Structure of ubiquitin refined at 1.8 Å resolution', *Journal of Molecular Biology*, vol. 194, no. 3, pp. 531–544, Apr. 1987, doi: 10.1016/0022-2836(87)90679-6.

[39] D. Finley, 'Recognition and Processing of Ubiquitin-Protein Conjugates by the Proteasome', *Annu. Rev. Biochem.*, vol. 78, no. 1, pp. 477–513, Jun. 2009, doi: 10.1146/annurev.biochem.78.081507.101607.

[40] E. Sakata, M. R. Eisele, and W. Baumeister, 'Molecular and cellular dynamics of the 26S proteasome', *Biochimica et Biophysica Acta (BBA) - Proteins and Proteomics*, vol. 1869, no. 3, p. 140583, Mar. 2021, doi: 10.1016/j.bbapap.2020.140583.

[41] R. J. Deshaies and C. A. P. Joazeiro, 'RING Domain E3 Ubiquitin Ligases', *Annu. Rev. Biochem.*, vol. 78, no. 1, pp. 399–434, Jun. 2009, doi: 10.1146/annurev.biochem.78.101807.093809.

[42] M. B. Metzger, J. N. Pruneda, R. E. Klevit, and A. M. Weissman, 'RING-type E3 ligases: Master manipulators of E2 ubiquitin-conjugating enzymes and ubiquitination', *Biochimica*

et Biophysica Acta (BBA) - Molecular Cell Research, vol. 1843, no. 1, pp. 47–60, Jan. 2014, doi: 10.1016/j.bbamcr.2013.05.026.

[43] N. Zheng and N. Shabek, 'Ubiquitin Ligases: Structure, Function, and Regulation', *Annu. Rev. Biochem.*, vol. 86, no. 1, pp. 129–157, Jun. 2017, doi: 10.1146/annurev-biochem-060815-014922.

[44] W. Li *et al.*, 'Genome-Wide and Functional Annotation of Human E3 Ubiquitin Ligases Identifies MULAN, a Mitochondrial E3 that Regulates the Organelle's Dynamics and Signaling', *PLoS ONE*, vol. 3, no. 1, p. e1487, Jan. 2008, doi: 10.1371/journal.pone.0001487.

[45] M. B. Metzger, V. A. Hristova, and A. M. Weissman, 'HECT and RING finger families of E3 ubiquitin ligases at a glance', *Journal of Cell Science*, vol. 125, no. 3, pp. 531–537, Feb. 2012, doi: 10.1242/jcs.091777.

[46] D. M. Wenzel and R. E. Klevit, 'Following Ariadne's thread: a new perspective on RBR ubiquitin ligases', *BMC Biol*, vol. 10, no. 1, p. 24, Dec. 2012, doi: 10.1186/1741-7007-10-24.

[47] J. M. Huibregtse, 'A family of proteins structurally and functionally related to the E6-AP ubiquitin-protein ligase', p. 5.

[48] P. de Bie and A. Ciechanover, 'Ubiquitination of E3 ligases: self-regulation of the ubiquitin system via proteolytic and non-proteolytic mechanisms', *Cell Death Differ*, vol. 18, no. 9, pp. 1393–1402, Sep. 2011, doi: 10.1038/cdd.2011.16.

[49] M. M. Savitski *et al.*, 'Multiplexed Proteome Dynamics Profiling Reveals Mechanisms Controlling Protein Homeostasis', *Cell*, vol. 173, no. 1, pp. 260-274.e25, Mar. 2018, doi: 10.1016/j.cell.2018.02.030.

[50] P. Grandi and M. Bantscheff, 'Advanced proteomics approaches to unravel protein homeostasis', *Drug Discovery Today: Technologies*, vol. 31, pp. 99–108, Apr. 2019, doi: 10.1016/j.ddtec.2019.02.001.

[51] B. Coll-Martínez and B. Crosas, 'How the 26S Proteasome Degrades Ubiquitinated Proteins in the Cell', *Biomolecules*, vol. 9, no. 9, p. 395, Aug. 2019, doi: 10.3390/biom9090395.

[52] L. Budenholzer, C. L. Cheng, Y. Li, and M. Hochstrasser, 'Proteasome Structure and Assembly', *Journal of Molecular Biology*, vol. 429, no. 22, pp. 3500–3524, Nov. 2017, doi: 10.1016/j.jmb.2017.05.027.

[53] A. Varshavsky, 'Naming a targeting signal', *Cell*, vol. 64, no. 1, pp. 13–15, Jan. 1991, doi: 10.1016/0092-8674(91)90202-A.

[54] H. Ella, Y. Reiss, and T. Ravid, 'The Hunt for Degrons of the 26S Proteasome', *Biomolecules*, vol. 9, no. 6, p. 230, Jun. 2019, doi: 10.3390/biom9060230.

[55] M.-K. Sung, J. M. Reitsma, M. J. Sweredoski, S. Hess, and R. J. Deshaies, 'Ribosomal proteins produced in excess are degraded by the ubiquitin–proteasome system', *MBoC*, vol. 27, no. 17, pp. 2642–2652, Sep. 2016, doi: 10.1091/mbc.e16-05-0290.

[56] J. C. Rosenbaum *et al.*, 'Disorder Targets Misorder in Nuclear Quality Control Degradation: A Disordered Ubiquitin Ligase Directly Recognizes Its Misfolded Substrates', *Molecular Cell*, vol. 41, no. 1, pp. 93–106, Jan. 2011, doi: 10.1016/j.molcel.2010.12.004.

[57] A. Varshavsky, 'N-degron and C-degron pathways of protein degradation', *Proc Natl Acad Sci USA*, vol. 116, no. 2, pp. 358–366, Jan. 2019, doi: 10.1073/pnas.1816596116.

[58] T. Ravid and M. Hochstrasser, 'Diversity of degradation signals in the ubiquitin–proteasome system', *Nat Rev Mol Cell Biol*, vol. 9, no. 9, pp. 679–689, Sep. 2008, doi: 10.1038/nrm2468.

[59] R. Menssen *et al.*, 'Exploring the Topology of the Gid Complex, the E3 Ubiquitin Ligase Involved in Catabolite-induced Degradation of Gluconeogenic Enzymes', *Journal of Biological Chemistry*, vol. 287, no. 30, pp. 25602–25614, Jul. 2012, doi: 10.1074/jbc.M112.363762.

[60] J. Regelmann *et al.*, 'Catabolite Degradation of Fructose-1,6-bisphosphatase in the Yeast *Saccharomyces cerevisiae*: A Genome-wide Screen Identifies Eight Novel *GID* Genes and Indicates the Existence of Two Degradation Pathways', *MBoC*, vol. 14, no. 4, pp. 1652–1663, Apr. 2003, doi: 10.1091/mbc.e02-08-0456.

[61] O. Santt *et al.*, 'The Yeast GID Complex, a Novel Ubiquitin Ligase (E3) Involved in the Regulation of Carbohydrate Metabolism', *MBoC*, vol. 19, no. 8, pp. 3323–3333, Aug. 2008, doi: 10.1091/mbc.e08-03-0328.

[62] M. E. R. Maitland *et al.*, 'The mammalian CTLH complex is an E3 ubiquitin ligase that targets its subunit muskelin for degradation', *Sci Rep*, vol. 9, no. 1, p. 9864, Dec. 2019, doi: 10.1038/s41598-019-46279-5.

[63] O. Francis, F. Han, and J. C. Adams, 'Molecular Phylogeny of a RING E3 Ubiquitin Ligase, Conserved in Eukaryotic Cells and Dominated by Homologous Components, the Muskelin/RanBPM/CTLH Complex', *PLoS ONE*, vol. 8, no. 10, p. e75217, Oct. 2013, doi: 10.1371/journal.pone.0075217.

[64] M. E. R. Maitland, M. Kuljanin, X. Wang, G. A. Lajoie, and C. Schild-Poulter, 'Proteomic analysis of ubiquitination substrates reveals a CTLH E3 ligase complex-dependent regulation of glycolysis', *FASEB j.*, vol. 35, no. 9, Sep. 2021, doi: 10.1096/fj.202100664R.

[65] H. Liu and T. Pfirrmann, 'The Gid-complex: an emerging player in the ubiquitin ligase league', *Biological Chemistry*, vol. 400, no. 11, pp. 1429–1441, Nov. 2019, doi: 10.1515/hsz-2019-0139.

[66] N. Kobayashi *et al.*, 'RanBPM, Muskelin, p48EMLP, p44CTLH, and the armadillo-repeat proteins ARMC8α and ARMC8β are components of the CTLH complex', *Gene*, vol. 396, no. 2, pp. 236–247, Jul. 2007, doi: 10.1016/j.gene.2007.02.032.

[67] F. Lampert *et al.*, 'The multi-subunit GID/CTLH E3 ubiquitin ligase promotes cell proliferation and targets the transcription factor Hbp1 for degradation', *eLife*, vol. 7, p. e35528, Jun. 2018, doi: 10.7554/eLife.35528.

[68] T. Pfirrmann, P. Villavicencio-Lorini, A. K. Subudhi, R. Menssen, D. H. Wolf, and T. Hollemann, 'RMND5 from Xenopus laevis Is an E3 Ubiquitin-Ligase and Functions in Early Embryonic Forebrain Development', *PLoS ONE*, vol. 10, no. 3, p. e0120342, Mar. 2015, doi: 10.1371/journal.pone.0120342.

[69] S. Qiao *et al.*, 'Interconversion between Anticipatory and Active GID E3 Ubiquitin Ligase Conformations via Metabolically Driven Substrate Receptor Assembly', *Molecular Cell*, vol. 77, no. 1, pp. 150-163.e9, Jan. 2020, doi: 10.1016/j.molcel.2019.10.009.

[70] B. Braun, T. Pfirrmann, R. Menssen, K. Hofmann, H. Scheel, and D. H. Wolf, 'Gid9, a second RING finger protein contributes to the ubiquitin ligase activity of the Gid complex required for catabolite degradation', *FEBS Letters*, vol. 585, no. 24, pp. 3856–3861, Dec. 2011, doi: 10.1016/j.febslet.2011.10.038.

[71] R. Menssen, K. Bui, and D. H. Wolf, 'Regulation of the Gid ubiquitin ligase recognition subunit Gid4', *FEBS Lett*, vol. 592, no. 19, pp. 3286–3294, Oct. 2018, doi: 10.1002/1873-3468.13229.

[72] S.-J. Chen, X. Wu, B. Wadas, J.-H. Oh, and A. Varshavsky, 'An N-end rule pathway that recognizes proline and destroys gluconeogenic enzymes', *Science*, vol. 355, no. 6323, p. eaal3655, Jan. 2017, doi: 10.1126/science.aal3655.

[73] A. Melnykov, S.-J. Chen, and A. Varshavsky, 'Gid10 as an alternative N-recognin of the Pro/N-degron pathway', *Proc Natl Acad Sci USA*, vol. 116, no. 32, pp. 15914–15923, Aug. 2019, doi: 10.1073/pnas.1908304116.

[74] C. Dong *et al.*, 'Recognition of nonproline N-terminal residues by the Pro/N-degron pathway', *Proc Natl Acad Sci USA*, vol. 117, no. 25, pp. 14158–14167, Jun. 2020, doi: 10.1073/pnas.2007085117.

[75] H. Liu *et al.*, 'The GID ubiquitin ligase complex is a regulator of AMPK activity and organismal lifespan', *Autophagy*, vol. 16, no. 9, pp. 1618–1634, Sep. 2020, doi: 10.1080/15548627.2019.1695399.

[76] UK10K Rare Diseases Group *et al.*, 'An organelle-specific protein landscape identifies novel diseases and molecular mechanisms', *Nat Commun*, vol. 7, no. 1, p. 11491, Sep. 2016, doi: 10.1038/ncomms11491.

[77] K. J. Roux, D. I. Kim, M. Raida, and B. Burke, 'A promiscuous biotin ligase fusion protein identifies proximal and interacting proteins in mammalian cells', *Journal of Cell Biology*, vol. 196, no. 6, pp. 801–810, Mar. 2012, doi: 10.1083/jcb.201112098.

[78] R. Rohatgi, L. Milenkovic, and M. P. Scott, 'Patched1 Regulates Hedgehog Signaling at the Primary Cilium', *Science*, vol. 317, no. 5836, pp. 372–376, Jul. 2007, doi: 10.1126/science.1139740.

[79] S. S. V. Vasquez, J. van Dam, and G. Wheway, 'An updated SYSCILIA gold standard (SCGSv2) of known ciliary genes, revealing the vast progress that has been made in the cilia research field', *MBoC*, vol. 32, no. 22, p. br13, Dec. 2021, doi: 10.1091/mbc.E21-05-0226.

[80] D. A. Hoey, M. E. Downs, and C. R. Jacobs, 'The mechanics of the primary cilium: An intricate structure with complex function', *Journal of Biomechanics*, vol. 45, no. 1, pp. 17–26, Jan. 2012, doi: 10.1016/j.jbiomech.2011.08.008.

[81] D. K. Song, J. H. Choi, and M.-S. Kim, 'Primary Cilia as a Signaling Platform for Control of Energy Metabolism', *Diabetes Metab J*, vol. 42, no. 2, p. 117, 2018, doi: 10.4093/dmj.2018.42.2.117.

[82] S. Pietrobono, S. Gagliardi, and B. Stecca, 'Non-canonical Hedgehog Signaling Pathway in Cancer: Activation of GLI Transcription Factors Beyond Smoothened', *Front. Genet.*, vol. 10, p. 556, Jun. 2019, doi: 10.3389/fgene.2019.00556.

[83] Y. Pan, C. B. Bai, A. L. Joyner, and B. Wang, 'Sonic hedgehog Signaling Regulates Gli2 Transcriptional Activity by Suppressing Its Processing and Degradation', *Mol Cell Biol*, vol. 26, no. 9, pp. 3365–3377, May 2006, doi: 10.1128/MCB.26.9.3365-3377.2006.

[84] F. Bangs and K. V. Anderson, 'Primary Cilia and Mammalian Hedgehog Signaling', *Cold Spring Harb Perspect Biol*, vol. 9, no. 5, p. a028175, May 2017, doi: 10.1101/cshperspect.a028175.

[85] A. Dummer, C. Poelma, M. C. DeRuiter, M.-J. T. H. Goumans, and B. P. Hierck, 'Measuring the primary cilium length: improved method for unbiased high-throughput analysis', *Cilia*, vol. 5, no. 1, p. 7, Dec. 2016, doi: 10.1186/s13630-016-0028-2.

[86] T. Saggese, A. A. Young, C. Huang, K. Braeckmans, and S. R. McGlashan, 'Development of a method for the measurement of primary cilia length in 3D', *Cilia*, vol. 1, no. 1, p. 11, Dec. 2012, doi: 10.1186/2046-2530-1-11.

[87] R. Bansal, S. E. Engle, T. K. Kamba, K. M. Brewer, W. R. Lewis, and N. F. Berbari, 'Artificial Intelligence Approaches to Assessing Primary Cilia', *JoVE*, no. 171, p. 62521, May 2021, doi: 10.3791/62521.

[88] S. Canterini *et al.*, 'Shortened primary cilium length and dysregulated Sonic hedgehog signaling in Niemann-Pick C1 disease', *Human Molecular Genetics*, vol. 26, no. 12, pp. 2277–2289, Jun. 2017, doi: 10.1093/hmg/ddx118.

[89] A. G. Vorobyeva and A. J. Saunders, 'Amyloid-β interrupts canonical Sonic hedgehog signaling by distorting primary cilia structure', *Cilia*, vol. 7, no. 1, p. 5, Dec. 2018, doi: 10.1186/s13630-018-0059-y.

[90] T. Kanamaru, A. Neuner, B. Kurtulmus, and G. Pereira, 'Balancing the length of the distal tip by septins is key for stability and signalling function of primary cilia', *The EMBO Journal*, vol. 41, no. 1, Jan. 2022, doi: 10.15252/embj.2021108843.

[91] J.-O. Shin *et al.*, 'Activation of sonic hedgehog signaling by a Smoothened agonist restores congenital defects in mouse models of endocrine-cerebro-osteodysplasia syndrome', *EBioMedicine*, vol. 49, pp. 305–317, Nov. 2019, doi: 10.1016/j.ebiom.2019.10.016.

[92] Morleo and Franco, 'The Autophagy-Cilia Axis: An Intricate Relationship', *Cells*, vol. 8, no. 8, p. 905, Aug. 2019, doi: 10.3390/cells8080905.

[93] Z. Tang *et al.*, 'Autophagy promotes primary ciliogenesis by removing OFD1 from centriolar satellites', *Nature*, vol. 502, no. 7470, pp. 254–257, Oct. 2013, doi: 10.1038/nature12606.

[94] S. Wang, M. J. Livingston, Y. Su, and Z. Dong, 'Reciprocal regulation of cilia and autophagy via the MTOR and proteasome pathways', *Autophagy*, vol. 11, no. 4, pp. 607–616, Apr. 2015, doi: 10.1080/15548627.2015.1023983.

[95] O. Pampliega *et al.*, 'Functional interaction between autophagy and ciliogenesis', *Nature*, vol. 502, no. 7470, pp. 194–200, Oct. 2013, doi: 10.1038/nature12639.

[96] I. Orhon, N. Dupont, O. Pampliega, A. M. Cuervo, and P. Codogno, 'Autophagy and regulation of cilia function and assembly', *Cell Death Differ*, vol. 22, no. 3, pp. 389–397, Mar. 2015, doi: 10.1038/cdd.2014.171.

[97] M.-H. Chen *et al.*, 'Cilium-independent regulation of Gli protein function by Sufu in Hedgehog signaling is evolutionarily conserved', *Genes Dev.*, vol. 23, no. 16, pp. 1910–1928, Aug. 2009, doi: 10.1101/gad.1794109.

[98] F. Massa *et al.*, 'The deubiquitinating enzyme Usp14 controls ciliogenesis and Hedgehog signaling', *Human Molecular Genetics*, vol. 28, no. 5, pp. 764–777, Mar. 2019, doi: 10.1093/hmg/ddy380.

[99] H. Moon *et al.*, 'Intestinal cell kinase, a protein associated with endocrine-cerebro-osteodysplasia syndrome, is a key regulator of cilia length and Hedgehog signaling', *Proceedings of the National Academy of Sciences*, vol. 111, no. 23, pp. 8541–8546, Jun. 2014, doi: 10.1073/pnas.1323161111.

[100] X. Wen, C. K. Lai, M. Evangelista, J.-A. Hongo, F. J. de Sauvage, and S. J. Scales, 'Kinetics of Hedgehog-Dependent Full-Length Gli3 Accumulation in Primary Cilia and Subsequent Degradation', *Mol Cell Biol*, vol. 30, no. 8, pp. 1910–1922, Apr. 2010, doi: 10.1128/MCB.01089-09.

[101] N. Yang, L. Li, T. Eguether, J. P. Sundberg, G. J. Pazour, and J. Chen, 'Intraflagellar transport 27 is essential for hedgehog signaling but dispensable for ciliogenesis during hair follicle morphogenesis', *Development*, vol. 142, no. 12, pp. 2194–2202, Jun. 2015, doi: 10.1242/dev.115261.

[102] S. Yoshida *et al.*, 'The novel ciliogenesis regulator DYRK2 governs Hedgehog signaling during mouse embryogenesis', *eLife*, vol. 9, p. e57381, Aug. 2020, doi: 10.7554/eLife.57381.

[103] C. A. Clement *et al.*, 'The primary cilium coordinates early cardiogenesis and hedgehog signaling in cardiomyocyte differentiation', *Journal of Cell Science*, vol. 122, no. 17, pp. 3070–3082, Sep. 2009, doi: 10.1242/jcs.049676.

[104] D. L. Egeberg *et al.*, 'Primary cilia and aberrant cell signaling in epithelial ovarian cancer', *Cilia*, vol. 1, no. 1, p. 15, Dec. 2012, doi: 10.1186/2046-2530-1-15.

[105] U. Emechebe *et al.*, 'T-box3 is a ciliary protein and regulates stability of the Gli3 transcription factor to control digit number', *eLife*, vol. 5, p. e07897, Apr. 2016, doi: 10.7554/eLife.07897.

[106] E. N. Kiprilov *et al.*, 'Human embryonic stem cells in culture possess primary cilia with hedgehog signaling machinery', *Journal of Cell Biology*, vol. 180, no. 5, pp. 897–904, Mar. 2008, doi: 10.1083/jcb.200706028.

[107] Hantel, Friederike and Liu, Huaize, 'Cilia-localized GID/CTLH ubiquitin ligase complex regulates protein homeostasis of Sonic Hedgehog signaling components', *Journal of Cell Science*, vol. 135, doi: 10.1242/jcs.259209.

[108] C. Gerhardt *et al.*, 'The transition zone protein Rpgrip1l regulates proteasomal activity at the primary cilium', *Journal of Cell Biology*, vol. 210, no. 1, pp. 1027–1045, Jul. 2015, doi: 10.1083/jcb.201408060.

[109] M. Hatayama and J. Aruga, 'Gli Protein Nuclear Localization Signal', in *Vitamins & Hormones*, vol. 88, Elsevier, 2012, pp. 73–89. doi: 10.1016/B978-0-12-394622-5.00004-3.

[110] Ł. Markiewicz, T. Uśpieński, B. Baran, S. M. Niedziółka, and P. Niewiadomski, 'Xpo7 negatively regulates Hedgehog signaling by exporting Gli2 from the nucleus', *Cellular Signalling*, vol. 80, p. 109907, Apr. 2021, doi: 10.1016/j.cellsig.2020.109907.

[111] B. Alberts, Ed., *Molecular biology of the cell*, 5th ed. New York: Garland Science, 2008.

[112] T. Sheng, S. Chi, X. Zhang, and J. Xie, 'Regulation of Gli1 Localization by the cAMP/Protein Kinase A Signaling Axis through a Site Near the Nuclear Localization Signal', *Journal of Biological Chemistry*, vol. 281, no. 1, pp. 9–12, Jan. 2006, doi: 10.1074/jbc.C500300200.

[113] M. T. Harreman, T. M. Kline, H. G. Milford, M. B. Harben, A. E. Hodel, and A. H. Corbett, 'Regulation of Nuclear Import by Phosphorylation Adjacent to Nuclear Localization Signals', *Journal of Biological Chemistry*, vol. 279, no. 20, pp. 20613–20621, May 2004, doi: 10.1074/jbc.M401720200.

[114] D. W. Chan *et al.*, 'Zic2 synergistically enhances Hedgehog signalling through nuclear retention of Gli1 in cervical cancer cells', *J. Pathol.*, vol. 225, no. 4, pp. 525–534, Dec. 2011, doi: 10.1002/path.2901.

[115] Y. Koyabu, K. Nakata, K. Mizugishi, J. Aruga, and K. Mikoshiba, 'Physical and Functional Interactions between Zic and Gli Proteins', *Journal of Biological Chemistry*, vol. 276, no. 10, pp. 6889–6892, Mar. 2001, doi: 10.1074/jbc.C000773200.

[116] V. Nguyen, A. L. Chokas, B. Stecca, and A. R. i Altaba, 'Cooperative requirement of the Gli proteins in neurogenesis', *Development*, vol. 132, no. 14, pp. 3267–3279, Jul. 2005, doi: 10.1242/dev.01905.

[117] K. Mizugishi, J. Aruga, K. Nakata, and K. Mikoshiba, 'Molecular Properties of Zic Proteins as Transcriptional Regulators and Their Relationship to GLI Proteins', *Journal of Biological Chemistry*, vol. 276, no. 3, pp. 2180–2188, Jan. 2001, doi: 10.1074/jbc.M004430200.

[118] E. W. Humke, K. V. Dorn, L. Milenkovic, M. P. Scott, and R. Rohatgi, 'The output of Hedgehog signaling is controlled by the dynamic association between Suppressor of Fused and the Gli proteins', *Genes Dev.*, vol. 24, no. 7, pp. 670–682, Apr. 2010, doi: 10.1101/gad.1902910.

[119] A. Szczepny *et al.*, 'Overlapping binding sites for importin β1 and suppressor of fused (SuFu) on glioma-associated oncogene homologue 1 (Gli1) regulate its nuclear localization', *Biochemical Journal*, vol. 461, no. 3, pp. 469–476, Aug. 2014, doi: 10.1042/BJ20130709.

[120] Z. Zhang *et al.*, 'Suppressor of Fused Chaperones Gli Proteins To Generate Transcriptional Responses to Sonic Hedgehog Signaling', *Mol Cell Biol*, vol. 37, no. 3, pp. e00421-16, Feb. 2017, doi: 10.1128/MCB.00421-16.

[121] M. Valiyaveettil *et al.*, 'Novel role of the muskelin–RanBP9 complex as a nucleocytoplasmic mediator of cell morphology regulation', *Journal of Cell Biology*, vol. 182, no. 4, pp. 727–739, Aug. 2008, doi: 10.1083/jcb.200801133.

[122] Q. Ding *et al.*, 'Mouse Suppressor of fused is a negative regulator of Sonic hedgehog signaling and alters the subcellular distribution of Gli1', *Current Biology*, vol. 9, no. 19, pp. 1119-S1, Oct. 1999, doi: 10.1016/S0960-9822(99)80482-5.

[123] P. Kogerman *et al.*, 'Mammalian Suppressor-of-Fused modulates nuclear–cytoplasmic shuttling of GLI-1', *Nat Cell Biol*, vol. 1, no. 5, pp. 312–319, Sep. 1999, doi: 10.1038/13031.

[124] N. Methot and K. Basler, 'Suppressor of fused opposes hedgehog signal transduction by impeding nuclear accumulation of the activator form of Cubitus interruptus', *Development*, vol. 127, no. 18, pp. 4001–4010, Sep. 2000, doi: 10.1242/dev.127.18.4001.

[125] H. Tukachinsky, L. V. Lopez, and A. Salic, 'A mechanism for vertebrate Hedgehog signaling: recruitment to cilia and dissociation of SuFu–Gli protein complexes', *Journal of Cell Biology*, vol. 191, no. 2, pp. 415–428, Oct. 2010, doi: 10.1083/jcb.201004108.

[126] A. F. Cooper *et al.*, 'Cardiac and CNS defects in a mouse with targeted disruption of suppressor of fused', *Development*, vol. 132, no. 19, pp. 4407–4417, Oct. 2005, doi: 10.1242/dev.02021.

[127] J. Svärd *et al.*, 'Genetic Elimination of Suppressor of Fused Reveals an Essential Repressor Function in the Mammalian Hedgehog Signaling Pathway', *Developmental Cell*, vol. 10, no. 2, pp. 187–197, Feb. 2006, doi: 10.1016/j.devcel.2005.12.013.

[128] J. F. Reiter and M. R. Leroux, 'Genes and molecular pathways underpinning ciliopathies', *Nat Rev Mol Cell Biol*, vol. 18, no. 9, pp. 533–547, Sep. 2017, doi: 10.1038/nrm.2017.60.

[129] F. Hildebrandt, T. Benzing, and N. Katsanis, 'Ciliopathies', *N Engl J Med*, vol. 364, no. 16, pp. 1533–1543, Apr. 2011, doi: 10.1056/NEJMra1010172.

[130] C. Wright, R. Healicon, C. English, and J. Burn, 'Meckel syndrome: what are the minimum diagnostic criteria?', *Journal of Medical Genetics*, vol. 31, no. 6, pp. 482–485, Jun. 1994, doi: 10.1136/jmg.31.6.482.

[131] T. W. Vogel, S. Manjila, and A. R. Cohen, 'Novel neurodevelopmental disorder in the case of a giant occipitoparietal meningoencephalocele: Case report', *PED*, vol. 10, no. 1, pp. 25–29, Jul. 2012, doi: 10.3171/2012.3.PEDS11559.

[132] C. C. N. Renaud and N. Bidère, 'Function of Centriolar Satellites and Regulation by Post-Translational Modifications', *Front. Cell Dev. Biol.*, vol. 9, p. 780502, Nov. 2021, doi: 10.3389/fcell.2021.780502.

[133] E. Odabasi, U. Batman, and E. N. Firat-Karalar, 'Unraveling the mysteries of centriolar satellites: time to rewrite the textbooks about the centrosome/cilium complex', *MBoC*, vol. 31, no. 9, pp. 866–872, Apr. 2020, doi: 10.1091/mbc.E19-07-0402.

[134] L. Gheiratmand *et al.*, 'Spatial and proteomic profiling reveals centrosome-independent features of centriolar satellites', *EMBO J*, vol. 38, no. 14, Jul. 2019, doi: 10.15252/embj.2018101109.

[135] V. Quarantotti *et al.*, 'Centriolar satellites are acentriolar assemblies of centrosomal proteins', *EMBO J*, vol. 38, no. 14, Jul. 2019, doi: 10.15252/embj.2018101082.

[136] L. Wang, K. Lee, R. Malonis, I. Sanchez, and B. D. Dynlacht, 'Tethering of an E3 ligase by PCM1 regulates the abundance of centrosomal KIAA0586/Talpid3 and promotes ciliogenesis', *eLife*, vol. 5, p. e12950, May 2016, doi: 10.7554/eLife.12950.

[137] S. C. Goetz, P. J. R. Ocbina, and K. V. Anderson, 'The Primary Cilium as a Hedgehog Signal Transduction Machine', in *Methods in Cell Biology*, vol. 94, Elsevier, 2009, pp. 199–222. doi: 10.1016/S0091-679X(08)94010-3.

[138] E. Odabasi, S. Gul, I. H. Kavakli, and E. N. Firat-Karalar, 'Centriolar satellites are required for efficient ciliogenesis and ciliary content regulation', *EMBO Rep*, vol. 20, no. 6, Jun. 2019, doi: 10.15252/embr.201947723.

[139] T. Akhshi and W. S. Trimble, 'A non-canonical Hedgehog pathway initiates ciliogenesis and autophagy', *Journal of Cell Biology*, vol. 220, no. 1, p. e202004179, Jan. 2021, doi: 10.1083/jcb.202004179.

[140] L. Huang and J. H. Lipschutz, 'Cilia and polycystic kidney disease, kith and kin: Cilia and PKD', *Birth Defect Res C*, vol. 102, no. 2, pp. 174–185, Jun. 2014, doi: 10.1002/bdrc.21066.

[141] G. Pigino, 'Intraflagellar transport', *Current Biology*, vol. 31, no. 10, pp. R530–R536, May 2021, doi: 10.1016/j.cub.2021.03.081.

[142] Y. Matsuyama *et al.*, 'Proteasomal non-catalytic subunit PSMD2 as a potential therapeutic target in association with various clinicopathologic features in lung adenocarcinomas: PSMD2 as potential target in lung adenocarcinoma', *Mol. Carcinog.*, vol. 50, no. 4, pp. 301–309, Apr. 2011, doi: 10.1002/mc.20632.

[143] O. Coux, K. Tanaka, and A. L. Goldberg, 'STRUCTURE AND FUNCTIONS OF THE 20S AND 26S PROTEASOMES', *Annu. Rev. Biochem.*, vol. 65, no. 1, pp. 801–847, Jun. 1996, doi: 10.1146/annurev.bi.65.070196.004101.

[144] J. Malicki and T. Avidor-Reiss, 'From the cytoplasm into the cilium: Bon voyage', *Organogenesis*, vol. 10, no. 1, pp. 138–157, Jan. 2014, doi: 10.4161/org.29055.

[145] C. Gerhardt, A. Wiegering, T. Leu, and U. Rüther, 'Control of Hedgehog Signalling by the Cilia-Regulated Proteasome', *JDB*, vol. 4, no. 3, p. 27, Sep. 2016, doi: 10.3390/jdb4030027.

[146] S. Herzig and R. J. Shaw, 'AMPK: guardian of metabolism and mitochondrial homeostasis', *Nat Rev Mol Cell Biol*, vol. 19, no. 2, pp. 121–135, Feb. 2018, doi: 10.1038/nrm.2017.95.

[147] D. Glick, S. Barth, and K. F. Macleod, 'Autophagy: cellular and molecular mechanisms', *J. Pathol.*, vol. 221, no. 1, pp. 3–12, May 2010, doi: 10.1002/path.2697.

[148] W.-X. Ding and X.-M. Yin, 'Mitophagy: mechanisms, pathophysiological roles, and analysis', *Biological Chemistry*, vol. 393, no. 7, pp. 547–564, Jul. 2012, doi: 10.1515/hsz-2012-0119.

[149] S. J. Ham, D. Lee, H. Yoo, K. Jun, H. Shin, and J. Chung, 'Decision between mitophagy and apoptosis by Parkin via VDAC1 ubiquitination', *Proc. Natl. Acad. Sci. U.S.A.*, vol. 117, no. 8, pp. 4281–4291, Feb. 2020, doi: 10.1073/pnas.1909814117.

[150] C. Dong, H. Zhang, L. Li, W. Tempel, P. Loppnau, and J. Min, 'Molecular basis of GID4-mediated recognition of degrons for the Pro/N-end rule pathway', *Nat Chem Biol*, vol. 14, no. 5, pp. 466–473, May 2018, doi: 10.1038/s41589-018-0036-1.

[151] S. Boulon *et al.*, 'PHAX and CRM1 Are Required Sequentially to Transport U3 snoRNA to Nucleoli', *Molecular Cell*, vol. 16, no. 5, pp. 777–787, Dec. 2004, doi: 10.1016/j.molcel.2004.11.013.

[152] J. Chrustowicz *et al.*, 'Multifaceted N-Degron Recognition and Ubiquitylation by GID/CTLH E3 Ligases', *Journal of Molecular Biology*, vol. 434, no. 2, p. 167347, Jan. 2022, doi: 10.1016/j.jmb.2021.167347.

8. Theses

1) Relative mRNA levels of *Ptch1* and *Gli1* are significantly decreased in NIH-3T3 cells deficient in the GID complex.

2) A dysfunctional GID complex does not influence the localisation of key components of the Shh signalling pathway.

3) Cells deficient in the GID complex show significantly decreased levels of GLI1 and GLI2 in the nucleus.

4) Ciliary levels of GLI2 and PTCH1 are significantly decreased in GID-deficient cells.

5) The GID complex is involved in the regulation of Shh signalling in NIH-3T3 cells.

6) Four subunits of the GID complex localise to the primary cilium in NIH-3T3 WT cells.

7) The GID complex and the primary cilium are connected by an intricate relationship.

V Selbstständigkeitserklärung

Hiermit erkläre ich, dass ich die vorliegende Dissertation mit dem Titel ,,The role of the GID complex at the primary cilium" selbstständig und nur mit Hilfe der im Anhang befindlichen Quellen angefertigt habe. Textstellen, welche wörtlich oder sinngemäß aus veröffentlichten Schriften entnommen wurden, sind als solche gekennzeichnet. Bei der Durchführung der Untersuchungen zur Generierung der Dissertationsergebnisse, habe ich die Satzung der Martin-Luther-Universität zur ,,Sicherung guter wissenschaftlicher Praxis" eingehalten. Die Arbeit habe ich weder im In- noch im Ausland in gleicher oder ähnlicher Form einer anderen Prüfungsbehörde vorgelegt. Die eingereichte schriftliche Version der Arbeit entspricht der Version der Dissertation auf dem elektronischen Speichermedium.

Halle (Saale), den

Friederike Hantel

VI Erklärung über frühere Promotionsversuche

Ich erkläre, dass ich mich an keiner anderen Hochschule einem Promotionsverfahren unterzogen bzw. eine Promotion begonnen habe.

Halle (Saale), den

Friederike Hantel

VII Danksagung